ABSTRACT

Title of dissertation: TOPICS IN SPIN ORBIT COUPLING
                            IN COLD ATOMS AND SEMICONDUCTORS:

                            Brandon Anderson, Doctor of Philosophy, 2011

Dissertation directed by: Associate Professor Victor Galitski
                            Department of Physics

This dissertation contains a collection of topics on the spin-orbit coupling of cold atoms and semiconductors.

We first consider the effects of an optically induced spin-orbit interaction on a system of Bosonic atoms. The spin-orbit term couples the emergent pseudo-spin-1/2 degree of freedom to momentum. The single particle energy spectrum has a low energy band characterized by two minima at non-zero momentum. At low temperatures, a many-body system will condense into these minima. In the presence of vanishing interactions, the ground state wavefunction is found to be a macroscopic superposition of of "left" and "right"-moving states. An experimentally observable signature of the condensate is predicted that can be observed using time-of-flight imaging.

We next consider the semiclassical dynamics of a trapped spin-orbit coupled system. We find non-linear dynamics parameterized by the value of the initial displacement of the trap, and the anisotropy of the spin-orbit energy spectrum. We show that the dynamics can give a Berry's phase, and propose an experiment to

measure this phase. We then propose a generalization of the 4-level scheme that allows for spin-orbit coupling described by a vector potential that is proportional to the angular momentum operator.

We propose a scheme for using atom interferometry to measure weak time-dependent accelerations. This proposal uses an ensemble of dilute trapped bosons with two pseudo-spin states coupled to a synthetic magnetic field, but with opposite effective charges. The synthetic field acts to couple spin to momentum continuously, which continuously imparts the acceleration on the phase of the internal states. We use time reversal pulses to reduce noise. The sensitivity of such a system is estimated to be $S \sim 10^{-7} \frac{\text{m/s}^2}{\sqrt{\text{Hz}}}$.

Finally, we predict a bulk manifestation of the spin-Hall effect in an inhomogeneous spin-orbit-coupled system. The phenomena is predicted in the framework of the spin diffusion equations generalized to include arbitrary Rashba and linear and cubic Dresselhaus terms. This framework shows that a bulk spin-density wave with a wavevector oriented perpendicular to an applied electric field will induce a charge-density wave characterized by a $\pi/2$-phase shift and a non-monotonic time-varying amplitude. The optimal values of spin-orbit coupling for observation of the effect are determined.

TOPICS IN SPIN-ORBIT COUPLING
COLD ATOMS AND SEMICONDUCTORS

by

Brandon Anderson

Dissertation submitted to the Faculty of the Graduate School of the
University of Maryland, College Park in partial fulfillment
of the requirements for the degree of
Doctor of Philosophy
2011

Advisory Committee:
Associate Professor Victor Galitski, Chair/Advisor
Adjunct Professor Jacob Taylor
Adjunct Professor Ian Spielman
Professor Mario Dagenais
Professor Sankar Das Sarma

Dedication

I dedicate this thesis to Jeffrey Mikeska. Jeff was a promising young scientist whose life was torn tragically short. He had a passion for science that was infectious, and inspired me at times when my own passion waned. Through the years and his battle with cancer, he never took his eyes of his dream of being a rocket scientist. He would have made an excellent scientist.

Before he died, his acceptance to the UT Aerospace Ph.D. program arrived in the mail.

Jeff, you never achieved your dream, but I dedicate this thesis to you.

Acknowledgments

I would first like to thank my advisor, Victor Galiski, for his encouragement and support over the past three and a half years. Naturally, Victor provided me with the research ideas and funding necessary for my intellectual development. But critically, he was always willing to make time in his incredibly busy schedule to talk not just about physics, but to help me in any way I needed. He provided encouragement when I was not feeling confident in my abilities, and provided guidance in my search for a career, and gave me the freedom to explore my own research when I was mature enough to work independently. Victor showed an interest in me far beyond his duties as my academic advisor, and for that I am deeply grateful.

Tudor Stansecu acted as a second advisor in the early days of my academic career, and was a pleasure to work with. Tudor's slow, methodical style of research is something I have tried to emulate ever since. I would like to thank Jacob Taylor for his help and support. Working with Jake was a pleasure, and he invested himself in my personal success as much as he did his own students. I would like to thank Ian Spielman and William Phillips for their lively and helpful conversations over the years. These stand out as some of the most intellectually stimulating conversations I've ever had, and I look forward to more in the future.

Perhaps more importantly, I thank the professors I had in undergrad who were responsible for both sparking my interest in physics, but also developing my skills so I could succeed at Maryland. I still remember the look on Joe Izen's as a crazy sophomore was telling him that he was going to take Quantum Mechanics, despite

I could never have done it without you. To my Dad, for nurturing my interest in science over the years. It's clear my mind is wired to enjoy science, but you guided me this way. To my Mom, for providing me love and encouragement whenever I have felt down in life. This dissertation is yours as much as it is mine.

Table of Contents

List of Abbreviations

BEC	Bose-Einstein Condensate
SOBEC	Spin-Orbit Coupled Bose-Einstein Condensate
TOF	Time of Flight
AC	Alternating Current
DC	Direct Current
SOI	Spin-Orbit Interaction
SOC	Spin-Orbit Coupling
SHE	Spin-Hall Effect
BIA	Bulk-Inversion Asymmetry
SIA	Structural Inversion Asymmetry

List of Figures

xiv

Chapter 1

Introduction

Spin is a fundamental property of quantum particles. The ability to couple spin and the orbital degrees of freedom gives rise to powerful tools in information processing and simulations. For example, if the spin of an electron could be coupled to it's center of mass motion in a semiconductor, then transport would allow the full $SU(2)$ spin degree of freedom [5] to be used for information processing. This could provide significant improvements over electron based devices and could lead to low power devices as well as new methods of information processing.

Spin-orbit coupling is a powerful tool for manipulation of spin in semiconductor systems. In these systems, the motion of the electrons through the electric fields around the atomic nuclei produce effective Zeeman fields. This relativistic correction to the motion of the electrons can be strong in some systems. Combined with the velocity dependence of the effective magnetic field, it is feasible to use this phenomena as a means to transport electron spin.

Simultaneously, new techniques in laser trapping and manipulation of atoms have opened the door for powerful experiments. Laser cooling and evaporation can be used to cool a small number of atoms into the regime where quantum effects become dominant. These systems, known as cold atomic systems, have already been used for metrology, quantum computation and quantum simulation. Recent

proposals and experiments have brought spin-orbit coupling to atomic physics to allow for simulation of solid-state systems as well as new phenomena that have no solid-state analogue.

1.1 Overview of Dissertation

This dissertation will cover spin-orbit coupling in both cold atoms and semi-conductors. It contains the result of several theoretical research projects as well as the background material relevant to each project. This structure of this dissertation is as follows. Chapter 2 through 5 contain the background, and Chapters 6 through 9 are the results of the research.

Chapter 2 contains an introduction to the interaction of light and atoms, and provides the background material needed to understand Chapter 3 and Chapter 4. Chapter 3 has an introduction to optically induced synthetic gauge fields in cold atomic systems. Two proposals for synthetic gauge fields with a non-commutative matrix structure, known as a non-Abelian field, are discussed and specialized to the case of spin-orbit coupling. Chapter 4 has an introduction to gravimetry using atom interference. Chapter 5 is an introduction to spin-orbit coupling in semiconductor systems and its relation to the spin-Hall effect. The relativistic origin of spin-orbit coupling is discussed as well as the effective magnetic field that it induces in semiconductors. This effective magnetic field is then shown to motivate spin-transport experiments.

Chapter 6 is a research proposal based upon work [6] done with Tudor Stanescu

and Victor Galitski. In this chapter, a many-body system of Bosons is considered under the influence of a synthetic spin-orbit coupling field. The spin-orbit coupling splits the energy bands and produces a double well structure in the lower band of the momentum-space dispersion. The minima of the double wells are exactly degenerate. At low temperatures, and in the presence of weak density-density interactions, the system is found to Bose-condense into a macroscopic superposition of all particles in the left well and all particles in the right well. The Gross-Pitaevskii equations are derived for the spin-orbit coupled condensate. Finally, an experimental signature is given that could be detected in time-of-flight experiments.

Chapter 7 contains unpublished work relating to synthetic spin-orbit coupling. The first section contains a semiclassical analysis of a trapped spin-orbit coupled system where the ground state is initially displaced. The dynamics are classified into regimes of large and small initial displacement, as well as spin-orbit couplings that are large and small. It is shown that the system will acquire a Berry's phase, and an experiment is proposed to measure the Berry's phase. In the second section, the 4-level scheme is generalized to next-nearest-neighbor couplings to allow for a $3D$ spin-orbit coupling. Certain optical configurations are considered, and a $3D$ spin-orbit coupling is found for which the vector potential is proportional to the pseudo-spin angular momentum operator.

Chapter 8 is a proposal for a new type of atom gravimeter that can measure time-dependent accelerations. The proposal uses the two pseudo-spins of an optically induced synthetic magnetic field to generate a continuous phase sensitivity of the external field to time-dependent gravitational signals. Methods for dealing with

noise through time reversal are discussed and the experimental feasibility is considered. It is estimated that the peak sensitivity of such a device is $S \sim 10^{-7} \frac{\mathrm{m/s}^2}{\sqrt{\mathrm{Hz}}}$. Appendix A contains additional calculations used in Chapter 8. The phase dependence on gravity is calculated in the path integral and operator formalism of quantum mechanics.

Chapter 9 is a theoretical proposal based upon work [7] done with Tudor Stanescu and Victor Galitski. The project predicts a bulk manifestation of the spin-Hall effect in semiconductor heterostructures. If a spin grating is allowed to relax in the presence of a perpendicular electric field, the system will induce a bulk charge density wave. This phenomena is predicted in a generalized spin-charge diffusion framework, and the diffusion equations are solved to maximize the phenomena.

Chapter 2

Interaction of Atoms and Light

In this section we provide a brief review of the interactions of light and atoms. Modern experimental techniques allow for the precision manipulation of atoms through magnetic and optical fields. This section provides an introduction into the basic physics of the coupling of light and atoms. Effects such as the AC Stark effect and Raman transitions will be discussed under the context of the rotating wave approximation, the dipole interaction and effective Hamiltonians.

2.1 Dipole Interaction

Neutral atoms have no net electric charge and a vanishing dipole moment. Thus, under the application of an electric field, a neutral atom should not experience a force. Fortunately, an interaction between light and atoms is possible since an applied electric field can induce a dipole moment. This induced dipole moment will then couple to the optical electric field through the dipole potential,

$$U = -\mathbf{d} \cdot \mathbf{E}. \tag{2.1}$$

In what follows we treat the electric field $\mathbf{E}$ as a classical, complex-valued field. However, the dipole term is treated as a quantum mechanical operator.

2.2 Dipole Operator and Two Level System

We approximate our atom as a two level system, with a ground state $|g\rangle$ and an excited state $|e\rangle$. This two level system can be pictured as a spin-1/2 system using the Bloch sphere picture, but we note that there is no requirement that the levels $|g\rangle$ and $|e\rangle$ be part of a real spin-1/2 system. The quantum Hamiltonian for such a system can be described by:

$$H_{atom} = \hbar\omega_0 |e\rangle \langle e| . \tag{2.2}$$

where ω_0 is the frequency splitting between the ground and excited states.

The classical dipole moment for an atom takes the form $\mathbf{d} = \sum_i q_i \mathbf{r}_i$, where q_i is a point charge at the position $\mathbf{r}_i$. Using the quantum-to-classical correspondence, the dipole operator takes the form $\hat{\mathbf{d}} = q\hat{\mathbf{r}}$, where $\hat{\mathbf{r}}$ is the electron position operator and $q = -e$ is the charge of the electron. We can then express the dipole operator through the matrix elements of our two level system:

$$\hat{\mathbf{d}} = \sum_{a,b} \langle a| e\hat{\mathbf{r}} |b\rangle |a\rangle \langle b| \tag{2.3}$$

where $a, b = e, g$ are the labels for the ground and excited states, and $\hat{\mathbf{d}}_{ab} = \langle a| q\hat{\mathbf{r}} |b\rangle$ are the dipole matrix elements. Consider the effect of the parity operator Π on the dipole matrix elements. Recall that for a neutral atom the states $|e\rangle$ and $|g\rangle$ will be states of definite parity, $\Pi |a\rangle = (-1)^{\pi_a} |a\rangle$, where π_a is the parity of the state a, and the position operator has odd parity, $\Pi \mathbf{r} \Pi^{-1} = -\mathbf{r}$. Thus, under a parity inversion

$$d_{ab} \rightarrow \langle a| \Pi^{-1}\Pi q\hat{\mathbf{r}}\Pi^{-1}\Pi |b\rangle \tag{2.4}$$

$$= (-1)^{\pi_a+\pi_b+1}d_{ab}. \tag{2.5}$$

It is therefore obvious that the diagonal matrix element of the dipole operator must vanish. However, it is possible that the off-diagonal matrix elements can be non-vanishing if the states $|e\rangle$ and $|g\rangle$ have opposite parity, $\pi_e = -\pi_g$.

We can now express the full Hamiltonian for our Atom-Laser system as:

$$H = \hbar\omega_0 |e\rangle \langle e| + \mathbf{E} \cdot \left(\mathbf{d}_{eg}\sigma_+ + \mathbf{d}_{eg}^*\sigma_-\right) \tag{2.6}$$

where $\sigma_+ = |e\rangle \langle g|$ and $\sigma_- = |g\rangle \langle e|$ are raising and lowering operators in the pseudo-spin space.

The physics that might be expected to emerge from this system is as follows. The laser field produces an oscillating electric field. When the frequency of the electric field is near the frequency splitting of the ground and excited state, the electrons in the atom will oscillate resonantly. This will allow an optical field to drive transitions between the ground to excited states.

2.2.1   Rotating Frame

We now discuss the dipole interaction in a rotating frame. The idea is to transfer the energy splitting between the ground and excited states into a time-dependent phase for the excited state. To do this we transform the eigenstates of our system with the *time-dependent* unitary operator $U = e^{-i\omega_0|e\rangle\langle e|t}$. This gives a new set of states $|\tilde{\psi}\rangle = U(t)|\psi\rangle$. The new Hamiltonian that describes these states can be found by rotating the states in the time-dependent Schrödinger's equation.

$$i\hbar\frac{d}{dt}|\psi\rangle = i\hbar\frac{d}{dt}U^\dagger(t)|\tilde{\psi}\rangle \tag{2.7}$$

Since the unitary transformation is time-dependent, the time derivative acts on the unitary rotation in addition to the state $|\tilde{\psi}\rangle$.

$$i\hbar\dot{U}^\dagger(t)\,|\tilde{\psi}\rangle + i\hbar U^\dagger(t)\frac{d}{dt}\,|\tilde{\psi}\rangle = H\,U^\dagger(t)\,|\tilde{\psi}\rangle\,. \tag{2.8}$$

Rearranging the term and left multiplying by $U(t)$ will produce the Hamiltonian in the rotating frame,

$$i\hbar\frac{d}{dt}\,|\tilde{\psi}\rangle \;=\; \left[U(t)HU^\dagger(t) - i\hbar U(t)\dot{U}^\dagger(t)\right]|\tilde{\psi}\rangle \tag{2.9}$$

$$\;=\; \tilde{H}\,|\tilde{\psi}\rangle \tag{2.10}$$

where the new Hamiltonian is:

$$\tilde{H} = U(t)HU^\dagger(t) + i\hbar\dot{U}(t)U^\dagger(t) \tag{2.11}$$

and $\dot{U} = \frac{d}{dt}U(t)$. Notice also that we have used the identity $\dot{U}U^\dagger = -U\dot{U}^\dagger$.

2.2.2 Rotating Wave Approximation

This transformation is generic and can be easily generalized to many-level systems. For the two-level case described above the rotating Hamiltonian takes the form:

$$\tilde{H} = \mathbf{E} \cdot \left(\mathbf{d}_{eg}\sigma_- e^{i\omega_0 t} + \mathbf{d}_{eg}^*\sigma_+ e^{-i\omega_0 t}\right)\,. \tag{2.12}$$

In the rotating frame, the dipole interaction can be seen to consist of two terms rotating at frequencies of opposite signs. The σ_+ term rotates at a positive frequency and corresponds to exciting the system from the ground to excited states. The σ_- term rotates with negative frequency and de-excites the system from the excited

to ground state. It is therefore useful to decompose the dipole operator into it's positive and negative frequency components,

$$\mathbf{d} = \mathbf{d}^{(+)} + \mathbf{d}^{(-)} \tag{2.13}$$

Here we have taken $\mathbf{d}^{(+)} = \mathbf{d}_{eg}\sigma_- e^{i\omega_0 t}$ and $\mathbf{d}_{eg}^*\sigma_+^{-i\omega_0 t}$ as the respective positive and negative frequency terms of the dipole operator.

A useful approximation can be made if we consider the optical field $\mathbf{E}$ created by a single laser beam. In this case we can assume it takes the form of

$$\mathbf{E} = \mathcal{E}\hat{\epsilon}(e^{i(\mathbf{k}\cdot\mathbf{x}-\omega t)} + e^{-i(\mathbf{k}\cdot\mathbf{x}-\omega t)}) \tag{2.14}$$

where $\hat{\epsilon}$ is the polarization of the light field and $\mathbf{k}$ and ω are the respective wavelength and frequency of light. We see that an electric field of this form can also be broken into positive and negative frequency components

$$\mathbf{E} = \mathbf{E}^{(+)} + \mathbf{E}^{(-)}, \tag{2.15}$$

where the $+(-)$ sign refer to the positive (negative) frequency components of the electric field.

This decomposition can be used to simplify the dipole interaction term in the Hamiltonian:

$$
\begin{align}
H_{AF} &= -\mathbf{d} \cdot \mathbf{E} \tag{2.16} \\
&= -(\mathbf{d}^{(+)} + \mathbf{d}^{(-)}) \cdot (\mathbf{E}^{(+)} + \mathbf{E}^{(-)}) \tag{2.17} \\
&= -\mathbf{d}^{(+)} \cdot \mathbf{E}^{(+)} - \mathbf{d}^{(-)} \cdot \mathbf{E}^{(-)} - \mathbf{d}^{(+)} \cdot \mathbf{E}^{(-)} - \mathbf{d}^{(-)} \cdot \mathbf{E}^{(+)} \tag{2.18}
\end{align}
$$

The first two terms have a time dependence of $e^{\pm i(\omega_0 + \omega)t}$ and rotate with frequencies $\omega_0 + \omega$. However, the last two terms rotate as $e^{\pm i\Delta t}$, i.e., with the frequency $\Delta =$

$\omega_0 - \omega$. If the frequency of of the laser is tuned near the transition frequency of the excited state, $|\omega_0 - \omega| \ll \omega_0 + \omega$, we expect the motion due to the fast moving terms to be averaged out on the time scales of the slow frequencies. This can be made formally exact by calculating transition amplitudes in perturbation theory, and noting that the fast time scales come with a factor of $1/(\omega_0 + \omega)$, whereas slow time scales come with a factor of $1/\Delta \gg 1/(\omega_0 + \omega)$. [8, 9] For our purposes it suffices to assume the time average of the fast terms is zero on the relevant times scales of atomic motion. For many cases the high frequency response of the electrons (femtoseconds) is faster than any modern detector can observe. [8]

In a frame rotating by $\omega_0 |e\rangle \langle e|$, and under the regime of the rotating wave approximation, the Hamiltonian for the atom-laser interaction system becomes

$$\tilde{H}_{RWA} = -\mathcal{E}\left(\langle g| \hat{\epsilon} \cdot \mathbf{d} |e\rangle \sigma_+ e^{-i\Delta t + i\mathbf{k} \cdot \mathbf{r}} + \langle e| \hat{\epsilon} \cdot \mathbf{d} |g\rangle \sigma_- e^{i\Delta t - i\mathbf{k} \cdot \mathbf{r}}\right). \qquad (2.19)$$

This Hamiltonian has the form of a raising operator rotating at frequency $-\Delta$, and a lowering operator rotating at frequency $+\Delta$. The time dependence can be eliminated with a transformation to a frame rotating at frequency Δ. This is analogous to the transformation in Sec. 2.2.1, with $U(t) = e^{i\Delta t |e\rangle \langle e|}$. The Hamiltonian in the rotating frame is:

$$H_{RWA} = -\hbar\Delta |e\rangle \langle e| - \hbar\left(\Omega\sigma_+ e^{i\mathbf{k} \cdot \mathbf{r}} + \Omega^*\sigma_- e^{-i\mathbf{k} \cdot \mathbf{r}}\right) \qquad (2.20)$$

where the Rabi frequency, defined as

$$\Omega = \frac{\mathcal{E} \langle e| \hat{\epsilon} \cdot \mathbf{d} |g\rangle}{\hbar}, \qquad (2.21)$$

is the characteristic frequency of an optically induced transition. The Hamiltonian

H_{RWA} is time-independent. Thus, the driven two level system can be transformed to a time-independent problem at the cost of terms rotating at frequencies of $\omega_0 + \omega$.

The spatial phase factor $e^{\pm i\mathbf{k}\cdot\mathbf{r}}$ will be shown to correspond to the atom absorbing or emitting a single unit of momentum $\mathbf{p} = \pm\hbar\mathbf{k}$. If the center of mass motion is not necessary, the electric dipole approximation can be applied, $\mathbf{k}\cdot\mathbf{r} \ll 1$, and this phase can be ignored. This approximation is reasonable, since the characteristic size of an atom $\sim .1nm$ is much less than the wavelength of optical light, $\sim 1000nm$. However, if the center of mass motion of the atom is considered, the spatial dependence of the phase can result in a spatially dependent force. This force is the optically induced gauge fields that will be discussed below.

2.3 Dynamics of the Two Level System

The dynamics of the two level system described by Eq. 2.20 can be explored by expanding the system in terms of its basis states, $|\tilde{\psi}\rangle = c_g(t)\,|g\rangle + c_e(t)\,|e\rangle$. Neglecting center of mass motion, the time-dependent Schrödinger's equation

$$i\hbar\frac{d}{dt}\,|\tilde{\psi}\rangle = [\hbar\Delta\,|e\rangle\,\langle e| + (\hbar\Omega\sigma_+ + \hbar\Omega^*\sigma_-)]\,|\tilde{\psi}\rangle \tag{2.22}$$

can then be expressed in terms of $c_g(t)$, $c_e(t)$ by left multiplying by the bras $\langle g|$ and $\langle e|$ respectively. This produces the following coupled equations of motion:

$$\dot{c}_g(t) = i\Omega c_e(t)$$

$$\dot{c}_e(t) = i\Delta c_e(t) + i\Omega^* c_g(t) \tag{2.23}$$

These equations can be exactly solved for time-independent Ω and Δ. However, two experimentally relevant situations are common, that of zero detuning, $\Delta = 0$ and that of large detuning, $\Delta \gg |\Omega|$. The intuition in these limits will be relevant for many experimentally relevant situations. These limits will now be discussed.

2.3.1 Rabi Oscillations

We now consider the zero detuning ($\Delta = 0$) limit of the equations of motion Eq. 2.23. In this limit, the equations of motion decouple

$$\ddot{c}_a = -|\Omega|^2 c_a(t), \tag{2.24}$$

where $a = e, g$. If the system is initially in the ground state, $c_g(0) = 1, c_e(0) = 0$, then the solution to these equations is given by

$$c_g(t) = \cos\left[|\Omega|t\right], \tag{2.25}$$

$$c_e(t) = i\frac{\Omega}{|\Omega|}\sin\left[|\Omega|t\right]. \tag{2.26}$$

These equations describe a system oscillating between the ground and excited states with probability $P_{ge} = \cos^2\left[|\Omega|t\right]$. These population oscillations are known as Rabi Oscillations. [8, 9] Also notice that the excited state acquires a phase $e^{i\phi_L} = i\Omega/|\Omega|$.

Consider now an optical pulse applied for a time $\Omega t = \pi/2$ to a state $|g\rangle$. Such a pulse will rotate the ground state into an even superposition

$$|\psi\rangle = \frac{1}{\sqrt{2}}\left(|g\rangle + e^{i\phi_L}|e\rangle\right). \tag{2.27}$$

Similarly, the excited state will be rotated into the orthogonal superposition. Such a pulse is called a "$\pi/2$" pulse since it rotates a vector on the Bloch sphere by

$\pi/2$. Similarly, a pulse for a time $\Omega t = \pi$ will act to interchange $|g\rangle \rightarrow e^{i\phi_L} |e\rangle$ and $|e\rangle \rightarrow e^{-i\phi_L} |g\rangle$. Such a pulse is equivalent to a rotation of π along the Bloch sphere.

2.3.2 Adiabatic Elimination

Consider now the large detuning limit, $\Delta \gg |\Omega|$. It is important to note that this limit can be consistent with the Rotating Wave Approximation, $\omega_0 + \omega \gg \Delta \gg |\Omega|$, and is indeed relevant for many experimental setups. [8, 9] In this limit, the driving energy of the field is small compared to the shift from resonance. One might therefore expect that an atom in the ground state will not be strongly excited.

If the atom is not strongly excited, the population of the excited state will reach a steady state given by $\dot{c}_e = 0$. This gives an excited state population of $c_e = -\frac{\Omega^*}{\Delta} c_g$. The equation of motion for the ground state thus becomes

$$\dot{c}_g = i\frac{|\Omega|^2}{\Delta} c_g \qquad (2.28)$$

with the solution $c_g(t) = c_g(0)e^{i\frac{|\Omega|^2}{\Delta}t}$. Thus, the coupling with the excited state acts to effectively raise the ground state energy $\Delta E = \hbar\frac{|\Omega|^2}{\Delta}$. This shift is known as the AC Stark shift, or light shift.

The intuition behind this solution can be seen by considering the equation of motion for c_e. In the large detuning limit, the evolution will be dominated by the detuning term, which is much greater than the Rabi coupling. However, in a manner similar to the rotating wave picture, this high frequency motion will be averaged out on long timescales. The time evolution of the upper state will then adiabatically follow the lower state. We have thus "adiabatically eliminated" the excited state

13

from the problem.

2.3.3 Dressed State Picture

A general solution to Eq. 2.23 for arbitrary detunings is also possible. While the limiting cases discussed above give intuition that will carry over to situations where an exact solution cannot be found, the full solution to this problem will help give more physical insight to the problem.

To solve the problem, express the Eq. 2.20 in matrix form:

$$H_{RWA} = -\hbar \begin{pmatrix} 0 & \Omega \\ \Omega^* & \Delta \end{pmatrix} \tag{2.29}$$

Diagonalization of H_{RWA} yields the two energy levels

$$E_{\pm}/\hbar = -\frac{\Delta}{2} \pm \sqrt{\left(\frac{\Delta}{2}\right) + |\Omega|^2} \tag{2.30}$$

and the corresponding eigenstates given by

$$|+\rangle = \cos(\theta)|e, \mathbf{p} + \hbar\mathbf{k}\rangle + e^{i\phi}\sin(\theta)|g, \mathbf{p}\rangle \tag{2.31}$$

$$|-\rangle = \sin(\theta)|e, \mathbf{p} + \hbar\mathbf{k}\rangle - e^{i\phi}\cos(\theta)|g, \mathbf{p}\rangle \tag{2.32}$$

where the Stückelberg angle θ is defined by

$$\tan(2\theta) = -\frac{\Delta}{2\Omega}, \tag{2.33}$$

and $e^{i\phi} = i\Omega/|\Omega|$. The effects of the optical fields can therefore be seen as mixing the ground and excited states. In doing so, the mixing introduces an avoided crossing of the energy levels, as can be seen in Fig. 2.1.

14

At large detuning, the energies and eigenstates can be expanded in powers of Ω/Δ. The energies are approximately given by

$$E_+ = -\Delta - \frac{|\Omega|^2}{4\Delta} \tag{2.34}$$

$$E_- = \frac{|\Omega|^2}{4\Delta} \tag{2.35}$$

with the approximate corresponding eigenstates

$$|+\rangle = |e\rangle + \frac{\Omega}{\Delta}|g\rangle \tag{2.36}$$

$$|-\rangle = |g\rangle - \frac{\Omega^*}{\Delta}|e\rangle. \tag{2.37}$$

The energy level E_- is just the light shift. The low energy eigenstate $|-\rangle$ can be seen to contain mostly the ground state, with only a small mixing of the excited state. This is consistent with the picture discussed in the adiabatic elimination section.

The $\Delta = 0$ limit is also of note for which the dressed state are $|\pm\rangle = \frac{1}{\sqrt{2}}(|g\rangle \pm |e\rangle)$, with corresponding energies $E_\pm = \pm\Omega$. The eigenstates are therefore even mixtures of the ground and excited states with opposite energies. Therefore, Rabi oscillations derive from the dressing of the uncoupled, or bare, states.

If the center of mass motion is considered, the phase $i\Omega/|\Omega|$ will come with an additional boost of $e^{i\mathbf{k}\cdot\mathbf{r}}$. Recall from quantum mechanics that a plane wave phase will act to boost the state by $\langle\mathbf{p}\rangle \to \langle\mathbf{p}\rangle + \hbar\mathbf{k}$. An optical pulse can therefore be viewed as a process where an atom in the ground state is excited while gaining the momentum of the optical field. Similarly, an excited state will decay and in the process give a unit of momentum to the background field.

15
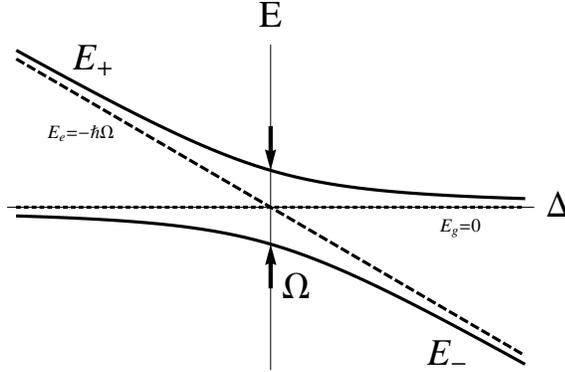
Figure 2.1 – The avoided crossings of the dressed state energy levels due to the mixing induced by the optical fields. The uncoupled states have energies of $E_g = 0$ and $E_e = -\hbar\Delta$, and meet at $\Delta = 0$. With the optical coupling, the far detuned states and energies asymptotically approach the uncoupled values. Near $\Delta = 0$ the crossing of the energy levels is avoided, and the energy levels of the dressed states are split by $\hbar\Omega$.

2.3.4 Two Level Atom in a Quantum Field

The semi-classical interaction is sufficient for describing the dynamics of an atom in an intense laser field. In this picture a dipole is seen to be driven by a classical field near resonance. However, the interaction of an atom and a quantum field can give a different physical intuition. A full treatment of this situation is beyond the scope of this thesis, but a schematic treatment is given below. A complete treatment is presented in. [10, 8, 9].

The promotion of the classical field to a quantum field can be performed by considering the atom-light interaction Hamiltonian

$$H = \hbar\omega_0 \left| e \right\rangle \left\langle e \right| + \hbar\omega \left(a^\dagger a + \frac{1}{2} \right) + \hbar g(a\sigma_+ + a^\dagger \sigma_-). \qquad (2.38)$$

16

This Hamiltonian can be rigorously derived for a two level atom using QED and the rotating wave approximation. The operators a and $a^\dagger$ are creation and annihilation operators for a single mode of a quantum field of frequency ω. This situation is a good approximation to a laser field, which is a coherent state [11] of single mode photons. The atom-laser interaction, $H_{AL} = \hbar g(a\sigma_+ + a^\dagger\sigma_-)$, is the quantum analogue of the dipole interaction for a quantum field. The classical Hamiltonian can be reclaimed by taking the expectation value of Eq. 2.38 in the coherent state $|\alpha\rangle$, defined by $a|\alpha\rangle = \alpha|\alpha\rangle$,

$$H = \hbar\omega_0 |e\rangle\langle e| + \hbar\omega\left(|\alpha|^2 + \frac{1}{2}\right) + \hbar g(\alpha\sigma_+ + \alpha^*\sigma_-) \tag{2.39}$$

This is just Eq. 2.20, up to an irrelevant constant, with $\Omega = g\alpha$.

The Hamiltonian in Eq. 2.38 is known as the Jaynes-Cummings model [12], and can be solved exactly. To interpret the results, consider a quantum field in the number state $a|N\rangle = \sqrt{N}|N-1\rangle$ with $N \gg 1$, and an atom in the state $|g\rangle$. The application of the atom-laser interaction term on the state $|N\rangle|g\rangle$ gives

$$H_{AL}|N\rangle|g\rangle = \hbar g(a\sigma_+ + a^\dagger\sigma_-)|N\rangle|g\rangle \tag{2.40}$$

$$= \hbar g\sqrt{N}|N-1\rangle|e\rangle. \tag{2.41}$$

If we consider the state $|N\rangle|e\rangle$ instead, a similar picture emerges

$$H_{AL}|N\rangle|e\rangle = \hbar g\sqrt{N+1}|N+1\rangle|e\rangle. \tag{2.42}$$

Thus, H_{AL} can be interpreted as the process of an atom (emitting)absorbing a photon with a corresponding electronic (de-)excitation with an effective coupling of $\Omega \sim g\sqrt{N}$. The momentum boost discussed in the previous section can now be

17

seen as the momentum kick due to the absorption or emission of the corresponding photon.

2.3.5 Spontaneous Emission

To conclude the discussion of two level systems, we briefly discuss spontaneous emission, one of the primary mechanisms of decoherence in atomic systems. Effecively, when an atom is in an excited state, the interaction with the electromagnetic field induces a probability for the atom to decay into a dipole allowed ground state. Note that a quantized electromagnetic field is required to describe spontaneous emission. If the atom is considered to interact with a classical field, then an excited state will be an stationary state of the system, and therefore stable.

The spontaneous emission rate can be calculated using Fermi's Gold Rule, [8, 9] to give

$$\Gamma = \frac{\omega^3 |\mathbf{d}_{ge}|^2}{3\pi\epsilon_0\hbar c^3} \tag{2.43}$$

where $\mathbf{d}_{ge}$ is the dipole matrix element between the states $|g\rangle$ and $|e\rangle$, ω is the frequency of the transition, ϵ_0 is the permittivity of free space, and c is the speed of light. Notice that the spontaneous emission rate goes as the cube of the transition frequency. This means that the rate of spontaneous emission is much higher for higher energy transitions.

To fully describe the effects of spontaneous emission, a density matrix formalism is required. This treatment will not be performed here, but the schematic effects are as follows. Spontaneous emission enters as a non-Hermitian driving term

in the equation of motion for the density matrix. The non-unitarity will cause the off-diagonal coherences of the density matrix to decay. Additionally, it will induce the diagonal elements of the excited state to decay so only the ground state is left. It can be seen that adding a large detuning from resonance will reduce the rate of excitation. This will, therefore, reduce the rate of decoherence in two photon transitions that will be discussed later. In the large detuning limit a two photon transition can be thought of as a virtual transition to an excited state.

2.4   Three or More Level Systems

The extension to an atom with three or more levels is straightforward. Recall that the two level treatment of an atom was equivalent to the Rotating Wave Approximation. More atomic levels can be considered if the driving frequency of the Electromagnetic field is near the resonance of additional atomic transitions. A more relevant situation is a system with multiple optical fields. When each field is near resonance with a different dipole transition, every level must be considered.

The following discussion will assume a scheme with a three level atom and two driving lasers. The atom will be in the "Λ"-scheme (See Fig. 2.2), where a single excited state, $|e\rangle$ is coupled to two ground states, $|g_1\rangle$, $|g_2\rangle$. The transition between the two ground states is dipole forbidden, $\langle g_1| \mathbf{d} |g_2\rangle = 0$. This means the higher energy ground state, $|g_2\rangle$, is metastable. The Hamiltonian for such a system is given by

$$H_A = \frac{\mathbf{p}^2}{2m} - \hbar\omega_{01} |g_1\rangle \langle g_1| - \hbar\omega_{02} |g_2\rangle \langle g_2| , \qquad (2.44)$$
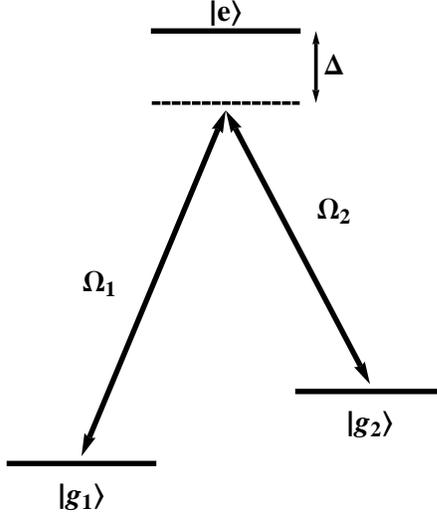
Figure 2.2 – A three level atom in the Λ scheme. Two ground states $|g_1\rangle$ and $|g_2\rangle$ are coupled by optical pulses Ω_1 and Ω_2 to a single excited state $|e\rangle$. The states are detuned from the excited state by a detuning Δ.

where ω_{0i} is the uncoupled energy for the state $|g_i\rangle$. We assume, $|\omega_{01} - \omega_{02}| \ll \omega_{0i}$, i.e. that the splitting between the ground states is much smaller than the splitting between the ground states and the excited states.

We now assume an optical field of the form

$$\mathbf{E}(\mathbf{r}, \mathbf{t}) = \hat{\varepsilon}_1 \mathcal{E}_1(\mathbf{r}, \mathbf{t}) \cos(\mathbf{k_1} \cdot \mathbf{r} - \omega_1 \mathbf{t}) + \hat{\varepsilon}_2 \mathcal{E}_2(\mathbf{r}, \mathbf{t}) \cos(\mathbf{k_2} \cdot \mathbf{r} - \omega_2 \mathbf{t}), \qquad (2.45)$$

where $\hat{\varepsilon}_i$, $\mathbf{k}_i$ and ω_i are the respective polarization vector, wavevector and frequency for the $|g_i\rangle \leftrightarrow |e\rangle$ transition. Additionally, the envelope $\mathcal{E}_i(\mathbf{r}, t)$ is assumed to have a slow variation in both space and time compared to the frequency and wavevector of the beam. Note that while this is not the most general form of an optical field, or a three level atom, most of the features necessary to understand optically induced synthetic gauge fields are present.

The dipole operator can be decomposed in a manner analogous to the two

level atom,

$$\mathbf{d} = \mathbf{d}^{(+)} + \mathbf{d}^{(-)} \tag{2.46}$$

$$= \langle g_1 | \mathbf{d} | e \rangle \sigma_1 + \langle g_2 | \mathbf{d} | e \rangle \sigma_2 + \langle e | \mathbf{d} | g_1 \rangle \sigma_1^\dagger + \langle e | \mathbf{d} | g_2 \rangle \sigma_2^\dagger \tag{2.47}$$

where $\sigma_i = |g_i\rangle \langle e|$. The Rotating Wave Approximation can now be applied to the light-atom interaction Hamiltonian. Note that there are now two optical frequencies and two dipole frequencies. We assume that the optical frequencies are such that terms that involve a different optical field and state are still "fast" rotating terms, e.g. $|\omega_1 - \omega_{01}| \ll |\omega_{10} - \omega_2|$. Thus, the the atom-field interaction Hamiltonian in the RWA is

$$H_{RWA}/\hbar = \Delta_1 |g_1\rangle \langle g_1| + \Delta_2 |g_2\rangle \langle g_2| + \frac{1}{2}\Omega_1 e^{i\mathbf{k}_1 \cdot \mathbf{r}} |g_1\rangle \langle e| + \frac{1}{2}\Omega_2 e^{i\mathbf{k}_1 \cdot \mathbf{r}} |g_2\rangle \langle e| + H.C.$$

$$\tag{2.48}$$

where

$$\Omega_i = -\frac{\langle g_i | \hat{\epsilon}_i \mathcal{E}_i | e \rangle}{\hbar} \tag{2.49}$$

is the Rabi frequency for beam $\mathcal{E}_i$.

The power of the Rotating Wave Approximation is now apparent. After dropping counter rotating terms, the atom-laser coupling is described by exactly the same Hamiltonian that would be written down from the state linkage diagram given. This is true for higher level atoms as well, as long as the polarization of the optical field is consistent with the angular momentum transferred between the dipole matrix elements of the transition.

2.5 Effective Hamiltonian

Consider now the case of large detuning from the excited state. Similar to the two level system, we expect the excited state to be negligibly populated, and to modify the dynamics of the ground states. This can be found by adiabatically eliminating the excited state in a manner analogous to the two level system. Alternatively, the dipole term can be treated as a perturbation to find an effective Hamiltonian. This method can be easily generalized to include many levels and allows the structure of the interaction to be visualized.

The structure of the three level atom suggests a natural starting place in perturbation theory. The three level atom can be viewed as a manifold of two ground states that are well separated from a excited state manifold. The treatment of excited state as a manifold allows for a direct generalization to the case of coupling to many excited states. Consider now the unperturbed Hamiltonian as the atomic ground, $\{|g_j\rangle\}$, and excited, $\{|e_k\rangle\}$ states. Furthermore, assume the dipole operator only couples the ground and excited state manifolds, and will not couple states inside either manifold. This implies that the relevant excited state manifold is the set of states that have absorbed a photon. This argument can be made precise using QED and using a quantized atom-field interaction. [10]

The effective Hamiltonian is now found perturbatively in H_{AL}/Δ, where Δ is the detuning of a one photon excitation between the ground and excited state manifold. The matrix elements can be found by projecting H_{AL} into the ground

and excited state manifolds. The resulting matrix elements are given by

$$\langle g_i | H_{eff} | g_j \rangle = \omega_{0i} \delta_{ij} - \langle g_i | \mathbf{d} \cdot \mathbf{E} | g_j \rangle + \frac{1}{2} \sum_{e_k} \langle g_i | \mathbf{d} \cdot \mathbf{E} | e_k \rangle \langle e_k | \mathbf{d} \cdot \mathbf{E} | g_j \rangle \left[\frac{1}{\Delta_{ik}} - \frac{1}{\Delta_{kj}} \right].$$

$$(2.50)$$

up to second order in H_{AL}, where $\Delta_{ij} = E_k - E_i + \hbar\omega$ and $\Delta_{kj} = E_k - E_j - \hbar\omega$. The first order term $\langle g_i | \mathbf{d} \cdot \mathbf{E} | g_j \rangle$ vanishes by the assumption that the dipole matrix elements of the interaction Hamiltonian vanish. The sum over the excited states in the second order term is naturally generalized to the case that there are many excited state manifolds.

The second order term now has a natural interpretation as a two photon transition from the ground state $|g_i\rangle$ to the excited state manifold, and then back to the state $|g_j\rangle$. Such a transition, known as a two photon Raman transition between the ground states $|g_i\rangle$ and $|g_j\rangle$, has an effective Rabi coupling given by

$$\Omega_R = \frac{1}{2} \sum_k \frac{\Omega_{ik} \Omega_{jk}^*}{\Delta_{ij}}, \qquad (2.51)$$

where Δ_{ij} is the two photon detuning. Additionally, the state $|j\rangle$ will experience an ac Stark shift of

$$\omega_{i,ac} = \sum_k \frac{|\Omega_{ik}|^2}{4\Delta_i}. \qquad (2.52)$$

Returning to the three level system, we find that our effective Hamiltonian for the two level system is given by

$$H_{eff} = \begin{pmatrix} \Delta_1 + \omega_{1,ac} & \Omega_R/2 \\ \Omega_R/2 & \Delta_2 + \omega_{2,ac} \end{pmatrix} \qquad (2.53)$$

where $\Omega_R = \frac{\Omega_1 \Omega_2}{2\Delta}$ is the two photon Raman coupling. Thus, in the large detuning

limit, the three level Λ scheme looks like an effective two level system with a one photon Rabi coupling.

2.5.1 Dark States

We can now introduce the concept of a dark state. Consider now a three level atom in the Λ scheme where an optical field pumps the ground state $|1\rangle$ to the excited state $|e\rangle$. Spontaneous emission will, over time, cause the atom to decay into both ground states. However, since the state $|1\rangle$ is continuously pumped, a sufficiently strong pump beam will win over spontaneous emission, and the steady state of the atom will be $|2\rangle$. Now consider the same setup, except with the pump beam applied between $|2\rangle$ and $|e\rangle$. Such a pump scheme has a steady state of $|1\rangle$.

Consider a general optical field Ω_1 connecting states $|1\rangle$ and $|e\rangle$, as well as an optical field Ω_2 connecting $|2\rangle$ and $|e\rangle$. There now must be some superposition of state $|1\rangle$ and $|2\rangle$ that does not couple to the combined optical fields. To find this state consider the atom-laser interaction

$$H_{al} = \begin{pmatrix} 0 & \Omega_1 & \Omega_2 \\ \Omega_1^* & 0 & 0 \\ \Omega_2^* & 0 & 0 \end{pmatrix}. \tag{2.54}$$

One of the eigenvectors of H_{al} is given by, up to normalization,

$$|D\rangle \sim \Omega_2 |1\rangle - \Omega_2 |1\rangle \tag{2.55}$$

and has eigenvalue $\lambda = 0$. The state $|D\rangle$, know as a dark state, has no matrix element with the atom-laser interaction. It is a dressed state of the optical field,

24

but it cannot absorb or emit photons from the laser, and therefore is dark. Further, it contains no component of the excited state, and therefore will not spontaneously emit.

More generally, a dark state state is an atomic dressed state for which there is no component of the excited state manifold. Since a dark state is a dressed state of the atom-laser interaction, this necessitates that there must be no projection of the dark state into the atom-laser Hamiltonian. In other words, a dark state is an eigenstate of the atom-laser interaction with zero eigenvalue. Recall we are considering an atom-laser interaction in a rotating frame where any diagonal terms have been eliminated. Thus, the requirement of zero eigenvalue is well defined. Physically, one might interpret a dark state as a dressed state for which the optical couplings of the ground state manifold destructively interfere completely. This destructive interference will prevent the atom from absorbing or emitting a photon, and thus the system remains optically dark.

Chapter 3

Synthetic Gauge Fields in Cold Atoms

The incredible degree of tunability and control available to cold atomic physicists in recent years has opened the doors to a variety of exciting physics, including precision metrological measurements, [13, 14, 15, 16, 17] simulations of well known problems from condensed matter and the possibility of quantum computation [18, 19, 20]. While atom-atom interactions occur naturally, all systems are charge-neutral, and this magnetic coupling has remained elusive. The desire to simulate quantum hall physics which requires the presence of a strong magnetic field, drove the development of optically induced synthetic magnetic fields. [21, 4, 22, 23] That is, the use of optical and magnetic fields to induce atomic center of mass dynamics analogous to a charged particle in a real magnetic field.

Simultaneously, the concept of a synthetic non-Abelian gauge field [24, 25, 6, 26, 27] for cold atoms was developed. Non-Abelian gauge fields were key to the understanding of high energy physics and the standard model, but had not taken a large role in the fields of either condensed matter or atomic physics. The realization that optical structures could produce an effective non-Abelian gauge field has allowed for both the simulation well known systems and the exploration of new systems without a solid state analogue.

In this chapter we review recent work done with synthetic fields. We will

begin with the N-level scheme [1], to demonstrate how optical coupling can induce a vector potential and spin-orbit coupling in an atom. We then treat the general case of the tripod scheme [24, 28] and show how more general non-Abelian synthetic fields can be generated. Then we will discuss Abelian synthetic magnetic fields in cold atoms from the same viewpoint. Finally we will conclude with a discussion of how the previous gauge fields can be viewed as adiabatic potentials arising from a Berry's phase.

3.1 N-pod Scheme and Spin-Orbit Coupling

We will begin with an example of a so-called "N-level" scheme, as defined in the paper [1]. This will introduce the idea of a synthetic non-Abelian gauge field from an experimental viewpoint of a coupled dispersion relation between different spin species. In this context, non-Abelian means the gauge potentials have a matrix structure that connect multiple internal states, and the gauge potentials do not commute with themselves. This is in contrast to an Abelian gauge field where the gauge field can have a matrix structure, but all gauge potentials commute.

Consider a system with N levels that are coupled in a ring topology. This geometry can be seen in Fig. 3.1(a) for $N = 4$, the state j is coupled to $j + 1$ with a coupling Ω_j. To complete the loop, state N is coupled to state 1. The single particle Hamiltonian takes the form

$$H = \sum_{j=1}^{N} \left[\left(\frac{\mathbf{p}^2}{2m} + \epsilon_j \right) |j\rangle \langle j| + \Omega_j |j\rangle \langle j - 1| + \text{H.C.} \right] \tag{3.1}$$

where the detuning ϵ_j is the detuning for the level $|j\rangle$, and the coupling Ω_j is the

coupling between the state $|j\rangle$ and $|j+1\rangle$, and the index j is summed mod N. The couplings Ω_j are the effective two-photon couplings that result from virtual two photon transitions to an excited state that has been adiabatically eliminated. We take the Raman couplings Ω_j to have the form

$$\Omega_j = \Omega e^{i\phi_j} e^{-i\mathbf{k}_j \cdot \mathbf{r}} \tag{3.2}$$

where Ω is an effective Rabi coupling, ϕ_j is the phase of the coupling, and $\hbar\mathbf{k}_j$ is the effective two photon momentum transfer. In general Ω and ϕ_j could have time or spatial dependence. However, to demonstrate the emergence of a non-Abelian gauge field in the form of spin-orbit coupling, it is only necessary to consider Ω, ϕ_j as homogeneous and time-independent. Further, the wavevectors are assumed to satisfy the property $\sum_j \mathbf{k}_j = 0$, i.e. there is no net momentum transfer for a state as it travels the closed loop.

We now assume that the Raman coupling Ω in Hamiltonian in Eq. 3.1 is much larger than all other energy scales, such as the kinetic energy, the detuning, and any external potentials applied. It therefore makes sense to diagonalize the Raman, or atom-laser coupling Hamiltonian,

$$H_{AL} = \sum_j \left[\Omega e^{i\phi_j - i\mathbf{k}_r \cdot \mathbf{r}} |j\rangle \langle j-1| + \text{H.C.} \right], \tag{3.3}$$

at the cost of potentially un-diagonalizing other terms. To perform this rotation, first define the states

$$|\tilde{j}\rangle = e^{-i\mathbf{K}_j \cdot \mathbf{r} + i\sum_{l=1}^{j-1}(\gamma_l - \bar{\gamma})} |j\rangle \tag{3.4}$$

which have been boosted by $\mathbf{K}_j = \frac{1}{N} \sum_l l\mathbf{k}_{l+j-1}$ and rephased so only the global phase $\bar{\gamma}$ appears. The cost of this transformation comes in the kinetic term, where

28

(a) Coupling scheme

Ω_{41}

$|1\rangle$ $|4\rangle$

Ω_{12} Ω_{34}

$|2\rangle$ $|3\rangle$

Ω_{23}

(b) Geometry

Ω_{12} Ω_{41}

$\mathbf{k}_1$ $\mathbf{k}_4$

BEC

$\hat{y}$

$\mathbf{k}_2$ $\mathbf{k}_3$

Ω_{23} Ω_{34}

$\hat{x}$

(c) Uncoupled dispersion

$|2\rangle$ $|1\rangle$

$|3\rangle$

$|4\rangle$

q_y q_x

$-\mathbf{K}_2$ $-\mathbf{K}_1$

$-\mathbf{K}_3$ $-\mathbf{K}_4$

(d) Coupled dispersion

Energy in units of E_L

6

4

2

0

-2

-1 0   1

$Quasimomentum$ q_y/k_L

0   -1

$Quasimomentum$ q_x/k_L
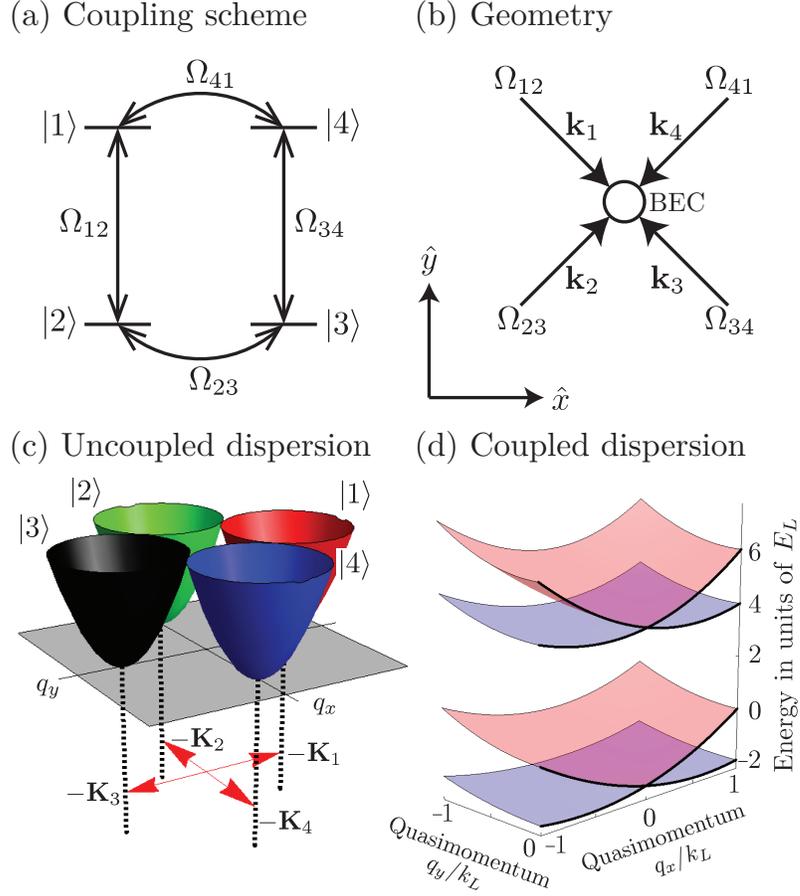
Figure 3.1 – (a) A four level atom connected with optical couplings through two-photon transitions in a closed loop topology. (b) The effective momentum transfer of each of the four optical couplings. The total momentum transfer of all four couplings vanishes. (c) Uncoupled dispersion relation of the undressed states. The momentum transfer from the optical beams transfers the minimum of the parabolic dispersion from a $\mathbf{p} = 0$ to $\mathbf{p} = -\mathbf{K}_j$ for the state $|j\rangle$. (d) The dispersion of the dressed state with $\epsilon = 0$. Two pairs of bands, each which has a Dirac point. Graphic taken from [1] and used with permission.

the spatially dependent phase $e^{-i\mathbf{K}_j\cdot\mathbf{r}}$ acts to boost the momentum operator,

$$e^{-i\mathbf{K}_j\cdot\mathbf{r}}\mathbf{p}e^{i\mathbf{K}_j\cdot\mathbf{r}} = \mathbf{p} + \hbar\mathbf{K}_j. \tag{3.5}$$

Thus, the kinetic term becomes

$$T = \sum_{j=1}^{N}\left[\frac{|\mathbf{p} + \hbar\mathbf{K}_j|^2}{2m}\right]|\tilde{j}\rangle\langle\tilde{j}| \tag{3.6}$$

$$= \sum_{j=1}^{N}\left[\frac{\mathbf{p}^2}{2m} + \frac{\hbar}{m}\mathbf{p}\cdot\mathbf{K}_j + \frac{\hbar^2\mathbf{K}_j^2}{2m}\right]|\tilde{j}\rangle\langle\tilde{j}| \tag{3.7}$$

The momentum boosts will eliminate the spatial dependence in H_{AL}, as the

terms

$$|j+1\rangle\langle j| \rightarrow \exp\left[i\frac{1}{N}\sum_l(\mathbf{k}_{l+j} - \mathbf{k}_{l+j-1})\cdot\mathbf{r}\right]|j+1\rangle\langle j| \tag{3.8}$$

$$= \exp\left[i\mathbf{k}_j\cdot\mathbf{r} - \frac{1}{N}\sum_j\mathbf{k}_j\cdot\mathbf{r}\right]|j+1\rangle\langle j| \tag{3.9}$$

$$= \exp\left[i\mathbf{k}_j\cdot\mathbf{r}\right]|j+1\rangle\langle j| \tag{3.10}$$

will cancel the spatially dependent phase in Ω_j. Notice that in Eq. 3.10 we have

used the fact that $\sum_j\mathbf{k}_j = 0$. In a similar manner, the phase $\phi'_j = \sum_{l=1}^{j-1}(\gamma_l - \bar{\gamma})$

will replace the phases ϕ_j with a single global phase. In the new basis, H_{AL} takes

the form

$$H_{AL} = \sum_j\left[\Omega e^{i\bar{\gamma}}|j\rangle\langle j-1| + \text{H.C.}\right]. \tag{3.11}$$

This term can be immediately diagonalized using the unitary transformation

$$U = \frac{1}{\sqrt{N}}\sum_{j=1}^{N}e^{i2\pi jk/N}|\tilde{j}\rangle\langle\tilde{k}|, \tag{3.12}$$

which can be thought of as a discrete Fourier transform of the set of cyclic atomic

levels. Applying Eq. 3.12 to Eq. 3.11, we find the four eigenvalues of H_{al} are given

by $E_l = -\Omega \cos\left(\frac{2\pi l}{N} - \bar{\gamma}\right)$. At certain "magic" phases of $\bar{\gamma} = 2\pi(p + 1/2)/N$, the spectrum will have a double degeneracy of the lowest energy eigenstates. Since we have assumed $\hbar\Omega$ is the largest energy scale in the problem, this degenerate subspace will be well separated compared to the rest of the remaining eigenstates of H_{AL}. We can therefore treat these two states as a slow, or adiabatic, ground state, and can adiabatically eliminate the excited states.

To lowest order we can now project our system into the degenerate subspace, and treat the two states as a "pseudo-spin-1/2" degree of freedom. The treatment of a set of low energy states as a pseudo-spin is a general feature of synthetic gauge fields. In this particular scheme the pseudo-spin states are taken as the low energy degenerate eigenstates. In the following section on the tripod scheme, a degenerate dark state manifold is used. The closed loop scheme has the advantage of using the lowest energy eigenstates as pseudo-spin, so the system does not have a lower energy state to decay to. This is in contrast to the dark states used in the tripod scheme where there exists a dressed state with lower energy than the dark states, thus making them metastable.

The behavior of the synthetic field now arises by examining the effect of the unitary operation in Eq. 3.12 on the diagonal terms of the original Hamiltonian. This unitary rotation will move the terms that were originally diagonal, such as the detuning and the kinetic term $\sum_j \mathbf{p} \cdot \mathbf{K}_j/m \, |\tilde{j}\rangle \langle \tilde{j}|$, and move them off the diagonal.

A special case of interest is when $\mathbf{K}_j$ are chosen to form the edges of a regular

N-gon. In this case, the momenta take the form

$$\mathbf{K}_j = -k_L \sin(2\pi j/N)\hat{e}_x + k_L \cos(2\pi j/N)\hat{e}_y. \qquad (3.13)$$

The effect of the unitary rotation on $\cos(2\pi j/N)$ can be seen by applying

$$\sum_{j,l} e^{i2\pi jl/N} \cos(2\pi j/N) |\tilde{j}\rangle \langle \tilde{l}| = \frac{1}{2} \sum_{j,l} \left(e^{i2\pi j(l+1)/N} + e^{i2\pi j(l-1)/N} \right) |\tilde{j}\rangle \langle \tilde{l}| \qquad (3.14)$$

$$= \frac{1}{2} \sum_{j} \left(|j \tilde{+} 1\rangle \langle \tilde{j}| + |j \tilde{-} 1\rangle \langle \tilde{j}| \right). \qquad (3.15)$$

Similarly, the sin term becomes $\sin(2\pi j/N) = \frac{i}{2} \sum_j \left(|j \tilde{+} 1\rangle \langle \tilde{j}| - |j \tilde{-} 1\rangle \langle \tilde{j}| \right)$. To see why these states are of interest, consider the projection of the rotated states into the 2×2 subspace formed by the two lowest energy eigenstates:

$$H_{2\times 2} = k_L \sigma_x q_y - k_L \sigma_y q_x. \qquad (3.16)$$

This effective Hamiltonian has the form of the Rashba spin-orbit interaction seen in semiconductor quantum wells. [29] Thus, purely through the application of optical fields, a cold atomic system could be used to simulate quantum wells in a semiconductor.

This scheme can be modified to include a linear Dresselhaus spin-orbit interaction through the application of a detuning from the Raman transition resonance. We chose a detuning of the form $H_\epsilon = \sum_j (-1)^j \epsilon |\tilde{j}\rangle \langle \tilde{j}|$. We specifically consider the case of $N = 4$, where the rotated H_ϵ looks like $H_\epsilon = \epsilon \sum_j |\tilde{j}\rangle \langle j \tilde{+} 2|$. This can

be expressed in matrix representation as

$$H_\epsilon = \begin{pmatrix} 0 & 0 & \epsilon & 0 \\ 0 & 0 & 0 & \epsilon \\ \epsilon & 0 & 0 & 0 \\ 0 & \epsilon & 0 & 0 \end{pmatrix} = \begin{pmatrix} 0 & \epsilon\hat{I} \\ \epsilon\hat{I} & 0 \end{pmatrix}, \tag{3.17}$$

where $\hat{I}$ in the second equality is the 2×2 identity matrix. We compare this to the

form of the non-diagonal momentum terms and see that they take the form

$$H_{\mathbf{q}} = \mathbf{q} \cdot \begin{pmatrix} \sigma_R & \sigma_R^* \\ \sigma_R^* & \sigma_R \end{pmatrix} \tag{3.18}$$

where $\sigma_R = k_L(\sigma_y \hat{e}_x - \sigma_x \hat{e}_y)$, and $\sigma_R^* = k_L(-\sigma_y \hat{e}_x - \sigma_x \hat{e}_y)$. To see the effect of H_ϵ,

we will now diagonalize

$$H_\epsilon + H_\Omega = \begin{pmatrix} -\hbar\Omega\hat{I} & \epsilon\hat{I} \\ \epsilon\hat{I} & \hbar\Omega\hat{I} \end{pmatrix}. \tag{3.19}$$

This block matrix can be diagonalized with a rotation of the super-matrix $R_{\sigma_y \otimes \hat{I}}(\theta) =$

$e^{-i\sigma_y \otimes \hat{I}\theta}$ where $\tan(2\theta) = \left(\frac{\epsilon}{\hbar\Omega}\right)$. Applying this rotation will bring the Hamiltonian

to a block diagonal form

$$H'_\epsilon + H'_\Omega = -\sqrt{\hbar^2\Omega^2 + \epsilon^2}\sigma_z \otimes \hat{I}. \tag{3.20}$$

This same rotation, when applied to to $H_{\mathbf{q}}$ will rotate the spin-orbit coupling to the

form

$$H'_{\mathbf{q}} = k_L\mathbf{q} \cdot \begin{pmatrix} \sigma_R - \sin(2\theta)\sigma_R^* & \cos(2\theta)\sigma_R^* \\ \cos(2\theta)\sigma_R^* & \sigma_R + \sin(2\theta)\sigma_R^* \end{pmatrix}. \tag{3.21}$$

Note that the term $\mathbf{q} \cdot \sigma_R^*$ has the form of the linear Dresselhaus spin-orbit interaction. Therefore, in the pseudospin subspace, a linear Dresselhaus spin orbit interaction can be induced through the application of an alternating detuning H_ϵ.

3.1.1 Coupled Dispersion

The origin of the spin-orbit coupling given above can be seen from a experimentally relevant standpoint as follows. Consider first the set of bare states, $\{|1\rangle, |2\rangle, |3\rangle, |4\rangle\}$. When the optical couplings are turned on, the optical fields act to shift the dispersions of state $|j\rangle$ from a parabola centered at $\mathbf{p} = 0$, to a parabola centered at $\mathbf{p} = -\mathbf{k}_j$ (see Fig. 3.1(c)). The uncoupled dispersion relations are then coupled into two sets of dispersions, each with a Dirac cone (Fig. 3.1(d)). Since the coupled dispersions also couple spin, the energy for each value of momentum will be spin-dependent.

This coupling of spin and momentum has a natural experimental signature. Consider a dressed state prepared with quasimomentum $\mathbf{q}$. Upon a time-of-flight measurement, the bare spins of the system will be offset in momentum by the value of their respective $\mathbf{k}_j$. This demonstrates an advantage of the ring-like coupling with no momentum transfer where the effect of a state traversing the ring of couplings is to acquire a phase. If the atom-light coupling were such that a net momentum were transferred, the picture would be modified. For each momentum there would be an infinite set of states that are coupled together, and differ by one unit of the momentum $\mathbf{k}_T = \sum_j \mathbf{k}_j$. Thus, for a dressed state with quasimomentum $\mathbf{q}$, a

time-of-flight expansion will yield an infinite set of momentum values for each bare state.

3.1.2 Adiabatic Corrections

By projecting into the low energy subspace, the dynamics of the high energy states is completely ignored. However, recall that when a ground state is coupled to an excited state with a far detuned optical beam, the ground state acquires an effective energy shift from the elimination of the excited state. Similarly, we expect that the two level effective spin-orbit Hamiltonian will acquire a correction due to the dynamics of the excited state. This correction can be calculated in perturbation theory in $1/\Omega$ in a manner analogous to Eq. 2.50. For the 4-level scheme the lowest order non-trivial, i.e., constant, correction is [1]

$$ H^{(3)} = -\frac{1}{2\Omega^2} \left[\sigma_x(q_y^3 - 3q_y q_x^2) - \sigma_y(q_x^3 - 3q_x q_y^2) \right] . \tag{3.22} $$

This has a 4-fold rotational symmetry in $\mathbf{q}$, $\boldsymbol{\sigma}$, but breaks the continuous symmetry of the Rashba spin-orbit interaction. This can be viewed as a restoration of the symmetry of the optical fields, which themselves have a 4-fold symmetry.

3.1.3 Interpretation as a Gauge Field

The spin-orbit coupling and kinetic terms can be expressed as

$$ \frac{(\mathbf{p} - \mathbf{A})^2}{2m} + \Phi, \tag{3.23} $$

where

$$\mathbf{A} = k_L \sigma_x \hat{e}_y - k_L \sigma_y \hat{e}_x \tag{3.24}$$

$$\Phi = -\frac{\mathbf{A}^2}{2m}. \tag{3.25}$$

The vector $\mathbf{A}$ has a matrix structure in spin space, and can be seen to shift the minimum of the kinetic energy from $\mathbf{p} = 0$ to $\mathbf{p} = \mathbf{A}$. In other words, for every spin direction, the vector potential produces a new kinetic energy minimum. Thus, we interpret $\mathbf{A}$ as a vector potential in a way analogous to how a vector potential in a magnetic field generates a new minima of kinetic energy at every point in space. We therefore say that we have induced a *synthetic gauge field*, with a vector potential $\mathbf{A}$ and a scalar potential Φ. This interpretation will be carried father in Sec. 3.4 where it will be shown this gauge field can be interpreted as a geometric phase, and is invariant under gauge transformations.

3.2   Tripod Scheme

Spin-orbit coupling is the most simple, non-trivial, non-Abelian gauge field possible. However, many other gauge fields can be simulated using cold atoms. One of the first proposals of a non-Abelian gauge field was the "tripod scheme." [28, 24] This scheme uses optical fields to couple three degenerate states to a single excited state (See Fig. 3.2).

This system can be described by the Hamiltonian

$$H_{AL} = \sum_{j=1}^{3} \left[\Omega_j(\mathbf{r}) \left| 0 \right\rangle \left\langle j \right| + \text{H.C.} \right], \tag{3.26}$$
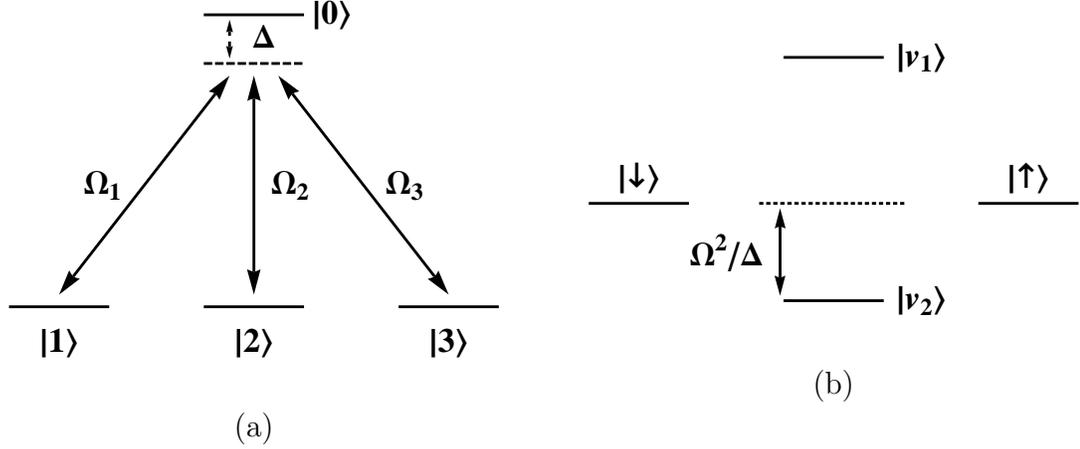
Figure 3.2 – The tripod scheme. Three ground states, $|1\rangle$, $|2\rangle$, $|3\rangle$, are connected to a single excited state $|0\rangle$ by optical pulses Ω_1, Ω_2, Ω_3 respectively. A detuning from the excited state is given by Δ. Upon diagonalization two dark states $|\uparrow\rangle$ and $|\downarrow\rangle$ emerge, as well as two bright states. The low energy bright state $|\nu_2\rangle$ is separated from the dark states by an energy Δ^2/Ω.

where $\Omega_j(\mathbf{r})$ is the single photon Rabi frequency for a transition from the state $|j\rangle$ to a state $|0\rangle$. Unlike the N-level scheme above, we do not make any assumptions about the form of the optical fields, except to assume they have spatial modulation. We also assume that the Rabi frequencies are much greater than the other scales of the problem, such as the kinetic energy, potential energy, and any detunings.

The emergence of the non-Abelian gauge field arises in a manner similar to the N-level scheme. Since the Rabi frequencies are the largest energy scales in the problem, it makes sense to diagonalize H_{AL}, at the possibility of generating other non-diagonal terms. This diagonalization is performed with the unitary rotation matrix $U(\mathbf{r})$, which can have a dependence on both space and time depending on the form of $\Omega_j(\mathbf{r})$. The result of this diagonalization is seen in Fig. 3.2. For an

arbitrary set of Rabi frequencies there will be a set of two dark states with energy between a single excited state and a single low energy state. The energies of the two bright states can be varied relative to the dark states through the detuning $\hbar\Delta$.

After applying the unitary rotation, we see that the dark states acquire spatial modulation. Therefore, when the unitary operator $U(\mathbf{r})$ is used to rotate to the dressed state basis, a new term arises from the non-commutativity of the position operator $\hat{\mathbf{r}}$ in $U(\mathbf{r})$, and the momentum operator $\hat{\mathbf{p}}$ in the kinetic energy term. The new terms are given by

$$U^\dagger(\mathbf{r})\frac{\hat{\mathbf{p}}^2}{2m}U(\mathbf{r}) = \frac{\hat{\mathbf{p}}^2}{2m} - \frac{1}{m}i\hbar U^\dagger\boldsymbol{\nabla}U \cdot \hat{\mathbf{p}} - \frac{\hbar^2}{2m}U^\dagger\nabla^2 U \tag{3.27}$$

$$= (\hat{\mathbf{p}} - \mathbf{A})^2 + \Phi \tag{3.28}$$

where

$$\mathbf{A} = i\hbar U^\dagger\boldsymbol{\nabla}U \cdot \tag{3.29}$$

is the vector potential, and

$$\Phi = \mathbf{A}^2 - \frac{\hbar^2}{2m}U^\dagger\nabla^2 U \tag{3.30}$$

has the form of a scalar potential.

We can now explicitly diagonalize H_{AL}. To do this, first parameterize the Rabi frequencies as

$$\Omega_1 = \Omega\sin(\theta)\cos(\phi)e^{iS_1}, \tag{3.31}$$

$$\Omega_2 = \Omega\sin(\theta)\sin(\phi)e^{iS_2}, \tag{3.32}$$

$$\Omega_3 = \Omega\cos(\theta)e^{iS_3}, \tag{3.33}$$

where $\Omega = \sqrt{|\Omega_1|^2 + |\Omega_2|^2 + |\Omega_3|^2}$. We can now construct the dark states

$$|\uparrow\rangle \;=\; \sin(\phi)e^{iS_{31}}|1\rangle - \cos(\phi)e^{iS_{32}}|2\rangle , \tag{3.34}$$

$$|\downarrow\rangle \;=\; \cos(\theta)\cos(\phi)e^{iS_{31}}|1\rangle + \cos(\theta)\sin(\phi)e^{iS_{32}}|2\rangle - \sin(\theta)|3\rangle . \tag{3.35}$$

The non-Abelian gauge field can then be calculated by projecting the rotated Hamiltonian into the dark state subspace. Performing this projection gives the vector potential

$$\mathbf{A}_{\uparrow\uparrow} \;=\; \hbar\left(\cos^2(\phi)\boldsymbol{\nabla}S_{23} + \sin^2(\phi)\boldsymbol{\nabla}S_{13}\right) \tag{3.36}$$

$$\mathbf{A}_{\uparrow\downarrow} \;=\; \hbar\cos(\theta)\left(\frac{1}{2}\sin(2\phi)\boldsymbol{\nabla}S_{12} - i\boldsymbol{\nabla}\phi\right) \tag{3.37}$$

$$\mathbf{A}_{\downarrow\downarrow} \;=\; \hbar\cos^2(\theta)\left(\cos^2(\phi)\boldsymbol{\nabla}S_{13} + \sin^2(\phi)\boldsymbol{\nabla}S_{23}\right) \tag{3.38}$$

and the scalar potential

$$\Phi_{\uparrow\uparrow} \;=\; \frac{\hbar^2}{2m}\left(\frac{1}{4}\sin^2(\phi)\left((\nabla S_{12})^2 + (\nabla\phi)^2\right)\right) \tag{3.39}$$

$$\Phi_{\uparrow\downarrow} \;=\; \frac{\hbar^2}{2m}\left(\frac{1}{2}\sin(2\phi)\nabla S_{12} - i\nabla\phi\right) \cdot \tag{3.40}$$
$$\left(\frac{1}{2}\sin(2\theta)\left(\cos^2\phi\nabla S_{13} + \sin^2\phi\nabla S_{23}\right) - i\nabla\theta\right)$$

$$\Phi_{\downarrow\downarrow} \;=\; \frac{\hbar^2}{2m}\left(\frac{1}{4}\sin^2(2\theta)\left(\cos^2\phi\nabla S_{13} + \sin^2\phi\nabla S_{23}\right)^2 + (\nabla\theta)^2\right) . \tag{3.41}$$

It is of note that the form of the vector and scalar potentials is entirely determined by the dressed states formed from atom-laser coupling, and not the strength of the coupling itself. The overall strength of the atom-laser coupling only enters in the adiabatic corrections that come from eliminating the dynamics of the excited states.

3.2.1   Spin-Orbit Coupling

There are now two ways we can simulate a spin-orbit coupled system using the tripod scheme. The first is to adiabatically eliminate the single excited state, to produce a ring-like coupling. If the Rabi frequencies are chosen to produce a ring-like coupling with no net momentum, this model then reduces to the $N = 3$ case of the N level scheme discussed in Sec. 3.1.

An earlier scheme to simulate spin-orbit coupling was given in Ref. [3]. In this scheme the optical couplings were chosen such that Ω_1 is produced by two laser beams propagating in the $x - y$ plane, which are offset at a relative angle η. The effect of these beams is to produce a standing wave along the $\hat{x}$ direction, and a plane wave along the $\hat{y}$ direction. The optical coupling Ω_2 is identical, except the standing wave in the $\hat{x}$ direction is phase shifted by $\pi/2$. The third coupling, Ω_3, is in the $\hat{y} - \hat{z}$ plane, oriented at an angle ξ relative to the $\hat{y}$ axis.

The form of these lasers naturally follow the parameterization given in Eqs. 3.32-3.33. The relevant parameters become $S_1 = S_2 = k_1 \cos(\eta/2)\, x$, $S_3 = k_3 \cos \xi$, and $\phi = k_1 \sin(\eta/2)\, y$. We can therefore apply the machinery above to immediately find the vector potential

$$\mathbf{A}_{\uparrow\uparrow} = \hbar \boldsymbol{\nabla} S, \tag{3.42}$$

$$\mathbf{A}_{\uparrow\downarrow} = -i\hbar \cos\theta\, \boldsymbol{\nabla}\phi, \tag{3.43}$$

$$\mathbf{A}_{\downarrow\downarrow} = \hbar \cos^2\theta\, \boldsymbol{\nabla} S, \tag{3.44}$$

which can be expressed using the Pauli matricies as

$$\mathbf{A}/\hbar = \frac{1}{2}(1+\cos^2(\theta))\boldsymbol{\nabla}S\,\hat{I} + \frac{1}{2}\sin^2(\theta)\boldsymbol{\nabla}S\,\sigma_z + \boldsymbol{\nabla}\phi\,\sigma_y \tag{3.45}$$

The term proportional to the identity matrix can be transformed away with the unitary transform $U = e^{-i\frac{1}{2}(1+\cos^2(\theta))\boldsymbol{\nabla}S\cdot\mathbf{r}}$. The remaining terms we can denote as

$$\mathbf{A} = mv\hat{x}\sigma_y + mv'\hat{y}\sigma_z, \tag{3.46}$$

where $v = \hbar k_1 \sin(\eta/2)\cos\theta/m$ and $v' = \hbar(k_1\cos(\eta/2) - k_3\cos\xi)\sin^2\theta/2m$. To match the notation in Sec. 6.2, we now redefine the σ matricies as follows $\sigma_y \to \sigma_1$, $\sigma_z \to \sigma_2$, and $\sigma_x \to \sigma_3$, which defines a right handed spin system.

Upon expanding the kinetic energy, $(\mathbf{p}-\mathbf{A})^2/2m$, a spin-orbit coupling

$$-\frac{1}{m}\mathbf{p}\cdot\mathbf{A} = -vp_x\sigma_1 - v'p_y\sigma_2 \tag{3.47}$$

arises. The tripod scheme is therefore capable of simulating spin orbit coupling. However, there are several drawbacks to this setup as opposed to the 4-level scheme given above. The first is that the adiabatic corrections to the spin-orbit Hamiltonian vanish as $1/\Omega_R$, the inverse of the two photon Raman coupling. This implies that large laser power will be necessary to eliminate adiabatic corrections to the spin-orbit term. This is in contrast to the 4-level scheme where adiabatic corrections converge as $1/\Omega_R^2$. [1] Second, there is no tripod scheme available in the alkali atoms, the most convenient set of atoms for cold atom experiments [1]. Any singlet state, such as a $F = 1$ hyperfine manifold, will not be isolated spectroscopically from a nearby set of states. For example, in ^{87}Rb, the $5^2P_{3/2}$, $F = 0$ manifold is only separated from the $F = 1$ manifold by 75MHz, this is much smaller than the energy splitting

41

between the ground state $5^2 S_{1/2}$, $F = 1$ manifold of ~ 6GHz. Therefore, in the rotating wave approximation, a coupling between between the ground state and the $F = 0$ state will also couple to states in the $F = 1$ manifold.

3.3 Synthetic Magnetic Fields

Synthetic fields in cold atoms can also be used to simulate magnetic fields. As discussed above, cold atoms have no net charge, and therefore do not experience the Lorentz force. The ability to simulate a magnetic field in cold atoms would allow for simulations of the quantum Hall effect [30, 31] or the spin Hall effect [4]. Early experiments on the quantum Hall effect used a rotating gas to simulate a magnetic field. However, since the effective magnetic field strength is proportional to the rotation frequency, the scope of these experiments is limited, and are unable to reach the quantum Hall regime. [32]

Several schemes for simulating magnetic fields using synthetic magnetic fields have also been proposed. [22, 21] This section will discuss the scheme proposed by [21] and extended by [4] to demonstrate the spin Hall effect. The scheme can be seen in Fig. 3.3. Consider a three level atom in the Λ scheme where the optical fields are counterpropagating Gaussian beams with spatially offset centers. For this coupling, the two beams will have a relative orbital angular momentum which is imparted on the atom under a two photon transition. Since a rotating frame is equivalent to a uniform magnetic field, it is expected that this atom-laser coupling will generate magnetic field like behavior.

(b)

(a)
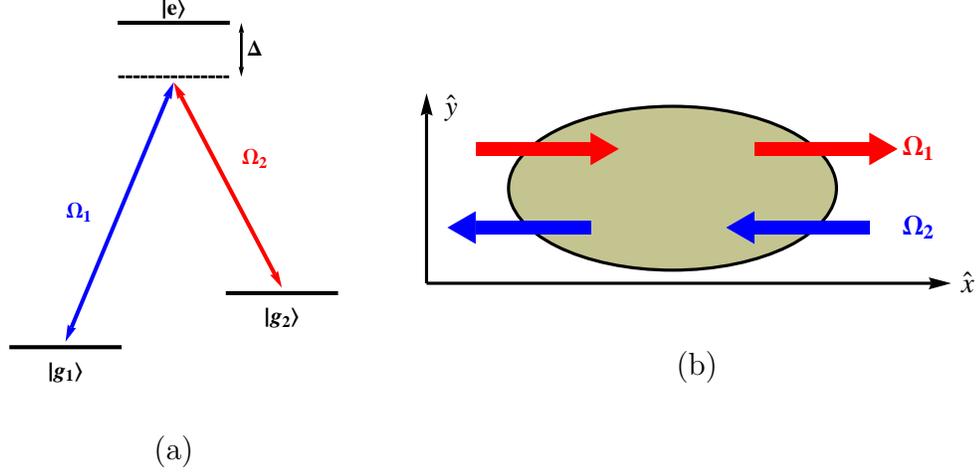
Figure 3.3 – The laser scheme for a synthetic magnetic field. An atom in the Λ scheme is coupled with two counter propagating pulses Ω_1 and Ω_2 with Gaussian profiles. The optical pulses have a relative angular momentum that is imparted on the dressed states of the atoms. The angular momentum is analogous to a charged particle in a magnetic field.

To see the origin of this field, consider the atom-laser Hamiltonian that describes the Λ-scheme

$$H_{AL} = \Delta \, |e\rangle \, \langle e| + \Omega_1(\mathbf{r}) \, |e\rangle \, \langle 1| + \Omega_2(\mathbf{r}) \, |e\rangle \, \langle 2| + H.C., \tag{3.48}$$

where

$$\Omega_j(\mathbf{r}) = \Omega_0 e^{-\frac{(x-x_j)^2}{\sigma_0^2}} e^{-ik_j y} \tag{3.49}$$

are the Rabi couplings and Δ is the detuning from the excited state. As before, we diagaonlize H_{AL} at the cost of other non-diagonal terms. The eigenvalues of H_{AL} are $\lambda = \{0, \frac{\Delta}{2} \pm \sqrt{\left(\frac{\Delta}{2}\right)^2 + \Omega^2}\}$, where $\Omega^2 = |\Omega_1|^2 + |\Omega_2|^2$. The corresponding

43

eigenstates are given by

$$|D\rangle = -\sin\phi e^{iS_2}|1\rangle - \cos\phi e^{iS_1}|2\rangle, \tag{3.50}$$

$$|-\rangle = \cos\theta\cos\phi e^{-iS_1}+|1\rangle\cos\theta\sin\phi e^{-iS_2}|2\rangle - \sin\theta|3\rangle, \tag{3.51}$$

$$|+\rangle = \sin\theta\cos\phi e^{-iS_1}+|1\rangle\sin\theta\sin\phi e^{-iS_2}|2\rangle + \cos\theta|3\rangle, \tag{3.52}$$

where $S = ky$, $\tan\phi = |\Omega_1|/|\Omega_2| = e^{-4(x_0)x/\sigma_0^2}$, $\tan\theta = 2\Omega/\Delta$, and we have assumed $x_1 = -x_2 = x_0$ and $k_1 = -k_2 = k/2$.

The vector potential for the dark state can now be calculated in the same way as the non-Abelian gauge fields,

$$\mathbf{A}_D = i\hbar\langle D|\boldsymbol{\nabla}|D\rangle = \hbar k\cos(2\theta)\hat{e}_y, \tag{3.53}$$

with a corresponding magnetic field given by

$$\mathbf{B}_{eff} = \boldsymbol{\nabla}\times\mathbf{A}_D = -2\hbar k\sin(2\theta)\boldsymbol{\nabla}\theta\times\hat{e}_y. \tag{3.54}$$

The optical coupling above gives

$$\mathbf{A}_D = -\frac{\hbar k}{1+e^{-x/d}}\hat{e}_y \tag{3.55}$$

where $d = \sigma_0^2/4x$, with a synthetic magnetic field of

$$\mathbf{B}_{eff} = \frac{\hbar k}{4d\cosh^2(x/2d)}\hat{e}_z. \tag{3.56}$$

For quantum Hall physics, only the dark ($\lambda = 0$) state is necessary to consider. However, as will be discussed later, we desire a synthetic magnetic field with two states that have opposite charges. To accomodate this second state, consider as well

the $\lambda_- = \frac{\Delta}{2} - \sqrt{\left(\frac{\Delta}{2}\right)^2 + \Omega^2}$ state. In the large detuning limit, $\Delta \gg \Omega$, the vector potential for this state becomes

$$\mathbf{A}_- = i\hbar \left\langle -|\,\boldsymbol{\nabla}\,|-\right\rangle = -\cos(2\theta)k\hat{e}_y, \tag{3.57}$$

with corrections of $\mathcal{O}(\Omega/\Delta)^2$. Thus, $\mathbf{A}_- = -\mathbf{A}_D$.

Notice however, that while there is an off-diagonal vector potential $\mathbf{A}_{-D} = i\hbar \left\langle -|\,\boldsymbol{\nabla}\,|D\right\rangle$, this term is small compared to the diagonal energy splitting of $\lambda_-/2$. This allows the off diagonal elements of the vector and scalar potential to be ignored in the adiabatic limit. Therefore, this setup will give two degrees of freedom that couple to a synthetic magnetic field with opposite effective charges, as is desired in Sec. 3.1. Note however, excited state $|-\rangle$ is subject to collisional decay.

3.4   Gauge Transformations and Dynamics

It is now worth considering the effects of gauge transformations for a synthetic gauge field. Recall that in systems with fundamental gauge fields, the scalar and vector gauge potentials are used to describe the system in the Hamiltonian or Lagrangian formalisms. In these formalisms, the vector and scalar potentials can be transformed through a series of gauge transformations. However, the Lagrangian equations of motion remain invariant under the same transformations. This can be understood as arising from a fundamental symmetry of the problem, which itself was induced by an overparameterization of the degrees of freedom necessary for the vector/scalar potential description.

Under a gauge transformation in classical gauge theory, the system is described

by the two potentials, $\mathbf{A}$ and Φ. For an Abelian gauge field, such as electromagnetism, these gauge fields transform according to

$$\mathbf{A} \rightarrow \mathbf{A} + \boldsymbol{\nabla}\alpha, \tag{3.58}$$

$$\Phi \rightarrow \Phi - \partial_t\alpha, \tag{3.59}$$

where $\alpha(\mathbf{r}, t)$ is an arbitrary function that parameterizes the change of gauge. In quantum mechanics, such a gauge transformation is implemented through a unitary rotation $U = e^{i\alpha(\mathbf{r},t)}$. This operator will transform the gauge potentials according to Eq. 3.58 and Eq. 3.59. Additionally, every quantum state will acquire the same overall phase $e^{i\alpha(\mathbf{r},t)}$. Consider now the effect of a gauge transformation on the momentum operator $\mathbf{p} \rightarrow U^{\dagger}\mathbf{p}U$. Using the coordinate representation of the momentum operator,

$$e^{-i\alpha}\mathbf{p}e^{i\alpha} = -ie^{-i\alpha}\boldsymbol{\nabla}e^{i\alpha} = -i\boldsymbol{\nabla} + \boldsymbol{\nabla}\alpha(\mathbf{r}, t) = \mathbf{p} + \boldsymbol{\nabla}\alpha(\mathbf{r}, t). \tag{3.60}$$

Therefore, the momentum operator is not gauge invariant. A gauge invariant observable related to momentum can be constructed by considering the operator $\mathbf{p} - \mathbf{A}$, which transforms as

$$\mathbf{p} - \mathbf{A} \rightarrow U^{\dagger}(\mathbf{p} - \mathbf{A})U \tag{3.61}$$

$$= U^{\dagger}\mathbf{p}U - \mathbf{A} \tag{3.62}$$

$$= \mathbf{p} - \boldsymbol{\nabla}\alpha - \mathbf{A} \tag{3.63}$$

$$= \mathbf{p} - (\mathbf{A} + \boldsymbol{\nabla}\alpha) \tag{3.64}$$

$$= \mathbf{p} - \mathbf{A}'. \tag{3.65}$$

46

We therefore see that the observable $\mathbf{p} - \mathbf{A}$ is gauge invariant for an Abelian gauge field.

Since the electromagnetic field is Abelian, i.e. it does not have a matrix structure, there is no possibility of a rotation among the components of the field. Now consider a gauge field with an internal degree of freedom, such as the pseudo-spin in the synthetic non-Abelian fields above. A more complex set of gauge transformations are now allowed, such rotations between the components of $\mathbf{A}$ and Φ. These additional symmetries allow the transformation $\alpha(\mathbf{r}, t)$ to be promoted to a matrix, $\boldsymbol{\alpha} \cdot \boldsymbol{\sigma}$, where $\boldsymbol{\alpha}(\mathbf{r}, t)$ is now a vector with one component for each generator of the internal space, $\boldsymbol{\sigma}$. Notice that the the gauge transformation can be local, in the sense that every point in space be transformed independently. In quantum mechanics this transformation is again represented by a unitary transformation, $U = \exp[i\boldsymbol{\alpha}(\mathbf{r}, t) \cdot \boldsymbol{\sigma}]$. Under such a gauge transformation the vector potential transforms as

$$\mathbf{A} \rightarrow U^{\dagger}\mathbf{A}U - iU^{\dagger}\boldsymbol{\nabla}U. \tag{3.66}$$

We therefore see that $\mathbf{p} - \mathbf{A}$ is again invariant under the transformation U.

For a physical gauge field, such as an electromagnetic field, gauge invariance is imposed as a physical law. This means that *only gauge invariant observables can be observed.* The most simple example of this is that the canonical momentum $\mathbf{p}$ is not an observable quantity in the presence of an electromagnetic field. A related observable is the mechanical momentum

$$m\dot{\mathbf{v}} = \mathbf{p} - e\mathbf{A}, \tag{3.67}$$

which was shown to be invariant above.

The case of a synthetic gauge field is starkly different. The structures in such fields arise from optical coupling of light and atoms, and have no relation to a fundamental symmetry of nature. Therefore gauge invariance is *not* required for these systems, and non-gauge invariant observables can be measured.

One way of viewing the consequence of the induced gauge is to directly consider the effect of the optical couplings on the bare states, $|i\rangle$, of the atoms. As long as the optical couplings are maintained, the dressed states are formed from superposition of boosted bare states $e^{i\mathbf{k}_i \cdot \mathbf{r}} |i\rangle$. The presence of the optical fields can generate eigenstates with non-zero momentum, but vanishing mechanical momentum. This is why the mechanical momentum of an eigenstate of a Hamiltonain with a synthetic field may have zero mechanical momentum, even if it has a finite canonical momentum. However, if the optical fields are turned off instantaneously, the bare states will retain their boost, and each bare state will fly away with a corresponding mechanical and canonical momentum $m\mathbf{v}_i = \mathbf{k}_i$.

For example, consider the momentum operator, $\mathbf{p}$, for the synthetic magnetic field in Sec. 3.3. For this scheme, the vector potential desciribing the magnetic field is given by

$$\mathbf{A} = \frac{\hbar k \hat{e}_y}{1 + e^{-x/d}}, \qquad (3.68)$$

which is the vector potential of a uniform magnetic field in the Landau gauge, up to a constant. Recall this field was generated in a three level system by two counter-propagating laser fields. Thus, this effective potential is composed of the states

$e^{iky/2}|1\rangle$ and $e^{-iky/2}|2\rangle$. The offset Gaussian profiles produces a spatially dependent superposition of these two states. We now examine the momentum distribution of the $|1\rangle$ component of the dark state $|D\rangle$. Ignoring the orbital wavefunction, a measurement of the momentum in the $\hat{e}_y$-direction of this component will give

$$\langle\hat{p}_{1y}\rangle \sim k/2\frac{1}{1+e^{-x/d}}, \tag{3.69}$$

where $\hat{p}_{1y} = \hat{p}_y|1\rangle\langle 1|$ is the momentum operator projected into the subspace for $|1\rangle$. Note the momentum in the $\hat{e}_y$ has spatial dependence on x. A similar result is valid for state $|2\rangle$.

Now consider the same setup for the synthetic magnetic field, except rotate the lasers by $\pi/2$ about the $\hat{e}_z$ axis. The induced vector potential will then be described by $\mathbf{A}' = -\hbar k\hat{e}_x 1 + e^{-y/d}$. This vector potential will have the same Lagrangian equations of motions as $\mathbf{A}$. However, an analogous momentum measurement of the dark state will yield

$$\langle\hat{p}_{1x}\rangle \sim -k/2\frac{1}{1+e^{-y/d}}, \tag{3.70}$$

where $\hat{p}_{1x} = \hat{p}_x|1\rangle\langle 1|$ is the momentum in the $\hat{e}_x$-direction of the projection on the state $|1\rangle$ onto the dark state $|D\rangle$. This measurement will give the same effective profile as the previous vector potential, just rotated by $\pi/2$, according to the rotation of the optical fields.

A more complete treatment will show that $\mathbf{A}$ and $\mathbf{A}'$ describe a system where all the gauge invariant observables are identical, but measurements of the bare states will have different spatial dependence. This is a property of all synthetic gauge fields. In these systems, gauge transformations can be performed physically, in the

sense that different optical configurations can produce vector potentials that are connected by gauge transformations. However, if the undressed degrees of freedom are measured, they will be manifestly gauge invariance. Therefore, a change of gauge can be used to calculate some observables, but care must be taken to transform to the original gauge upon measurement of the undressed states, or any measurements made after the synthetic fields are instantaneously turned off.

Finally, we note that synthetic gauge fields differ from gauge fields experienced in nature in another dramatic way. Classical gauge fields are dynamic, in the sense that the field itself is generated by its coupling to matter particles. The matter particles can then generate their own fields, i.e., they can be sources or sinks of the field. Synthetic gauge fields are static, in that they are generated independent of matter particles, and are not a physical entity in and of themselves. This limits the analogy with real gauge fields as well as the systems they can simulate. However, other schemes for producing synthetic gauge fields may be possible. For instance, an atom in a cavity could produce fluctuations that will generate field fluctuations. At the time of writing, there has only been one proposal for a dynamical gauge field. [33]

3.5   Berry's Phase

We will now demonstrate the connection between a synthetic gauge field and Berry's phase in an adiabatic system. Consider a quantum Hamiltonian $H(\lambda)$ that is a function of a vector of parameters $\lambda = (\lambda_1, \ldots, \lambda_n)$. For every value of the

parameters λ the system will have a set of eigenfunctions

$$H(\lambda) \, |\psi_n(\lambda)\rangle = E_n(\lambda) \, |\psi_n(\lambda)\rangle . \tag{3.71}$$

Now, allow the parameters $\lambda = \lambda(t)$ to vary slowly in time and consider the state $|\psi_n(\lambda(0))\rangle$ at $t = 0$. If the variation is slow compared to the other time scales of the problem, the adiabatic theorem states that the system will remain in the same eigenstate, $|\psi_n(\lambda(t))\rangle$, up to an overall phase.

To find this phase consider the time-dependent Schrödinger equation, and assume the state has a phase $e^{i\phi(t)} \, |\lambda(t)\rangle$.

$$i\hbar \frac{d}{dt} e^{i\phi(t)} \, |\psi_n(\lambda(t)), t\rangle = H(\lambda(t)) \, |\psi_n(\lambda(t)), t\rangle . \tag{3.72}$$

Using Eq. 3.71, and left multiplying by $\langle\psi_n(\lambda)|$ gives

$$\hbar \frac{d}{dt} \phi(t) = i\hbar \, \langle\psi_n(\lambda)| \frac{d}{dt} \, |\psi_n(\lambda)\rangle - E_n(\lambda(t)). \tag{3.73}$$

We see that the adiabatic motion resulted in not only the dynamical phase $e^{-i \int dt \, E(\lambda(t))/\hbar}$, but also a new phase

$$\phi_B = \int_0^T dt \, i\hbar \, \langle\psi_n(\lambda)| \boldsymbol{\nabla}_\lambda \, |\psi_n(\lambda)\rangle \cdot \frac{d\lambda}{dt} \tag{3.74}$$

known as a geometric, or Berry's phase. The meaning of the word "geometric" can be understood if the Berry's phase is expressed as

$$\phi_B = \oint i\hbar \, \langle\psi_n(\lambda)| \boldsymbol{\nabla}_\lambda \, |\psi_n(\lambda)\rangle \cdot d\lambda , \tag{3.75}$$

where we have assumed $\lambda(t)$ to trace a closed path as it varies from time $t = 0$ to $t = T$. The quantity $A_B = i\hbar \, \langle\psi_n(\lambda)| \boldsymbol{\nabla}_\lambda \, |\psi_n(\lambda)\rangle$ is known as Berry's connection,

and can be interpreted as a vector potential. We see the phase ϕ_B depends only on the path that λ takes, and not on the dynamics of the evolution. Thus, only the geometry of parameter space is relevant as long as the variation is sufficiently slow.

Since the integral is around a closed curve, the Berry's phase is unambiguously defined. If $|\psi_n(\lambda)\rangle$ is rephased by $e^{i\alpha(\lambda)}$, the Berry's phase will gain a term $-\hbar \oint \boldsymbol{\nabla}_\lambda \alpha(\lambda) \cdot d\lambda$. However, the line integral of a gradient vanishes, so Berry's phase is invariant. We note that λ must be varied in a closed loop for ϕ_B to be well defined. If it is not, such a transformation could be made to eliminate the phase.

The synthetic magnetic field of Sec. 3.3 can now be interpreted as a Berry's phase. Consider the dark state $|D\rangle = \sin\phi\,|1\rangle - \cos\phi e^{iS}\,|2\rangle$. As discussed above, the dark state has a spatial dependence through the parameters ϕ and S. If the atom is sufficiently cold so the variation in the optical fields is adiabatic compared to the electron degrees of freedom, the atom will remain in the dark state. This is analogous to the Born-Oppenheimer approximation. By moving through space in a closed loop, the dark state acquires a flux $e^{i\oint \mathbf{A}_b(\mathbf{r})\cdot d\mathbf{r}}$, which is analogous to the flux a charge particle will experience as it moves through a real magnetic field described by a vector potential $\mathbf{A}(\mathbf{r})$.

Synthetic non-Abelian gauge fields can be interpreted as a non-Abelian Berry's phase. If the Hamiltonian $H(\lambda)$ has a degenerate subspace $\{|\psi_n(\lambda)\rangle\}$ such that $H(\lambda)\,|\psi_n(\lambda)\rangle = E\,|\psi_n(\lambda)\rangle$, the above derivation of Berry's phase can be repeated for all states in the degenerate subspace. However, since the states are degenerate

it makes sense to right multiply by $|\psi_m(\lambda)\rangle$ as well. The Berry's connection

$$\mathbf{A}_{mn} = i\hbar \langle\psi_m(\lambda)| \boldsymbol{\nabla}_\lambda |\psi_n(\lambda)\rangle \qquad (3.76)$$

now has a matrix structure. The generalized Berry's phase is a unitary matrix given by

$$e^{i\phi_B} = P\exp[i\oint i\hbar \langle\psi_m(\lambda)| \boldsymbol{\nabla}_\lambda |\psi_n(\lambda)\rangle \cdot \mathrm{d}\lambda], \qquad (3.77)$$

where P denotes a path ordered exponential in λ-space. A synthetic non-Abelian gauge field thus originates in the same way a synthetic magnetic field does. As the atom travels through slowly varying optical fields, the pseudospins follow their eigenstates. However, the degeneracy of the eigenstates gives rise to an ambiguity of which pseudospin is which, and the subspace can transform into itself.

Chapter 4

Atom Interferometry

We now provide a brief review of traditional atom interferometry as is necessary for Chap. 8. In recent years, atom interferometry has emerged as a powerful tool for precision measurements of gravity, gradiometry, gyroscopy [34, 35, 36], metrology [37, 38, 39] and inertial sensing [40]. The ability to cool atoms to low temperatures has opened up the door for experiments where interference is performed on atoms. Recall that the de Broglie wavelength of a particle is given by

$$\lambda_{dB} = 2\pi\hbar/p = \frac{\hbar}{\sqrt{2\pi M k_b T}}, \tag{4.1}$$

where M is the mass of the particle and $k_b T$ is the thermal energy. The ability to cool atoms to the μK regime has opened the doors for the ability to use the matter wave principle as a measuring tool. For example, a ^{87}Rb atom cooled to $T \sim 1\mu$K will have a de Broglie wavelength of $\lambda \sim .5\mu$m, comparable to the wavelength of light in the visible spectrum.

The general scheme for an atom interferometer is analogous to an optical interferometer. A diffraction grating or beam splitter is used to place a beam of atoms into a motional superposition. The beam is then allowed to propagate, and at some future point recombined to produce an interference pattern. The period of free evolution will undergo phase evolution that can be coupled to the environment. Upon recombining the beam-split matter waves, an interference signal will result

that can be used to measure the environmental coupling in the free evolution period.

If the two diffracted beams of atoms are set up so that one travels at a higher gravitational potential than the other, the phase accumulated will depend on the gravitational potential in the region the matter wave traverses. Such a scheme has proven a powerful test of gravitational measurements, and recent experiments have surpassed corner cubes [35] as the most precise measurements of gravity to date.

There are several schemes to accomplish such an interference measurement. We will now focus on the use of Raman pulses in atom interferometry to perform a measurement of gravity. Consider a three level atom in the Λ scheme, as discussed in Sec. 2.4, initially polarized in the state $|1, \mathbf{p}\rangle$. Now apply a Raman pulse using two counter-propagating beams with wavevectors $\mathbf{k}_1 \simeq -\mathbf{k}_2$. As discussed above, a pulse application for a time $\int \Omega \mathrm{d}t = \pi/2$ will place the system in the state

$$|\psi\rangle = \frac{1}{\sqrt{2}} \left(|1, \mathbf{p}\rangle + e^{i\phi_L} |2, \mathbf{p} + \hbar \mathbf{k}_{eff}\rangle \right), \tag{4.2}$$

where ϕ_L is the phase of the laser, and $\mathbf{k}_{eff} = \mathbf{k}_1 + \mathbf{k}_2$. Additionally, a pulse for a time $\Omega t = \pi$ will act to interchange the state

$$|1, \mathbf{p}\rangle \quad \rightarrow \quad e^{i\phi_L} |2, \mathbf{p} + \hbar \mathbf{k}_{eff}\rangle, \tag{4.3}$$

$$|2, \mathbf{p} + \hbar \mathbf{k}_{eff}\rangle \quad \rightarrow \quad e^{-i\phi_L} |1, \mathbf{p}\rangle. \tag{4.4}$$

We can now interpret a $\pi/2$-pulse as the analogue of an optical beamsplitter, and a π pulse as mirror. It is clear that a pulse sequence of $\frac{\pi}{2} - \pi - \frac{\pi}{2}$, with pulses separated by a time T, will act to split the beam and then recombine it at a future time $2T$. The spatial splitting and recombination of the beam is true only for the case of a constant gravitational field.
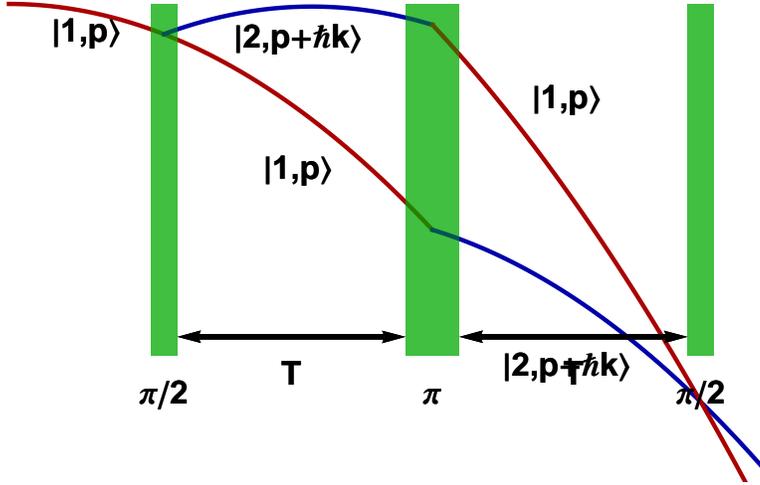
Figure 4.1 – The space-time diagram for the two spin states of an atom in the $\pi/2 - \pi - \pi/2$ pulse sequence. The first $\pi/2$ pulse separates the beam spatially, analogous to a beamsplitter. The π pulse acts as a mirror to ensure the atoms overlap at a future time. The final $\pi/2$ pulse converts the phase coherence accumulated along the two paths into a population measurement which can be used to extract information about the gravitational potential.

This scheme can be used to make a measurement of gravity if the beam of atoms is initially oriented parallel to the direction of gravity. (See Fig. 4.1) If the beam of atoms is allowed to freely fall, and $\mathbf{k}_{eff}$ is also oriented along the direction of gravity, the two beams will spatially separate and follow different paths. One beam of atoms will spend more time at a higher gravitational potential than the other, and therefore accumulate phase faster. Despite the influence of gravity, the two beams will once again recombine so that a phase measurement can be performed.

The phase accumulated for such an interferometer has two contributions, the phase due to free evolution, ϕ_{evol}, and the phase imprinted by the laser beams, ϕ_{laser}.

The free evolution phase can be calculated using the path integral formulation of quantum mechanics. [5] In the semi-classical limit, the propagator is dominated by the phase $e^{iS_{cl}/\hbar}$, where,

$$S_{cl} = \int_{t_i}^{t_f} dt\, L[\mathbf{r}(t), \dot{\mathbf{r}}(t)] \tag{4.5}$$

is the action of the classical path connecting the points $\mathbf{r}(t_i)$ and $\mathbf{r}(t_f)$. The net phase due to the difference in the two paths is given by

$$\Delta\phi_{evol} = \frac{S_{cl}^u - S_{cl}^l}{\hbar} = \frac{1}{\hbar} \oint L[\mathbf{r}(t), \dot{\mathbf{r}}(t)], \tag{4.6}$$

where $S_{cl}^{u/l}$ is the classical action of the upper/lower path. For the case of a free particle in a constant gravitational field, this phase vanishes.

The phase imprinted by the lasers has the form $\phi_i = \mathbf{k}_i \cdot \mathbf{r}_i - \omega_i t_i$, where $\mathbf{k}_i$, ω_i are the respective wavevector and frequency of pulse i, and $\mathbf{r}_i$, t_i are the respective position of the atom and time at which the laser is applied. Following the pulse sequence in 4.1, we see that the net phase difference due to the lasers is

$$\Delta\phi_{lasers} = \phi_1 - \phi_{2a} - \phi_{2b} + \phi_3, \tag{4.7}$$

where

$$\phi_1 = 0 \tag{4.8}$$

$$\phi_{2a} = k_{eff}\left[-\frac{1}{2}gT^2 + v_0 T\right], \tag{4.9}$$

$$\phi_{2b} = k_{eff}\left[-\frac{1}{2}gT^2 + \left(v_0 + \frac{\hbar k_{eff}}{m}\right)T\right], \tag{4.10}$$

$$\phi_3 = \left[-2gT^2 + \left(2v_0 + \frac{\hbar k_{eff}}{m}\right)T\right], \tag{4.11}$$

where v_0 is the initial velocity of the atoms and the pulses 1, $2a/2b$ and 3 were applied

at the respective times $t = 0, T, 2T$. Calculating the total phase shift therefore gives

$$\Delta\phi_{lasers} = -k_{eff}gT^2. \tag{4.12}$$

Fig. **??** shows the experimental result of such a gravitational measurement made by the Chu group. [2] The data shows the local variation in gravity over time, and phenomena such as the tides are clearly visible. This class of experiments has proven to be the most precise measurements of the Earth's surface gravity to date, and future experiments promise measurements of General Relativity and the gravitational constant G_N [16, 17, 15, 41].
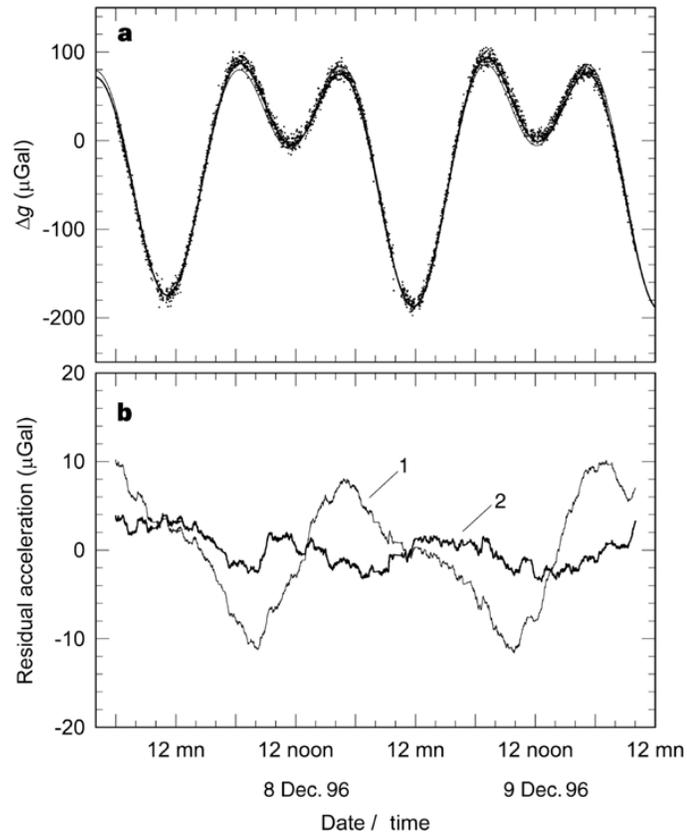
Figure 4.2 – **??**(a): Two days of experimental data of the Earth's surface gravity measured by Steven Chu's group. Each data point is one minute of data. The variation of the tides are clearly visible, and are compared to two tidal models given by solid lines. $1\mu\text{Gal} = 10^{-8}\text{m/s}^2$. **??**(b): Difference of the experimental data between two models given by trace 1 and trace 2. [2]

Chapter 5

Spin-Orbit Coupling and the Spin-Hall Effect

5.1   Spin-orbit Coupling in Semiconductors

The spin-orbit coupling that is discussed above is a simulation of spin-orbit coupling in semiconductors [42, 43, 29, 44, 42, 43]. Spin-orbit coupling can lead to a class of transport effects such as the spin-Hall effect or anomalous-Hall effect. [45, 46, 47] This chapter will provide an introduction to spin-orbit coupling in semiconductors, and the spin-Hall effect. The material in this section will provide the background information for the work on the bulk spin-Hall effect in Chap. 9

The phenomena of spin-orbit coupling can be qualitatively described as a relativistic correction of the Schrödinger equation. Consider a particle of charge e with spin $s = 1/2$, moving in an electric field $\mathbf{E}$, and moving at a velocity $\mathbf{v}$. Transforming the system to the particle's rest frame, the particle sees a magnetic field $\mathbf{B} = \frac{1}{c}\mathbf{E} \times \mathbf{v} = \frac{1}{mc}\mathbf{E} \times \mathbf{p}$. This magnetic field has a corresponding Zeeman shift of

$$H_{SO} \sim \boldsymbol{\mu} \cdot \mathbf{B} = \frac{e\hbar}{2mc}\boldsymbol{\sigma} \cdot \mathbf{B} = -\frac{e\hbar}{2m^2c^2}\boldsymbol{\sigma} \times \boldsymbol{\nabla}V, \tag{5.1}$$

where $\boldsymbol{\sigma}$ are the Pauli matricies, m is the mass of the particle, c is the speed of light, and V is the potential of the electric field. A full treatment of spin-orbit coupling can be derived using the Dirac equation, and reproduces Eq. 5.1 up to a factor of 2. This factor is a result of ignoring the transformation into a rotating frame. The

full spin-orbit interaction term is given by

$$H_{SO} = -\frac{e\hbar}{4m^2c^2}\boldsymbol{\sigma} \cdot (\boldsymbol{\nabla}V \times \mathbf{p}) \quad\quad\quad (5.2)$$

and is known as the Thomas-Pauli spin-orbit interaction.

Since the spin-orbit interaction comes with a factor of $1/c^2$, it is negligible except for the cases of strong electric fields or large velocities. The first system where the spin-orbit correction was necessary was atomic systems, where the spin-orbit interaction is, in part, responsible for the fine structure splitting. The large electric fields near the atomic nucleus provide a radial electric field that allows the Pauli term to be expressed as $H_{SO} \sim \mathbf{L}\cdot\mathbf{S}$, where $\mathbf{S}$ is the spin of the electron, and $\mathbf{L}$ is the orbital angular momentum of the electron. This is where the term spin-orbit coupling arose.

The second example of where spin-orbit coupling is relevant is in semiconductor structures. Due to Kramer's theorem, the band structure in semiconductors must be degenerate, with the state $E(\mathbf{k},\uparrow) = E(-\mathbf{k},\downarrow)$. If additionally, the crystal structure is inversion symmetric, i.e. invariant under $\mathbf{r} \to -\mathbf{r}$, then the band structure has the symmetry $E(\mathbf{k},\uparrow) = E(-\mathbf{k},\uparrow)$ and $E(\mathbf{k},\downarrow) = E(-\mathbf{k},\downarrow)$. These combine to force the relation $E(\mathbf{k},\uparrow) = E(\mathbf{k},\downarrow)$, and therefore, there can be no spin splitting in the band structure.

If the structure is not inversion symmetric, then the spin-orbit coupling term can change the band structure to split the energy of the spin structure. There are two ways inversion symmetry can be broken. The first is the system can have a region where the normal crystal structure is broken. This is what happens in

61

semiconductor quantum wells, where two different semiconductors are placed in contact. This symmetry breaking is known as a structural inversion asymmetry (SIA), and leads to the Rashba spin-orbit interaction. The second situation where inversion symmetry can be broken is when the unit cell of the crystal structure itself lacks inversion symmetry. In this case, there can be a spin-orbit coupling in the bulk of the semiconductor, leading to the Dresselhaus spin-orbit interaction. This is known as bulk inversion asymmetry (BIA).

We now specialize to group III-V semiconductors, such as GaAs. This class of materials has a tetrahedral unit cell, and therefore is not bulk inversion symmetric. The effect of bulk inversion asymmetry was treated by Dresselhaus [44] in Zincblende materials and later by D'yakanov and Perel [48]. The effect of the asymmetry is to induce a momentum-dependent magnetic field $H(\mathbf{k}) = \frac{\hbar}{2}\boldsymbol{\sigma} \cdot \boldsymbol{\Omega}(\mathbf{k})$, where the momentum dependent Zeeman frequency is

$$\boldsymbol{\Omega}_{D_3}(\mathbf{k}) = \beta_3 \left(k_x(k_y^2 - k_z^2), k_y(k_z^2 - k_z^2), k_z(k_x^2 - k_y^2) \right), \tag{5.3}$$

where β_3 is an effective coupling constant, and $\mathbf{k} = (k_x, k_y, k_z)$. This is known as the cubic Dresselhaus spin-orbit interaction. Note the functional similarity with the adiabatic corrections for the 4-level scheme given by Eq. 3.22.

Now consider the effect of a one-dimensional confining potential so that the semiconductor system becomes effectively two dimensional. Such a situation occurs, for example, when a thin layer GaAs is placed between two layers of AlGaAs, known as a heterostructure. Since AlGaAs and GaAs have nearly identical lattice constants, but different chemical potentials, an effective one-dimensional confining potential is

created in the middle layer.

The confining potential has two effects. First, the cubic Dresselhaus term is modified, as the momentum oriented perpendicular to the plane of confinement is quantized. Second, if the top and bottom layer of the heterostructure have different doping, the trapping potential of the quantum well becomes asymmetric and a new spin-orbit coupling can appear. This term has an effective Zeeman field of

$$\boldsymbol{\Omega}_R(\mathbf{k}) = \alpha\,(\mathbf{k} \times \mathbf{n}) \tag{5.4}$$

where α is a coupling parameter and $\boldsymbol{n}$ is a vector normal to the plane of confinement. This coupling is known as the Rashba spin-orbit interaction.

The form of the Dresselhaus spin-orbit interaction depends on the axis of confinement of the heterostructure. We now consider only heterostructures grown along the axis [001]. The momentum, k_z, oriented perpendicular to the well can now be replaced by by a quantum average of the lowest mode of a square well potential. Thus, $\langle k_z \rangle = 0$, and $\langle k_z^2 \rangle = (\pi/a)^2$ where a is the width of the model quantum well. This average gives an effective Zeeman field of

$$\boldsymbol{\Omega}_{D_1}(\mathbf{k}) = \beta_1(-k_x, k_y, 0) \tag{5.5}$$

where $\beta_1 = \beta_3\langle k_z^2 \rangle$ is the effective linear Dresselhaus coupling constant. We also note that for well oriented along this axis, the Rashba term looks like

$$\boldsymbol{\Omega}_R(\mathbf{k}) = \alpha\,(\mathbf{k} \times \hat{e}_z)\,. \tag{5.6}$$

Therefore, the general form of the spin-orbit interaction in a semiconductor quantum well is the sum of Ω_{D_1}, Ω_{D_3} and Ω_R.

5.2 Spin Relaxation Mechanisms

The presence of a momentum dependent Zeeman term has been shown to lead to spin relaxation in semiconductors. Since the spin-orbit term in the Hamiltonian does not commute with any component of the spin operator, there is no spin conservation along any spin direction. In the presence of impurities this can lead to scattering through several mechanisms, including the Elliott-Yafet mechanism, D'yakanov-Perel mechanism, Bir-Aronov-Pikus mechanism, and the nuclear hyperfine exchange interaction. [43, 48]

In two dimensional electron systems the D'yakanov-Perel mechanism is the dominant mechanism, so we will confine our discussion to this mechanism only. The effective Zeeman field $\mathbf{\Omega}(\mathbf{k}) \cdot \boldsymbol{\sigma}$ depends on the direction of momentum, $\mathbf{k}$. The scattering off an impurity will act to change the direction of $\mathbf{k}$, and thus the direction of the effective Zeeman field. Therefore, impurity scattering will act to randomize the axis of spin precession, and cause a loss of spin information over time.

Consider the limit where the average spin precession frequency $\Omega(\mathbf{k})_{av}$ is less than the momentum relaxation time τ_p, i.e., $\Omega(\mathbf{k})_{av} \leq \tau_p$. Between scatterings the spin will precess an angle $\delta\theta \sim \Omega_{av}\tau_p$ before rotating about a different, randomly oriented, axis and the spin undergoes a random walk of $n = t/\tau_p$ steps in a time t. For n steps of a random walk, the angle will precess as $\theta_n \sim n\delta\theta$. Therefore if we define the spin precession time, τ_s, as the time when $\theta_n \sim 1$, we can estimate a spin relaxation rate as $1 \sim \Omega_{av}\tau_p\sqrt{\tau_s/\tau_p}$ to give

$$\frac{1}{\tau_s} = \Omega_{av}^2 \tau_p. \tag{5.7}$$

Therefore, the spin lifetime is inversely proportional to the momentum scattering time.

5.3 Spin Currents and the Spin-Hall Effect

The spin-Hall effect is a collection of effects that are found in spin-orbit coupled semiconductor systems. The canonical manifestation is an accumulation of spin at the boundaries of a spin-orbit coupled system under the application of an electric field. This can be considered analogous to the Hall effect where the application of an electric field will induce boundary charge accumulation. This spin-Hall effect is still not well understood, and there has been much controversy in the origin of the effect.

To motivate the spin-Hall effect we now define the concept of a spin current. There is no universally agreed on definition of a spin current, but we use the form

$$j_k^i = C \frac{1}{2} \langle \{ \sigma_i, v_k \} \rangle \tag{5.8}$$

where C is a constant that varies from definition to definition, $\{ \cdot, \cdot \}$ is an anti-commutator, and $\langle \cdot \rangle$ is the average of single particle wavefunctions. The anti-commutator is necessary since spin-orbit coupling modifies the velocity operator $v_k = \frac{1}{i\hbar} [H, r_k]$, to induce an anomalous velocity that is analogous to the kinetic momentum discussed above. It is desirable for the spin current to follow a continuity equation analogous to charge current, $\partial_t \mathbf{S} + \mathbf{\nabla} \cdot \mathbf{j} = 0$. However, due to spin-orbit coupling the spin operator does not commute with the Hamiltonian, and spin is not a conserved quantity. This leads to source terms on the right hand side of the

continuity equation for the spin current.

This definition of a spin current then allows for a spin-Hall conductivity, analogous to σ_{xy} in the Hall effect. This is defined as

$$\sigma^{SH} = -j_y^z / E_x \tag{5.9}$$

which is the response of the S_z component of spin in the $\hat{e}_y$ direction to an electric field in the $\hat{e}_x$ direction. For a time-independent electric field, the spin-Hall conductivity can be seen to vanish in the bulk for k-linear spin-orbit couplings. This can be explained by noting that semiconductors are not spin polarized in the absence of a magnetic field. If the bulk could support a steady state spin current then the bulk would become spin polarized. Note that this result is in contrast to the universal spin-Hall conductivity $\sigma^{SH} = e/4\pi\hbar$ that was predicted in the absence of impurities.

The relation of spin currents to the boundary accumulation of spin is therefore unclear. The spin-Hall effect can be treated without reference to spin currents using the Boltzmann equation. In the dirty limit where the spin lifetime τ_s is much larger than the momentum relaxation time, $\tau \gg \tau_s$, the kinetic equation can be reduced to a diffusion equation. The general form of the diffusion equation, in the absence of an electric field, is given by

$$(\partial_t - \mathcal{D}\nabla^2)\rho_i = (\Gamma^{ij} - P^{ijk}\partial_k + \mathbf{C}^{ij} \cdot \boldsymbol{\nabla})\rho_j, \tag{5.10}$$

where ρ_0 is the charge density and $\rho_{1,2,3} \equiv \rho_{x,y,z}$ are spin densities. The parameters Γ^{ij} describe the Dyakonov-Perel spin relaxation [49], $\mathcal{D} = \tau v_F^2/2$ is the diffusion constant, $P^{ijk} = -P^{jik}$ characterize the precession of the spin polarization and and $\mathbf{C}^{ij}$ describe the coupling between the spin and charge degrees of freedom.

These diffusion equations have been generalized to include a dc electric field for the Rashba case. In Sec. 9.2 these equations are generalized to include linear and cubic Dresselhaus terms.

The diffusion equation formalism has also yielded ambiguous predictions of the spin-Hall effect. The appearance of spin accumulation in the presence of a dc electric field is highly dependent on the boundary conditions of the system. [50, 51, 52, 53] These boundary conditions themselves are dependent on the microscopic Hamiltonian of the system. For example, a reflective boundary will not see any S_z spin accumulation. However, a boundary with a strong spin-orbit scattering will see spatially oscillating polarizations of both S_z and S_y in a region near the boundary. Finally, we note that the if a spin current is applied, the above spin transport mechanisms will induce charge accumulation on the boundaries. This is known as the inverse spin-Hall effect.

Chapter 6

Spin-Orbit Coupled Bose-Einstein Condensates

6.1 Introduction

The single particle spin-orbit Hamiltonian described in Chapter 5 is analogous to the spin-orbit Hamiltonian an electron sees in semiconductor quantum wells. At low temperatures, the many-particle physics of these systems is dictated by the Pauli exclusion principle. Since no two electrons can occupy the same state, the electrons will occupy all the lowest energy levels up to the Fermi energy. Above the Fermi energy, there will only be a very small electron occupation. Many important properties of these systems, such as transport, are determined only by electrons near the Fermi surface.

This picture is greatly contrasted to a system of Bosons. At low temperatures the many-body ground state can condense such that there is a macroscopic occupation of particles in the same quantum state. The Bose condensed phase, like the Fermi surface, is crucially linked to the spin of the particle. Due to the spin-statistics theorem [54], half-integer spin wavefunctions must be antisymmetric when two particles are interchanged, whereas integer spin particles must have wavefunctions that are symmetric under the interchange of two particles.

In the previous discussion of effective spin-orbit coupling in cold atomic systems there were no underlying assumption made on the spin of the atoms in question.

Such a scheme could be implemented in either a Bosonic or a Fermionic species of atom. In this chapter we consider a many-body system of Bosons under the influence of an effective spin-orbit coupling cooled to below the condensation temperature, called the spin-orbit coupled Bose-Einstein condensate, or "SOBEC." We show that such a system can have a ground state that is a macroscopic superposition of the two degenerate ground states of the problem. We consider the isotropic limit where the double degeneracy becomes continuous, and find that a condensate is not stable. The Gross-Pitaevskii equations are derived for the anisotropic case, and the Bogoliubov spectrum is reproduced. Finally, we find an experimental signature of a SOBEC that can be measured through time of flight imaging. This work was done in collaboration with Tudor Stanescu and Victor Galitski, and was published in [6].

6.2 Spin-orbit interacting Hamiltonian and single-particle physics

We start with an effective spin-orbit coupled Hamiltonian analogous to the single particle Hamiltonian of an electron in a semiconductor quantum well. We will consider a system of the form

$$\hat{\mathcal{H}} = \frac{\mathbf{p}^2}{2m}\breve{1} - vp_x\breve{\sigma}_1 - v'p_y\breve{\sigma}_2, \tag{6.1}$$

where $\mathbf{p}$ is the momentum operator, $\sigma_{1,2}$ are the first two Pauli matricies in pseudo-spin-1/2 space, and v,v' are the spin-orbit coupling parameters. As discussed above, this Hamiltonian can reproduce any combination of Rashba or linear Dresselhaus spin-orbit interaction. Much of the physics that follows depends only on the form of the effective Hamiltonian, and not on the scheme used, such as the tripod or

4-level scheme. Where relevant, the following discussion will assume the tripod scheme unless otherwise noted, and the pseudo-spin-1/2 states will be the dark states defined in Eq. 3.35.

Now, we concentrate on the generic case characterized by anisotropic spin-orbit interactions and assume for concreteness that $v > v' > 0$. The special cases where $v = \pm v'$ and $v' = 0$ will be discussed later. The trap potential and the inter-particle interaction are initially disregarded and discussed in the following sections. The single-particle spectrum of Hamiltonian (6.1) is (see Fig. 6.1):

$$E_\lambda(\mathbf{p}) = \frac{\mathbf{p}^2}{2m} + \lambda\sqrt{v^2 p_x^2 + v'^2 p_y^2},$$ (6.2)

where $\lambda = \pm 1$ labels the bands. The corresponding eigenfunctions $\vec{\phi}_{\lambda \mathbf{p}}(\mathbf{r}) = e^{i\mathbf{p}\mathbf{r}}\vec{U}_\lambda(\chi_{\mathbf{p}})$
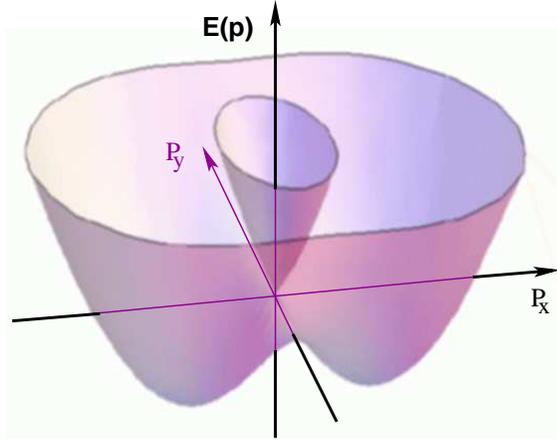
Figure 6.1 – Schematic picture of the band structure described by Eq. (6.2) with $v/v' = 2.5$ for a constant value of p_z. The inside sheet represents the $\lambda = +1$ band, while the outside sheet corresponds to $\lambda = -1$ and has a double-well structure with minima at $p_x = \pm mv$ and $p_y = 0$.

70

are spinors with components

$$U_\lambda(\chi_{\mathbf{p}}) = \frac{1}{\sqrt{2}} \begin{pmatrix} 1 \\ -i\lambda \frac{\cos(\chi_{\mathbf{p}}) + i\Delta \sin(\chi_{\mathbf{p}})}{\sqrt{\cos^2(\chi_{\mathbf{p}}) + \Delta^2 \sin^2(\chi_{\mathbf{p}})}} \end{pmatrix} \tag{6.3}$$

where $\chi_{\mathbf{p}}$ is the azimuthal angle in the (p_x, p_y)-plane and $\Delta = v'/v < 1$. The unitary matrix $U_{\alpha\lambda}(\chi_{\mathbf{p}})$ diagonalizes the Hamiltonian (6.1) (where $\alpha = \uparrow, \downarrow$ corresponds to the pseudo-spin index and $\lambda = \pm 1$ labels the eigenstates). It can be seen from Eq. (6.2) that the single particle spectrum contains two minima at $\lambda = -1$ with momenta $p_y = p_z = 0$ and $p_x = \pm mv \neq 0$ (see Fig. 6.1). The eigenfunctions for these two states are given by

$$\psi_{L/R} = \frac{1}{\sqrt{2}} \begin{pmatrix} 1 \\ \pm 1 \end{pmatrix} e^{\mp imvx} \tag{6.4}$$

where the top sign corresponds to the "left-movers", and the bottom sign corresponds to the "right-movers." The left and right moving states have non-zero canonical momentum, $\langle \mathbf{p} \rangle = \mp mv\mathbf{e}_x$. However, their kinetic momentum $\langle \mathbf{p} - \mathbf{A} \rangle = 0$ vanishes, so a pure left or right moving state will remain stationary as long as the laser fields are maintained, even in the absence of a trapping potential. This is also true for the more general ground state

$$\Psi_{\mathrm{dw}}(\mathbf{r}) = \sqrt{w_{\mathrm{L}}} \begin{pmatrix} 1 \\ -i \end{pmatrix} e^{-imvx + i\phi_{\mathrm{L}}} + \sqrt{w_{\mathrm{R}}} \begin{pmatrix} 1 \\ i \end{pmatrix} e^{imvx + i\phi_{\mathrm{R}}}, \tag{6.5}$$

consisting of a superposition of left and right movers. We have taken $w_{\mathrm{L}}, w_{\mathrm{R}} \geq 0$ and ϕ_{L} and ϕ_{R} as the respective weights and phases of the left and right moving states subjected to the constraint $w_{\mathrm{L}} + w_{\mathrm{R}} = 1$.

The exact degeneracy of the lowest energy states is not accidental, but is inherited from a time-reversal-like symmetry of the effective Hamiltonian. This can be seen by defining an anti-unitary "time-reversal" operator as $T = i\sigma_2 K$, where K is the complex conjugation operator [5]. We see that the action of T is to take $\mathbf{p} \to -\mathbf{p}$ and $\boldsymbol{\sigma} \to -\boldsymbol{\sigma}$. This is exactly analogous to time reversal for real spins in quantum mechanics. Applying the time-reversal operator to the Hamiltonian in Eq. 6.2 gives:

$$
\begin{aligned}
T\hat{\mathcal{H}}T^{-1} &= T\left(\frac{\mathbf{p}^2}{2m} + v p_x \sigma_1 + v' p_y \sigma_2\right)T^{-1} & (6.6)\\
&= \left(\frac{(T\mathbf{p}T^{-1})^2}{2m} + v(Tp_xT^{-1})(T\sigma_1 T^{-1}) + v'(Tp_yT^{-1})(T\sigma_2 T^{-1})\right) & (6.7)\\
&= \frac{(-\mathbf{p})^2}{2m} + v(-p_x)(-\sigma_1) + v'(-p_y)(-\sigma_2) & (6.8)\\
&= \frac{\mathbf{p}^2}{2pm} + v p_x \sigma_1 + v' p_y \sigma_2 & (6.9)\\
&= \hat{\mathcal{H}} & (6.10)
\end{aligned}
$$

where we have inserted $\hat{1} = TT^{-1}$ where relevant to transform the $\mathbf{p}$ and $\boldsymbol{\sigma}$ operators independently. The Hamiltonian thus has a time-reversal like symmetry, and we can apply Kramer's theorem [5] to show that there must be a pair of degenerate lowest energy eigenstates. These states are related by the time reversal operator, i.e. $\psi_\mathrm{L} = e^{i\phi}T\psi_\mathrm{r}$, up to an overall phase, ϕ.

It is worth noting that the time-reversal like symmetry depends on the absence of effective Zeeman-like fields of the form $H_Z = \mathbf{B}\cdot\boldsymbol{\sigma}$. The presence of such a term in the Hamiltonian will explicitly break time-reversal symmetry, and thus the two-fold degeneracy of the ground state is not guaranteed. In the case that $\mathbf{B} = B\hat{e}_1$ the

degeneracy is explicitly broken, but in the limit that $B_1 = 0$ an accidental symmetry can remain as long as $|B| \ll mv^2$.

Note that rotations in the manifold of the double-well ground-states are distinct from rotations in the pseudo-spin Hilbert space, as real-space and pseudo-spin coordinates are mixed up by the spin-orbit interaction. The two-fold degeneracy of the single-particle ground state is preserved if the system is placed in a harmonic trap. For a potential $V_{\text{trap}} = m\omega^2 \mathbf{r}^2/2$, we can write the Schödinger equation in momentum representation: the trap potential plays the role of "the kinetic energy" and the real kinetic term produces a double-well potential in momentum space, see Fig. 6.1. The tunnelling processes connect the degenerate vacua in momentum space [55]. However, they do not eliminate the double-degeneracy of the single-particle states, which is protected by the Kramers-like symmetry (see Section 6.4.2).

It is instructive to consider the limits of the effective spin-orbit Hamiltonian. We first consider the limit where $v' = 0$. In this limit we see that the spin-orbit field only couples to the matrix σ_1 corresponding to the persistent spin helix [56, 57] in semiconductors. This spin-orbit coupling can be removed via the unitary transformation $U = \exp[-imvx\sigma_1]$ to allow the Hamiltonian to be immediately diagonalized. If we assume a harmonic trapping potential the eigenstates takes the form $\psi_{n,\alpha}(\mathbf{r}) = e^{-imvx\sigma_1}\phi_n(\mathbf{r})\chi_\alpha$, where $\phi_n(\mathbf{r})$ is the n-th harmonic oscillator wavefunction and $\chi_\uparrow = (1,0)^\dagger$, $\chi_\downarrow = (0,1)^\dagger$ are the eigenspinors of the σ_3 operator. This spin-orbit coupling can thus be viewed as two uncoupled bands where the location of the momentum space energy minima are shifted in opposite directions in
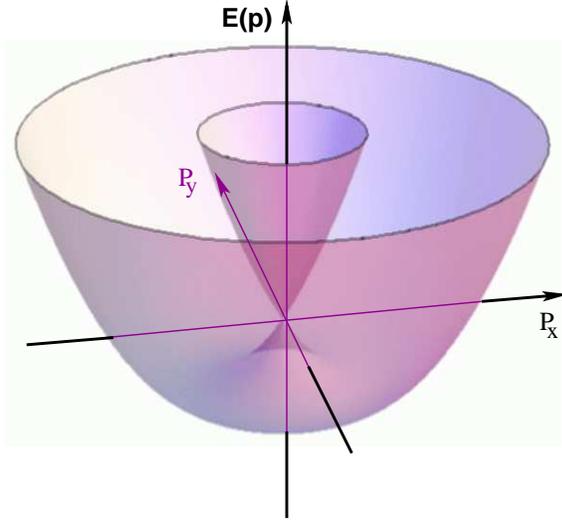
Figure 6.2 – Schematic picture of the band structure described by Eq. (6.2) for the isotropic Rashba-type case with $v = v'$ for $p_z = 0$. The inside sheet represents the $\lambda = +1$ band, while the outside sheet corresponds to $\lambda = -1$ and has minima on a one-dimensional circle $\sqrt{p_x^2 + p_y^2} = mv$.

momentum space. A weak Zeeman term of the form $H_Z = \Delta\sigma_3$ will not commute with the spin-orbit term, and will couple the bands. This situation is analogous to the spin-orbit coupling of Yu et. al. [27].

In the isotropic limit $\Delta = v'/v \to 1$, the transition temperature formally vanishes. Note that in the isotropic case $v = v'$ the spin-orbit term of the Hamiltonian (6.1) is equivalent to the Rashba model [29] and can be reduced to the latter via the rotation $\exp\left(i\pi\check{\sigma}_2/4\right)$ in the pseudo-spin space. In this case, the spectrum (6.2) has minima on a one-dimensional circle $\sqrt{p_x^2 + p_y^2} = mv$ (see Fig. 6.2). The single-particle ground-state is infinitely degenerate and the most general expression for the

corresponding wave-function is

$$\Psi_{\mathrm{ring}}(\mathbf{r}) = \int\limits_{0}^{2\pi} \frac{d\chi}{2\pi} \sqrt{w(\chi)} \, \vec{U}_{-}(\chi) e^{i\phi(\chi)} e^{[imv(x\cos\chi + y\sin\chi)]}, \qquad (6.11)$$

where $w(\chi) > 0$ is the angle-dependent weight of the Bose-condensate on a circle $[\int d\chi/(2\pi)w(\chi) = 1]$ and $\phi(\chi)$ is the angle-dependent phase. An especially interesting class of ground states corresponds to $w(\chi)$ not vanishing anywhere on the circle. In this case, the phase $\phi(\chi)$ must satisfy the constraint $\phi(\chi+2\pi) - \phi(\chi) = 2\pi n$, with $n \in \mathbb{Z} = \pi_1(S^1)$ being an integer winding number. Therefore, there may exist a number of topologically distinct ground states (characterized by the winding number), which can not be deformed into one another via any continuous transformation.

6.3 Bose-Einstein Condensation

At low temperatures, the many-body Bose system (6.1) is expected to condense into the single-particle states corresponding to the double-well minima. The transition temperature of this double-well spin-orbit coupled BEC, ("SOBEC"), can be calculated using standard text-book procedures [58]. Let us assume that near and below the transition the band with $\lambda = +1$ does not contribute and that we can expand the spectrum near the minima of the $\lambda = -1$ band (6.2). We define the momentum $\mathbf{q}$ in the vicinity of the left/right minima as follows: $\mathbf{p} = \pm mv\mathbf{e}_x + \mathbf{q}$, with $q \ll mv$. Eq. (6.2) leads to the anisotropic spectrum:

$$\delta E(\mathbf{q}) = \frac{q_x^2 + q_z^2}{2m} + \left[1 - \left(\frac{v'}{v}\right)^2\right] \frac{q_y^2}{2m}. \qquad (6.12)$$

The transition temperature is

$$T_{\rm c} = \frac{\pi}{2} \left[\frac{4}{\zeta(3/2)} \right]^{\frac{3}{2}} \left[1 - \left(\frac{v'}{v} \right)^2 \right]^{\frac{1}{3}} \frac{n^{\frac{2}{3}}}{m}.$$ (6.13)

We see that if $n^{1/3} \left[1 - (v'/v)^2 \right]^{1/6} \ll mv$, our approximation is justified and, in particular, the density of particles in the upper band $\lambda = +1$ is exponentially small.

In the isotropic limit we see that the condensation temperature formally vanishes. This is because energetically costly fluctuations only occur along the radial and out of plane axes in momentum space. This transition into the ring SOBEC is similar to a "weak-crystallization transition" discussed by Brazovsky [59] (see also, Refs. [60, 61, 62]). In this case, the phase volume of fluctuations is very large, which drives the (classical) transition first order. Even though the transition temperature into the ring SOBEC vanishes in the thermodynamic limit, in a finite trapped system, the energy scale for the crossover into this state will be non-zero.[63]

6.4   Effects of density-density interaction

We must now consider the effects of interactions on the spin-orbit coupled BEC. In the absence of interactions, the many-body ground state for a system of N particles will take the form $|N - n, n\rangle$, where $N - n, n$ is the fraction of particles in the left and right moving states respectively. This set of ground states are $N+1$-fold degenerate and the most general many-body ground state for a SOBEC will then take the form:

$$||\Psi_N\rangle = \sum_{n=0}^{N} \frac{c_n}{\sqrt{n!(N-n)!}} \left(\hat{B}_L^\dagger \right)^n \left(\hat{B}_R^\dagger \right)^{N-n} ||{\rm vac}\rangle,$$ (6.14)

where $\hat{B}_{L/R}^\dagger$ are the corresponding creation operators and c_n are arbitrary coefficients satisfying $\sum_n |c_n|^2 = 1$. We expect that interactions will break the macroscopic degeneracy of the many-body ground state and favor a single or small subset of the non-interacting ground states. The form of the interactions are important. If the interactions preserve time-reversal symmetry, the many-body ground state must still maintain a two-fold degeneracy due to the Kramer's like symmetry. On the other hand, if interactions break time reversal symmetry even this degeneracy can be lifted and the system is expected to pick a single ground state. In the following we consider the effect of density-density interactions. This may be in contrast to some experimentally relevant situations where the interactions will explicitly break Kramer's symmetry. [27]

Before we proceed we note that this system is distinct from the previous work done on a two-component Bose condensates [64, 65] where it was found that the ground state for such a system is ferromagnetic with a fully polarized pseudo-spin. The arguments for such a ground state depend on the ability to factorize the spin and orbital degrees of freedom. This is not true for the spin-orbit coupled system where spin and momentum are fully coupled. However, we note that this is possible in the persistent spin helix [56] limit, so in such a limit the systems should coincide.

To find the many-body ground state for a spin-orbit BEC we now add the density-density interaction Hamiltonian $\hat{\mathcal{H}}_{\text{int}} = \frac{1}{2} \int d^3\mathbf{r} d^3\mathbf{r}' \hat{n}(\mathbf{r}) V_{\text{int}}(\mathbf{r}-\mathbf{r}') \hat{n}(\mathbf{r}')$, where $\hat{n}(\mathbf{r}) = \sum_\mu \hat{\psi}_\mu^\dagger(\mathbf{r}) \hat{\psi}_\mu(\mathbf{r})$ and $\hat{\psi}_\mu(\mathbf{r})$ is the field operator, which is initially defined in terms of the creation/annihilation operators for the original hyperfine states. The effective interaction in pseudo-spin space can be obtained by first applying the po-

sition dependent rotation matrix $R_{\mu\alpha}(\mathbf{r})$ and then dropping terms connected to the bright states. The effective interaction then takes the standard form:

$$\hat{\mathcal{H}}_{\text{int}} = \frac{1}{2V} \sum_{\mathbf{p},\mathbf{p}',\mathbf{q}} V_{\text{int}}(\mathbf{q}) \hat{b}^{\dagger}_{\alpha\mathbf{p}} \hat{b}_{\alpha\mathbf{p}+\mathbf{q}} \hat{b}^{\dagger}_{\beta\mathbf{p}'} \hat{b}_{\beta\mathbf{p}'-\mathbf{q}}, \tag{6.15}$$

where $\hat{b}^{\dagger}_{\alpha\mathbf{p}}$ is the creation operator for a state with momentum $\mathbf{p}$ and pseudo-spin α in the dressed state subspace.

In the limit of weak interactions, $V_{\text{int}} \ll mv^2/2$, we expect the low temperature physics to be dominated by the $\lambda = -1$ low energy band in Eq. 6.2. A second, momentum-dependent rotation is then required to rotate to the eigenstates of the effective spin-orbit coupled Hamiltonian. We perform this rotation defined by $\hat{B}_{\lambda\mathbf{p}} = U^{\dagger}_{\lambda\alpha}(\mathbf{p})\hat{b}_{\alpha\mathbf{p}}$ and $\hat{B}^{\dagger}_{\lambda\mathbf{p}} = \hat{b}^{\dagger}_{\alpha\mathbf{p}}U_{\alpha\lambda}(\mathbf{p})$, where $U_{\alpha\lambda}(\mathbf{p}) = U_{\alpha\lambda}(\chi_{\mathbf{p}})$ is defined in Eq. 6.3 and there is an implicit sum over the pseudo-spin α. The low-energy physics can then be captured by projecting out the $\lambda = +1$ band and considering operators with momenta near the momentum space double wells. Thus, it is convenient to express the Hamiltonian in terms of left/right-moving operators, defined as $\hat{B}_{L/R\ \mathbf{q}} = \hat{B}_{-1\ \mp(\mathbf{q}+m\mathbf{v})}$ and the corresponding unitary matricies $U_{L/R\ \alpha}(\mathbf{q}) = U_{-1\ \alpha}(\mp(\mathbf{q} + m\mathbf{v}))$. This leads to the following interaction Hamiltonian

$$\hat{\mathcal{H}}_{\text{int}} = \frac{1}{2V} \sum_{\mathbf{p},\mathbf{p}',\mathbf{q}} \sideset{}{'}\sum_{\{\sigma_i\}} V_{\text{int}}(\mathbf{q}_{\sigma}) \hat{B}^{\dagger}_{\sigma_1\mathbf{p}} \hat{B}_{\sigma_2\mathbf{p}+\mathbf{q}} \hat{B}^{\dagger}_{\sigma_3\mathbf{p}'} \hat{B}_{\sigma_4\mathbf{p}'-\mathbf{q}}$$
$$\times U^{\dagger}_{\sigma_1\alpha}(\mathbf{p}) U_{\alpha\sigma_2}(\mathbf{p}+\mathbf{q}) U^{\dagger}_{\sigma_3\alpha'}(\mathbf{p}') U_{\alpha'\sigma_4}(\mathbf{p}'-\mathbf{q}). \tag{6.16}$$

where the prime sign in the sum over the left and right indices $\sigma_i = \text{L/R} = \mp$ is restricted by the condition $\sigma_1 + \sigma_3 = \sigma_2 + \sigma_4$, i.e., the numbers of left- and right-movers are conserved, and $\mathbf{q}_{\sigma} = \mathbf{q} - (\sigma_1 - \sigma_2)mv\mathbf{e}_x$. We stress that equation (6.16)

is valid in the limit of weak interactions (relative to the spin-orbit coupling) and low temperatures, when only single particle states with momenta in the vicinity of the two minima are occupied.

6.4.1 Generalized Bogoliubov transformation

Next, we introduce the projection operators $\hat{\mathcal{P}}_{N,n} = \hat{\mathcal{P}}_{N,n}^2$ that select the subspace characterized by n left-moving and $(N-n)$ right-moving quasiparticles. The Hamiltonian can be expressed as $\hat{\mathcal{H}} = \sum_{n=0}^{N} \hat{\mathcal{P}}_{N,n} \hat{\mathcal{H}} \hat{\mathcal{P}}_{N,n} = \sum_{n=0}^{N} \hat{\mathcal{H}}_n$. An important observation is that the Hamiltonian containing the interaction term (6.16) preserves the number of left- and right-movers and thus we can consider different "sectors," $\hat{\mathcal{H}}_n$, independently. Our goal is to diagonalize each term $\hat{\mathcal{H}}_n$ using a mean-field scheme and reduce the many-body Hamiltonian to the form

$$\hat{\mathcal{H}} = \sum_{n=0}^{N} \hat{\mathcal{P}}_{N,n} \left[\mathcal{E}_0(n) + \sum_{\mathbf{q},\sigma} \Omega_\sigma(n, \mathbf{q}) \hat{\beta}_{n,\sigma,\mathbf{q}}^\dagger \hat{\beta}_{n,\sigma,\mathbf{q}} \right] \hat{\mathcal{P}}_{N,n}, \tag{6.17}$$

where $\mathcal{E}_0(n)$ is the contribution of the $(n, N-n)$ sector to the condensate energy, while $\Omega_\sigma(n, \mathbf{q})$ represents the spectrum of quasi-particle excitations. To obtain the mean-field result, we use a Bogoliubov-type approximation in which the operators corresponding to $\mathbf{q} = \mathbf{0}$ are replaced within each sector $(n, N-n)$ by c-numbers, $\hat{B}_{L\,0} \to \sqrt{n_0}\, e^{i\phi/2}$ and $\hat{B}_{R\,0} \to \sqrt{N_0 - n_0}\, e^{-i\phi/2}$. Next, we notice that at low temperatures, the momenta of uncondensed bosons are $q \ll mv$. Thus, we can expand the products of U-vectors in (6.16) in terms of the deviations $\mathbf{q}$ from the

minima of the energy bands

$$
\begin{aligned}
\vec{U}_{\mathrm{L}}^{\dagger}(\mathbf{q}_1)\vec{U}_{\mathrm{L}}(\mathbf{q}_2) &= \vec{U}_{\mathrm{R}}^{\dagger}(\mathbf{q}_1)\vec{U}_{\mathrm{R}}(\mathbf{q}_2) \approx 1 - \frac{\Delta^2}{8}\frac{(q_{1y}-q_{2y})^2}{(mv)^2}, \\
\vec{U}_{\mathrm{R}}^{\dagger}(\mathbf{q}_1)\vec{U}_{\mathrm{L}}(\mathbf{q}_2) &= \vec{U}_{\mathrm{L}}^{\dagger}(\mathbf{q}_1)\vec{U}_{\mathrm{R}}(\mathbf{q}_2) \approx \frac{\Delta}{2}\frac{q_{1y}+q_{2y}}{mv},
\end{aligned}
\tag{6.18}
$$

with $\Delta = v'/v < 1$ and corrections of order $\mathcal{O}(q_{1,2}^3)$ and $\mathcal{O}(q_{1,2}^2)$, respectively. Consequently, contributions to the mean-field Hamiltonian can be expanded in the small parameter $x_{\mathbf{q}} = \Delta^2 q_y^2/(mv)^2$. In the zero-order approximation, i.e., neglecting contributions of order $x_{\mathbf{q}}$ and higher, the mean-field Hamiltonian for the $(n, N-n)$ sector is

$$
\begin{aligned}
\hat{\mathcal{H}}_n^{(0)} &= \frac{N}{2V}\sum_{\mathbf{q}} V_{\mathrm{int}}(\mathbf{q})\left[\hat{\vec{B}}_{\mathbf{q}}^{\dagger}\begin{pmatrix} s(\mathbf{q})+1+\delta & \sqrt{1-\delta^2}e^{-i\phi} \\ \sqrt{1-\delta^2}e^{i\phi} & s(\mathbf{q})+1-\delta \end{pmatrix}\hat{\vec{B}}_{\mathbf{q}} \right. \\
&\quad \left. + \hat{\vec{B}}_{\mathbf{q}}^{\mathrm{T}}\begin{pmatrix} (1+\delta)e^{i\phi} & \sqrt{1-\delta^2} \\ \sqrt{1-\delta^2} & (1-\delta)e^{-i\phi} \end{pmatrix}\hat{\vec{B}}_{-\mathbf{q}} + \mathrm{h.c.}\right],
\end{aligned}
\tag{6.19}
$$

where $\delta = 2n/N - 1$, $\hat{\vec{B}}_{\mathbf{q}}^{T} = \left(\hat{B}_{L\mathbf{q}}, \hat{B}_{R\mathbf{q}}\right)$ is the annihilation operator in a spinor notation, $s(\mathbf{q}) = 2\delta E(\mathbf{q})/\left[n_0 V_{\mathrm{int}}(\mathbf{q})\right]$, and $\delta E(\mathbf{q})$ is the anisotropic spectrum (6.12) near the minima. We now introduce new bosonic operators $\hat{B}_{-,\mathbf{q}} = \sqrt{1-n/N}\hat{B}_{L,\mathbf{q}}e^{-i\phi/2} - \sqrt{n/N}\hat{B}_{R,\mathbf{q}}e^{i\phi/2}$ and $\hat{B}_{+,\mathbf{q}} = \sqrt{n/N}\hat{B}_{L,\mathbf{q}}e^{-i\phi/2} + \sqrt{1-n/N}\hat{B}_{R,\mathbf{q}}e^{i\phi/2}$. The Hamiltonian becomes diagonal for the $\hat{B}_{-}$-particles, which have the "free" spectrum $\delta E(\mathbf{q})$, and has the standard Bogoliubov form [58] for the $\hat{B}_{+}$-particles. Introducing the new operators $\hat{\beta}_{-,\mathbf{q}} \equiv \hat{B}_{-,\mathbf{q}}$ and $\hat{\beta}_{+,\mathbf{q}} \equiv (1-A_{\mathbf{q}}^2)^{-1/2}\left(\hat{B}_{+,\mathbf{q}} + A_{\mathbf{q}}\hat{B}_{+,-\mathbf{q}}^{\dagger}\right)$, with $A_{\mathbf{q}} = -s(\mathbf{q}) - 1 + \sqrt{[s(\mathbf{q})+1]^2 - 1}$, we get

$$
\hat{\mathcal{H}}_n^{(0)} = \mathcal{E}_0^{(0)} + \sum_{\mathbf{q}}\left\{\Omega_-(\mathbf{q})\hat{\beta}_{-,\mathbf{q}}^{\dagger}\hat{\beta}_{-,\mathbf{q}} + \Omega_+(\mathbf{q})\hat{\beta}_{+,\mathbf{q}}^{\dagger}\hat{\beta}_{+,\mathbf{q}}\right\},
\tag{6.20}
$$

where $\mathcal{E}_0^{(0)}$ is the condensate energy [58] in the zero-order approximation, $\Omega_-(\mathbf{q}) = \left\{ q_x^2 + q_z^2 + q_y^2 \left[1 - (v'/v)^2 \right] \right\} / (2m)$ is the anisotropic free particle quadratic spectrum and $\Omega_+(\mathbf{q}) = \sqrt{\left[\Omega_-(\mathbf{q}) + nV_{\text{int}}(\mathbf{q}) \right]^2 - n^2 V_{\text{int}}^2(\mathbf{q})}$ is an anisotropic sound similar to the conventional Bogoliubov phonon mode in a BEC. At this level of approximation the condensate energy is n-independent (i.e., it is the same for any particular sector characterized by n left movers and $(N - n)$ right movers) and, consequently, the degeneracy of the non-interacting ground state (6.14) is preserved. In the first order approximation, the mean-field Hamiltonian (6.19) acquires sector-dependent corrections of order $x_\mathbf{q} \ll 1$. Following the above recipe, we introduce a set of new operators $\hat{B}_{\pm,\mathbf{q}}$ that diagonalize the $\hat{B}_\mathbf{q}^\dagger \hat{B}_\mathbf{q}$ term in the Hamiltonian (6.19) but not the other terms. Next, we diagonalize the full Hamiltonian [up to terms of order $\mathcal{O}(x_\mathbf{q}^2)$] via a generalized Bogoliubov-type transformation

$$\hat{\beta}_{-,\,\mathbf{q}} = \hat{B}_{-,\mathbf{q}} + x_\mathbf{q} D_\mathbf{q} \hat{B}_{-,-\mathbf{q}}^\dagger \tag{6.21}$$

$$+ x_\mathbf{q} F_{1\mathbf{q}} \hat{B}_{+,\mathbf{q}} + x_\mathbf{q} F_{2\mathbf{q}} \hat{B}_{+,-\mathbf{q}}^\dagger$$

$$\hat{\beta}_{+,\,\mathbf{q}} = (1 - A_\mathbf{q}^2)^{-1/2} \left(\hat{B}_{+,\mathbf{q}} + A_\mathbf{q} \hat{B}_{+,-\mathbf{q}}^\dagger \right. \tag{6.22}$$

$$\left. + x_\mathbf{q} C_{1\mathbf{q}} \hat{B}_{-,\mathbf{q}} + x_\mathbf{q} C_{2\mathbf{q}} \hat{B}_{-,-\mathbf{q}}^\dagger \right).$$

In the equations (6.21) and (6.22) we already anticipated that some of the terms are corrections of order $x_\mathbf{q}$. The coefficients are determined by requiring that the β-operators obey standard commutation relations [to order $\mathcal{O}(x_\mathbf{q})$] and that the off-diagonal contributions to the Hamiltonian vanish. Assuming for simplicity that we have a point-like interaction, i.e., $V_{\text{int}}(\mathbf{q}) = V_{\text{int}}$ is momentum-independent for

momenta in a range that is relevant for the problem, the groundstate energy in the $(n, N - n)$ sector is

$$
\begin{aligned}
\mathcal{E}_0(n) \;=\;& \frac{V_{\text{int}} N^2}{2V} + \frac{V_{\text{int}} N}{2V} \sum_{\mathbf{q} \neq 0} \frac{1}{1 - A_{\mathbf{q}}^2} \left\{ [2 + s(\mathbf{q})] A_{\mathbf{q}}^2 + 2A_{\mathbf{q}} \right. \\
& \left. - \frac{x_{\mathbf{q}}}{8} \left[A_{\mathbf{q}}^2 (\cos(4\xi) + 3) - A_{\mathbf{q}}(\cos(4\xi) - 5) \right] \right\} + \mathcal{O}(x_{\mathbf{q}}^2),
\end{aligned}
\tag{6.23}
$$

where $\cos^2(\xi) = n/N$. The relevant coefficient of the generalized Bogoliubov transformation (6.21-6.22) has the form

$$
\begin{aligned}
A_{\mathbf{q}} \;=\;& -1 - \frac{s}{2} + \frac{1}{2}\sqrt{s(4+s)} - \frac{x_{\mathbf{q}}}{32\sqrt{s(4+s)}} \left(2 + s\sqrt{s(4+s)} \right) \\
& \times [-4 - 5s + (4 + s)\cos(4\xi)] + \mathcal{O}(x_{\mathbf{q}}^2).
\end{aligned}
\tag{6.24}
$$

Explicitly evaluating (6.23) with $A_{\mathbf{q}}$ given by Eq. (6.24) shows that, at this level of approximation, the energy of the condensate becomes sector-dependent, $\mathcal{E}_0(n) \approx \mathcal{E}_0^{(0)} + \mathcal{E}_0^{(1)}(n)$, and is minimal for $n = 0$ and $n = N$. Thus, the density-density interaction reduces the large $(N + 1)$-fold degeneracy of the ground state to a two-fold degeneracy. Consequently, in the limit of vanishing interactions $V_{\text{int}} \to +0$, the most general expression for the many-body wave-function is

$$
||\Psi_N\rangle = \frac{1}{\sqrt{N!}} \left[\sqrt{w_{\text{L}}} e^{i\phi_{\text{L}}} \left(\hat{B}_{\text{L}}^\dagger \right)^N + \sqrt{w_{\text{R}}} e^{i\phi_{\text{R}}} \left(\hat{B}_{\text{R}}^\dagger \right)^N \right] ||\text{vac}\rangle,
\tag{6.25}
$$

where $w_{\text{L/R}}$ represents the fraction of the left/right movers and $\phi_{\text{L/R}}$ are arbitrary phases. Notice that Eq. (6.25) describes a fragmented or entangled BEC, unless $w_{\text{L}} w_{\text{R}} = 0$. i.e., the many-body state (6.25) does not correspond to the condensation into one single-particle state.

We reiterate that the left- and right-movers in the condensate have non-zero momentum, but zero velocity and do not actually move while the laser fields responsible for the spin-orbit coupling are present. We also note that equation (6.25) describes a so-called N00N state,[66, 67] which is quantum correlated state with properties that can be exploited in applications such as quantum sensing and quantum metrology. This suggests that the possibility of using spin-orbit coupled condensates as qubits deserves to be further investigated.

We conclude the section by motivating the macroscopic entanglement of (6.25). Considering the $v' \to 0$ limit in a harmonic trap, for which the left and right moving states can be exactly expressed by $\psi_\sigma = e^{-i\sigma m v x} \phi_0(\mathbf{r}) \begin{pmatrix} 1 \\ -i\sigma \end{pmatrix}$, where $\phi_0(\mathbf{r})$ is the ground state of the harmonic oscillator. Such a state has minimum uncertainty, $\Delta p \Delta x = \hbar/2$. The presence of repulsive interactions will act to increase Δx, which by the uncertainty relation will act to localize the uncertainty of the state in momentum space, assuming the overall uncertainty is unperturbed. Therefore, position space repulsive interactions can be pictured as momentum space attractive interactions. The existence of a macroscopically entangled state was independently predicted in a similar system in [68], but in the limit of strong interactions. It is therefore plausible that a macroscopically entangled state can exist for all interaction strengths, as long as the interactions are of the density-density form.

In practice, the time-reversal-like symmetry of a system with synthetic spin-orbit coupling will be broken by perturbations due to imperfections in the laser fields and spin-dependent interaction terms. Due to the completeness of the pseudo-spin-

1/2 degree of freedom, any perturbation of the optical or magnetic fields will add a new term to the single particle Hamiltonian

$$H' = h_0 + \mathbf{h} \cdot \boldsymbol{\sigma} \tag{6.26}$$

where h_0 is a perturbation proportional to the identity matrix, and the perturbation $\mathbf{h}$ is a pseudo-spin dependent magnetic field. It can be seen that the components of h_0, h_y and h_z will preserve the degeneracy of the ground state, but h_x will produce an energy splitting between the ground states of $\delta E \sim \langle h_x \sigma_x \rangle$. Furthermore, a perturbation of h_y and h_z will produce off-diagonal couplings between the left and right moving ground states. The off diagonal components will not destroy the N00N state. However, even a small energy splitting will produce a relative energy shift between the two degenerate ground states of $\Delta E = N \delta E$, which can be large for a macroscopic number of particles, even if the original perturbation is small. Thus, even small time-reversal symmetry breaking perturbations can lead to a large energy splitting, and a preference of one ground state over the other. Additionally, the energy scale ΔE will give the time scale for the damping of the condensate. This indicates that symmetry breaking perturbations will lead to small lifetimes of N00N states.

6.4.2 Gross-Pitaevskii equations

In this section we derive the Gross-Pitaevskii equations for a spin-orbit coupled BEC. Let us consider the density-density interaction potential as a contact pseudo-potential, $V_{\text{int}}(\mathbf{r} - \mathbf{r}') = V_{\text{int}} \delta(\mathbf{r} - \mathbf{r}')$, where $V_{\text{int}} = \frac{4\pi\hbar^2}{m} a$ and a is the inter-atomic

scattering length. The full many body Hamiltonian can be written as

$$\hat{\mathcal{H}} = \sum_{\mu,\nu} \int d^3r \ \hat{\psi}_\mu^\dagger(\mathbf{r}) h_{\mu\nu} \hat{\psi}_\nu(\mathbf{r}) \tag{6.27}$$
$$+ \frac{V_{\text{int}}}{2} \sum_{\mu,\nu} \int d^3r \ \hat{\psi}_\mu^\dagger(\mathbf{r}) \hat{\psi}_\nu^\dagger(\mathbf{r}) \hat{\psi}_\nu(\mathbf{r}) \hat{\psi}_\mu(\mathbf{r}),$$

in terms of field operators $\hat{\psi}_\mu(\mathbf{r})$ for the original hyperfine states, $\mu \in \{0,1,2,3\}$. In Eq. (6.27) we used the notation $h_{\mu\nu} = \left(\frac{\mathbf{p}^2}{2m} + V_{\text{trap}} + H_{a-l} \right)_{\mu\nu}$ for the single particle Hamiltonian in the presence of a trap potential V_{trap}, in addition to the spatially varying laser fields that interact with the atom, H_{a-l}. In the adiabatic approximation, after projecting onto the dressed state subspace, the first term in Eq. (6.27) becomes $\sum_{\mathbf{p};\alpha,\beta} \hat{b}_{\alpha\mathbf{p}}^\dagger \left[(\mathbf{p}^2/2m + V_{\text{trap}}) \ \check{1} - vp_x\check{\sigma}_2 - v'p_y\check{\sigma}_3 \right]_{\alpha\beta} \hat{b}_{\beta\mathbf{p}}$, where $\hat{b}_{\alpha\mathbf{p}}^\dagger$ and $\hat{b}_{\alpha\mathbf{p}}$ are the creation and annihilation operators for bosons with pseudo-spin $\alpha = \uparrow, \downarrow$. The interaction term is given by equation (6.15). Before writing down the Gross-Pitaevskii equations, let us summarize the three different representations used for describing the system of bosons interacting with the spatially modulated laser fields.

i) *Hyperfine states representation*: This is the most straightforward way to describe the motion of the bosons and their interaction with the trap potential (V_{trap}) and the laser fields (H_{a-l}), as well as the density-density interaction (second term in Eq. (6.27)). The field operator that creates a particle in the hyperfine state $\mu \in \{0,1,2,3\}$ at point $\mathbf{r}$ is $\hat{\psi}_\mu^\dagger(\mathbf{r})$, while the creation of a free-moving particle with momentum $\mathbf{p}$ is described by $\hat{c}_{\mu\mathbf{p}}^\dagger = \int d^3r \ e^{i\mathbf{p}\mathbf{r}} \hat{\psi}_\mu^\dagger(\mathbf{r})$. By performing the position-dependent rotation $R_{\mu\alpha}$ which diagonalizes the atom-laser Hamiltonian *and* projecting onto the dressed state subspace we switch to the pseudo-spin representa-

tion.

ii) *Pseudo-spin representation (dressed state representation)*: This is the natural framework for describing the low-energy physics of the atomic system interacting with the laser field. The creation operator for free-moving particles with spin $\alpha \in \{\uparrow, \downarrow\}$ and momentum $\mathbf{p}$ is $\hat{b}_{\alpha\mathbf{p}}^{\dagger}$. We can define the corresponding field operator as $\hat{\tilde{\psi}}_{\alpha}^{\dagger}(\mathbf{r}) = \sum_{\mathbf{p}} e^{-i\mathbf{p}\mathbf{r}} \hat{b}_{\alpha\mathbf{p}}^{\dagger}$. Note that the field operators in the hyperfine and pseudo-spin representations are related via the position-dependent rotation, $\hat{\psi}_{\mu}^{\dagger}(\mathbf{r}) = \sum_{\alpha} R_{\mu\alpha}(\mathbf{r}) \hat{\tilde{\psi}}_{\alpha}^{\dagger}(\mathbf{r})$. Diagonalizing the single-particle spin-orbit coupled Hamiltonian, $H = (\mathbf{p}^2/2m + V_{\text{trap}})\check{1} - vp_x\check{\sigma}_2 - v'p_y\check{\sigma}_3$, generates a set of eigenstates described by the spinor eigenfunctions $\vec{\phi}_{\sigma n}(\mathbf{r})$. The quantum number $\sigma = \pm$ can be viewed as labeling right (left) moving states.

iii) *Right/left moving states representation*: This is the representation corresponding to the eigenstates of the spin-orbit coupled single particle Hamiltonian. In Section 6.1 we have shown that in the absence of a trap potential the single particle spectrum for the generic case $v \neq v'$ is characterized by two minima at non-zero momenta. This double-degeneracy is protected by a Kramers-like symmetry which is not broken by the trapping potential $V_{trap}(\mathbf{r})$.

In the derivation below we find it convenient to use the following parametrization for the eigenfunctions:

$$\vec{\phi}_{\sigma n}(\mathbf{r}) = e^{i\sigma mvx} \begin{pmatrix} u_{\sigma n}^{\uparrow}(\mathbf{r}) \\ i\sigma u_{\sigma n}^{\downarrow}(\mathbf{r}) \end{pmatrix}, \tag{6.28}$$

where $\sigma = \pm$ and n is a set of quantum numbers. The Kramers-like symmetry

implies that

$$
u^\uparrow_{-\sigma n}(\mathbf{r}) = \left[u^\downarrow_{\sigma n}(\mathbf{r}) \right]^*,
$$

$$
u^\downarrow_{-\sigma n}(\mathbf{r}) = \left[u^\uparrow_{\sigma n}(\mathbf{r}) \right]^*, \tag{6.29}
$$

and the corresponding energies are degenerate, $E_{-\sigma n} = E_{\sigma n} = E_n$. Because $\langle \phi_{-\sigma n} | \phi_{\sigma n} \rangle = 0$, the two states are linearly independent. The creation operator for a left/right moving particle described by the eigenstate $\vec{\phi}_{\sigma n}$ is $\hat{B}^\dagger_{\sigma n}$. The field operators in the pseudo-spin representation can be expressed in terms of $\hat{B}_{\sigma n}$ operators as

$$
\hat{\tilde{\psi}}_\uparrow(\mathbf{r}) = \sum_n \left[e^{imvx} u^\uparrow_{+n}(\mathbf{r}) \hat{B}_{+n} + e^{-imvx} u^\uparrow_{-n}(\mathbf{r}) \hat{B}_{-n} \right],
$$

$$
\hat{\tilde{\psi}}_\downarrow(\mathbf{r}) = \sum_n \left[i e^{imvx} u^\downarrow_{+n}(\mathbf{r}) \hat{B}_{+n} - i e^{-imvx} u^\downarrow_{-n}(\mathbf{r}) \hat{B}_{-n} \right], \tag{6.30}
$$

where the terms with $\sigma = +$ and $\sigma = -$ correspond to the right and left moving modes, respectively. Finally, note that in the translation invariant case, $V_{\mathrm{trap}} = 0$, we introduced the eigenfunctions $\vec{\phi}_{\lambda \mathbf{p}}(\mathbf{r}) = e^{i\mathbf{p}\mathbf{r}} \vec{U}_\lambda(\chi_{\mathbf{p}})$, with $U_{\alpha\lambda}(\chi_{\mathbf{p}})$ given by equation (6.3), and the corresponding creation operators, $\hat{B}_{\lambda \mathbf{p}}$. We then defined the left/right movers for the low energy band $\lambda = -1$ and small momenta $q < mv$ as $\hat{B}_{L/R\ \mathbf{q}} = \hat{B}_{(-1)\ \mp(\mathbf{q}+m\mathbf{v})}$. Alternatively, we can directly define the eigenfunctions $\vec{\phi}_{\sigma \mathbf{q}}(\mathbf{r})$ in the left/right moving representation using the parametrization (6.28), with no restriction for $\mathbf{q}$. The correspondence between the two representations is given by: $\mathbf{p} = \sigma(\mathbf{q} + m\mathbf{v})$ and $\lambda = -\mathrm{sign}(q_x + mv)$. This generalizes our definition of the left/right moving modes to arbitrary energy. Notice however, that a left (right) "moving" state from the high energy band $\lambda = +1$ has in fact a positive (negative) momentum.

To write the Gross-Pitaevskii equation in the pseudo-spin representation we

use the standard procedure and calculate the commutator $[\hat{\tilde{\psi}}_\alpha(\mathbf{r}), \hat{\mathcal{H}}]$, where $\hat{\mathcal{H}}$ is the many-body Hamiltonian expressed in terms of pseudo-spin field operators. Using Eq. (6.27) and the relations between representations summarized above we obtain

$$i\frac{\partial}{\partial t}\widetilde{\psi}_\alpha(\mathbf{r}, t) = \sum_\beta \left\{ \left[\frac{-\nabla^2}{2m} + V_{\text{trap}}(\mathbf{r})\right]\check{1} + iv\frac{\partial}{\partial x}\check{\sigma}_2 \right. \tag{6.31}$$
$$\left. + iv'\frac{\partial}{\partial y}\check{\sigma}_3 \right\}_{\alpha\beta} \widetilde{\psi}_\beta(\mathbf{r}, t) + V_{\text{int}}\left(|\widetilde{\psi}_\uparrow|^2 + |\widetilde{\psi}_\downarrow|^2\right)\widetilde{\psi}_\alpha(\mathbf{r}, t).$$

Relation (6.31), which is a system of two coupled non-linear differential equations, represents the time-dependent Gross-Pitaevskii equation for a spin-orbit coupled Bose-Einstein condensate wave-function. Similar equations can be written in the left/right moving states representation. For simplicity, we will address here only the translation invariant case $V_{\text{trap}} = 0$. The field operator for the left/right moving modes can be written in terms of the corresponding $\hat{B}_{\sigma\mathbf{q}}$ operators as

$$\hat{\Phi}_\sigma(\mathbf{r}) = \sum_{\alpha, \mathbf{q}} \phi_{\sigma\mathbf{q}}^\alpha(\mathbf{r})\hat{B}_{\sigma\mathbf{q}}. \tag{6.32}$$

The non-interacting part of the Hamiltonian is diagonal in terms of left/right moving operators, with eigenvalues that depend on the momentum $\mathbf{q}$ only. At low-energies, these eigenvalues are given by the anisotropic spectrum $\delta E(\mathbf{q}) = (q_x^2 + q_z^2)/(2m) + q_y^2/(2m_y)$ with $m_y = m\left[1 - (v'/v)^2\right]^{-1}$. In general, the interacting Hamiltonian is given by equation (6.16), but in the low-energy limit we neglect all corrections of order $x_\mathbf{q} = \Delta^2 q_y^2/(mv)^2$ and higher coming from the momentum-dependent matrices

$U_{\alpha\sigma}(\mathbf{q})$. In this limit we obtain

$$i\frac{\partial}{\partial t}\Phi_\sigma(\mathbf{r}, t) = \left(\frac{(-i\partial_x - \sigma mv)^2}{2m} - \frac{\partial_y^2}{2m_y} - \frac{\partial_z^2}{2m}\right)\Phi_\sigma(\mathbf{r}, t)$$
$$+V_{\text{int}}\left(|\Phi_L|^2 + |\Phi_R|^2\right)\Phi_\sigma(\mathbf{r}, t), \qquad (6.33)$$

where $\partial_j = \partial/\partial x_j$, $j \in \{x, y, z\}$. The time-independent Gross-Pitaevskii equations can be obtained by looking for a stationary solution of the form $\Phi_\sigma(\mathbf{r}, t) = \Phi_{0\sigma}(\mathbf{r})e^{-i\mu t}$, where μ is the chemical potential which determined by the condition $N = \int d^3r\,(|\Phi_L|^2 + |\Phi_R|^2)$, with N being the total number of bosons. We note that by linearizing $\Phi_\sigma(\mathbf{r}, t)$ with respect to the deviations from the stationary solution we obtain an excitation spectrum consisting in two modes, $\Omega_\pm(\mathbf{q})$, identical with those found using the generalized Bogoliubov treatment.

6.5 Experimental signature of spin-orbit coupled BEC: measuring a SOBEC qubit

A straightforward way to detect experimentally the new type of BEC would be to probe the momentum distribution of the density of the particles via time-of-flight expansion. After removing the trap *and* the laser fields, the boson gas represents a system of free particles, each characterized by a certain momentum and a hyperfine state index. In a TOF experiment one determines the momentum distribution by measuring the particle density at various times after the release of the boson cloud. The operator associated with a density measurement is $\hat{\rho}(\mathbf{r}) = \sum_\mu \hat{\psi}_\mu^\dagger(\mathbf{r})\hat{\psi}_\mu(\mathbf{r})$, where $\hat{\psi}_\mu^\dagger(\mathbf{r})$ is the creation operator for a particle in the hyperfine state μ positioned at point $\mathbf{r}$. Determining the density profile involves a simultaneous measurement of

$\hat{\rho}(\mathbf{r})$ for all the values of $\mathbf{r} \in \mathcal{V}$ corresponding to a ceratin region in space where the boson cloud is located. To insure formal simplicity, we consider a coarse-grained space, i.e., we treat $\mathbf{r}$ as a discrete variable. This is simply a technical trick and does not influence the final result. Our goal is to find the most likely spatial distributions of the particles at a given moment t after the release of the atoms. In the limit of large particle numbers, the actual measured density profiles will involve only small fluctuations away from these "most likely" distributions.

For a system of N bosons, the result of the measurement is a set of eigenvalues $\{\sum_\mu n_{\mathbf{r}\mu}\}_{(\mathbf{r}\in\mathcal{V})}$ that label an eigenvector of the density operator

$$||\Phi_{\{n_{\mathbf{r}\mu}\}}\rangle = \prod_{\mu,\mathbf{r}\in\mathcal{V}} \frac{1}{\sqrt{(n_{\mathbf{r}\mu})!}} \left[\hat{\psi}_\mu^\dagger(\mathbf{r})\right]^{n_{\mathbf{r}\mu}} ||\text{vac}\rangle, \tag{6.34}$$

where the occupation numbers satisfy the constraint $\sum_{\mu,\mathbf{r}} n_{\mathbf{r}\mu} = N$, and the factors $1/\sqrt{(n_{\mathbf{r}\mu})!}$ insure the normalization to unity. Note that $n_{\mathbf{r}\mu}$ is an integer representing the number of particles located in a certain "cell" $\mathbf{r}$ of the coarse-grained space. At time t after the release, the many-body state of N bosons that were initially in a BEC groundstate described by Eq. (6.25) is

$$||\widetilde{\Psi}_N(t)\rangle = \mathcal{N} \sum_\sigma \sqrt{w_\sigma}\, e^{i\phi_\sigma} \tag{6.35}$$

$$\sum_{\{n_{\mathbf{r}\mu}\}_\mathcal{V}} \left\{ \prod_{\mu,\mathbf{r}\in\mathcal{V}} \frac{1}{(n_{\mathbf{r}\mu})!} \left[Q_\mu^\sigma(\mathbf{r},t)\hat{\psi}_\mu^\dagger(\mathbf{r})\right]^{n_{\mathbf{r}\mu}} ||\text{vac}\rangle \right\},$$

where $\mathcal{N}$ is a normalization factor, σ labels the left ($\sigma = L \equiv -1$) and right ($\sigma = R \equiv +1$) modes and $||\widetilde{\Psi}_N(0)\rangle = ||\Psi_N\rangle$. The coefficients Q_μ^σ are normalized so that $\sum_{\mathbf{r},\mu} |Q_\mu^\sigma(\mathbf{r},t)|^2 = 1$. The second summation in (6.35) is over all possible spatial distributions of N particles and, in the continuous limit, it becomes a path integral.

Equation (6.35) represent the expansion of the many-body wave-function in terms eigenstates (6.34) of the density operator. The probability $\mathcal{P}[\{n_{\mathbf{r}\mu}\}]$ of measuring a certain density profile $n_{\mathbf{r}\mu}$ is determined by the coefficient of the corresponding term. If we focus, for simplicity, on the case when there are only left (right) movers in (6.25), this probability is proportional to $\prod_{\mathbf{r},\mu} |Q_\mu^\sigma(\mathbf{r},t)|^{2n_{\mathbf{r}\mu}}/(n_{\mathbf{r}\mu})!$, with $\sigma = L(R)$. The probability $\mathcal{P}[\{n_{\mathbf{r}\mu}\}]$ has a maximum for $n_{\mathbf{r}\mu}^0 = N|Q_\mu^\sigma(\mathbf{r},t)|^2$ corresponding, in the continuous limit, to a stationary point of the path integral in equation (6.35). For large particle number, $\mathcal{P}[\{n_{\mathbf{r}\mu}\}]$ becomes sharply peaked at $n_{\mathbf{r}\mu}^0$ and the actually measured density profiles will exhibit only relatively small deviations from the stationary profile. Therefore, at time t after release, the density of the boson cloud is

$$\rho(\mathbf{r},t) = N \sum_\mu |Q_\mu^\sigma(\mathbf{r},t)|^2. \tag{6.36}$$

If both w_R and w_L are non-zero, the result of a measurement will be either a "right moving" density profile [$\sigma = R$ in (6.36)] with a probability w_R, or a "left moving" profile [$\sigma = L$ in (6.36)] with a probability w_L, assuming that the two profiles are spatially well separated. We are not addressing here the interesting effects of the interference between left and right moving condensates. These effects are negligible if the left and right moving density profiles are spatially separated, but become important otherwise, e.g. at small times after the release.

Next we determine explicitly the coefficients $Q_\mu^\sigma(\mathbf{r},t)$ for the exactly solvable model of bosons with "Ising-type" spin-orbit coupling, $v \neq v' = 0$, placed in a harmonic trap, $V_{\text{trap}}(\mathbf{r}) = m\omega^2 r^2/2$.[3] In this case, the operators $\hat{B}_\sigma^\dagger$ from Eq.

(6.25) are creation operators for the single particle ground states

$$\vec{\phi}_{\sigma 0}(\mathbf{r}) = \varphi_0(\mathbf{r})e^{i\sigma mvx}\frac{1}{\sqrt{2}}\begin{pmatrix} 1 \\ i\sigma \end{pmatrix}, \tag{6.37}$$

where $\varphi_0(\mathbf{r})$ represents the groundstate wavefunction of the harmonic oscillator. The spinor (6.37) is written in the dressed state basis. Performing the position-dependent rotation $R_{\mu\alpha}$ [see Eq. (3.35)], we can express the operators $\hat{B}_\sigma^\dagger$ in terms of creation operators for particles in a certain hyperfine state located at point $\mathbf{r}$, $\hat{\psi}_\mu^\dagger(\mathbf{r})$, or their Fourier components corresponding to free moving particles, $\hat{c}_{\mu\mathbf{k}}^\dagger = \sum_{\mathbf{r}} e^{i\mathbf{k}\mathbf{r}}\hat{\psi}_\mu^\dagger(\mathbf{r})$. The time evolution after the release can be easily described in terms of time evolution for the $\hat{c}_{\mu\mathbf{k}}^\dagger$ operators, $\hat{c}_{\mu\mathbf{k}}^\dagger(t) = \exp(-i\epsilon_\mathbf{k}t)\,\hat{c}_{\mu\mathbf{k}}^\dagger$, where $\epsilon_\mathbf{k} = k^2/(2m)$ is the free particle spectrum. Consequently, the many-body state $||\widetilde{\Psi}_N(t)\rangle$ can be obtained by making in Eq. (6.25) the substitution $\hat{B}_\sigma^\dagger \to \sum_{\mathbf{r},\mu} Q_\mu^\sigma(\mathbf{r},t)\hat{\psi}_\mu^\dagger(\mathbf{r})$ with

$$Q_\mu^\sigma(\mathbf{r},t) = \sum_{\alpha,\mathbf{k},\mathbf{r}'} \left[\vec{\phi}_{\sigma 0}\right]_\alpha (\mathbf{r}')R_{\mu\alpha}^*(\mathbf{r}')e^{i\mathbf{k}(\mathbf{r}-\mathbf{r}')}e^{-i\epsilon_\mathbf{k}t}. \tag{6.38}$$

Finally, introducing this expression of Q_μ^σ in equation (6.36) we obtain for the measured density profile the expression

$$\begin{aligned} \rho(\mathbf{r},t) &= N\frac{\Gamma^3}{[2\pi(1+\tau^2)]^{\frac{3}{2}}} e^{-\frac{\Gamma^2(y^2+z^2)}{1+\tau^2}} \left[\sin^2\theta\; e^{-\frac{\Gamma^2}{1+\tau^2}\left(x-\frac{\lambda mvt}{m}\right)^2}\right. \\ &+ \frac{(1-\lambda\cos\theta)^2}{2} e^{-\frac{\Gamma^2}{1+\tau^2}\left(x-\frac{(\lambda mv+mv_a)t}{m}\right)^2} \\ &\left.+ \frac{(1+\lambda\cos\theta)^2}{2} e^{-\frac{\Gamma^2}{1+\tau^2}\left(x-\frac{(\lambda mv-mv_a)t}{m}\right)^2}\right], \end{aligned} \tag{6.39}$$

where $\Gamma = \sqrt{m\omega}$ is the inverse characteristic length of the trap potential, $\tau = \omega t$ is time in units of ω^{-1}, $\theta \in [0\pi/2]$ and v_a are tunable parameters characterizing the

92

laser field, and $v = v_a \cos\theta$ [see the paragraph containing Eq. (3.35)]. In equation

(6.39) the density was normalized so that $\int d^3r\, \rho(\mathbf{r}, t) = N$. The density profile for

a "left moving" density distribution ($\sigma = -1$) is shown in Fig. 6.3 for three different

times after the release of the boson cloud. The parameters of the calculation are

$\theta = \pi/3$ and $v_a = 6\sqrt{\omega/m}$. Notice the three-peak structure of the density, corre-

sponding to the three exponential terms in equation (6.39). The relative weights of

the peaks are $\cos^4(\theta/2)$ (large peak), $1/2 \sin^2\theta = 2\sin^2(\theta/2)\cos^2(\theta/2)$ (middle peak)

and $\sin^4(\theta/2)$ (small peak) and their characteristic velocities are $-\sigma v_a(1 - \cos\theta)$,

$\sigma v_a \cos\theta$ and $\sigma v_a(1 + \cos\theta)$, respectively. The "left" and "right moving" distribu-

tions are symmetric with respect to a $x \rightarrow -x$ reflection (see also Fig. 6.4). Notice

that the total momentum corresponding to a distribution described by equation

(6.39) vanishes. By analyzing the transformation (3.35) to the dressed state basis,

we observe that $\sin\theta$ is the coefficient of the hyperfine state $|3\rangle$. Consequently, the

middle peak in the density distribution (6.39) consists of particles in this particular

hyperfine state. The other two peaks contain mixtures of states $|1\rangle$ and $|2\rangle$. A state-

selective measurement of particles in the hyperfine state $|3\rangle$ would reveal a single

peak structure moving to the left or to the right with a velocity $v = v_a \cos\theta$. The

dependence of the density profile $\rho(\mathbf{r}, t)/N$ on θ and on the ratio $\gamma = v_a/\sqrt{\omega/m}$ for

$\mathbf{r} = (x, 0, 0)$ and $t = \omega^{-1}$ is shown in Fig. 6.4.

6.6   Summary and conclusions

To summarize, in this chapter we have introduced and discussed in detail a new type of many-body system consisting of pseudo spin-1/2 bosons with spin-orbit interactions. We have shown that at low temperatures the system condenses into a new type of entangled BEC, the spin-orbit coupled Bose-Einstein condensate (SOBEC). The novelty of this state stems from the coupling of an internal degree of freedom, the pseudo-spin created as a result of an atom interacting with a spatially modulated laser field, to the real space motion of the particles. As a result, the single-particle spectrum is characterized by degenerate minima at finite momenta and, consequently, the bosons condense at low temperatures into an entangled quantum state with non-zero momentum. For an arbitrary spin-orbit coupling, the single particle spectrum has a double-well structure in momentum space (see Fig. 6.1) with minima at non-zero momenta. In this case, a system of N non-interacting bosons is characterized by a large $(N+1)$-fold degeneracy of the many-body ground state. Weak density-density interactions reduce this large degeneracy to a two-fold degeneracy. The corresponding ground state wave-function describes a superposition of left-moving and right-moving condensates with weights w_L and $w_R = 1 - w_L$, respectively. Performing a time-of-flight expansion of the condensed bosons results in a characteristic three-peak structure (see Fig. 6.4). The total momentum of the density profile is identically zero, but the peaks are moving along the $\hat{x}$-direction with velocities proportional to the $\mathbf{k}$-vector of the laser field modulation in that direction. The probability of measuring a left- (right-) moving condensate is w_L (w_R)

94

and the signature of a left- (right-) moving state consists in the middle and small peaks moving left (right), while the large peak moves in the opposite direction.

In conclusion, the spin-orbit coupled BEC can be viewed as a state occurring at the interface between spintronics and cold atom physics, with nontrivial properties that have a significant potential for applications. We note here that the ground-state of the double-well SOBEC [see Eq. (6.25)] represents a N00N state,[66, 67] similar to those recently proposed for the construction of a gravimeter bases on atom interferometry.[37] Therefore, the study of a SOBEC state in the context of quantum entanglement and quantum interference is highly relevant. In addition, the double degeneracy associated with the pseudo-spin degree of freedom makes this state a natural candidate for a qubit. A possible way to measure such a qubit was described in the last section. Time-dependent laser fields [similar to those, which lead to the spin-orbit-coupled Hamiltonian (6.1)] could be used as "gates" to perform unitary rotations in the space of degenerate ground states. Note that the coupling of the spin to the orbital motion yields a protecting mechanism against decoherence, due to momentum conservation, and suggest that the spin-orbit coupled condensates are interesting candidates for fault tolerant quantum computation. Finally, we note that for a symmetric Rashba-type spin-orbit coupling, the system is characterized by a single-particle spectrum that has a continuous set of minima along a circle in momentum space. This results in a huge degeneracy that may lead to possible phases with non-trivial topological properties, making the study of the symmetric SOBEC a potentially very interesting problem.
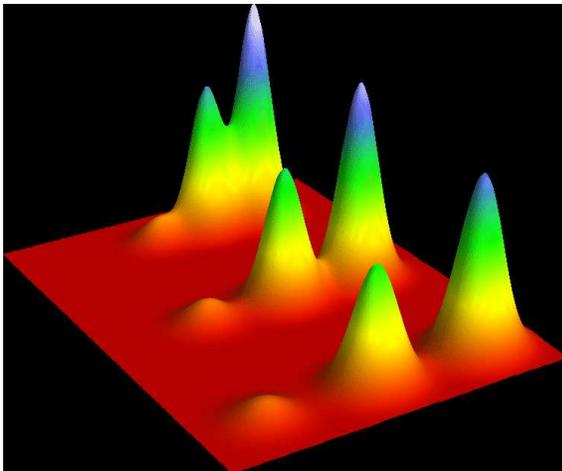
Figure 6.3 – Density of particles at three different moments, $t_1 = 0.4\omega^{-1}$, $t_2 = 0.6\omega^{-1}$, and $t_3 = 0.8\omega^{-1}$, after both the trap and the laser fields are removed at $t = 0$. For clarity, the density distributions are shifted along the y-axis. This time-of-flight expansion corresponds to a many-body ground state (6.25) and is obtained using the single-particle eigenfunctions for the exactly-solvable model of trapped bosons with Ising-type spin-orbit coupling ($v \neq v' = 0$) [3] with $v_a = 6(\omega/m)^{1/2}$. This "left moving" density distribution is measured with a probability w_L, while there is a w_R probability to observe a "right moving" distribution which corresponds to a $x \to -x$ reflection (see also Fig. 6.4). Notice the characteristic three-peak structure. To resolve the BEC peaks, the spin-orbit coupling energy scale should be larger than the trap level spacing, i.e., $mv^2 \gg \omega$. In the opposite limit the phenomenon of real-space BEC separation is smeared out by finite-size effects (6.25).
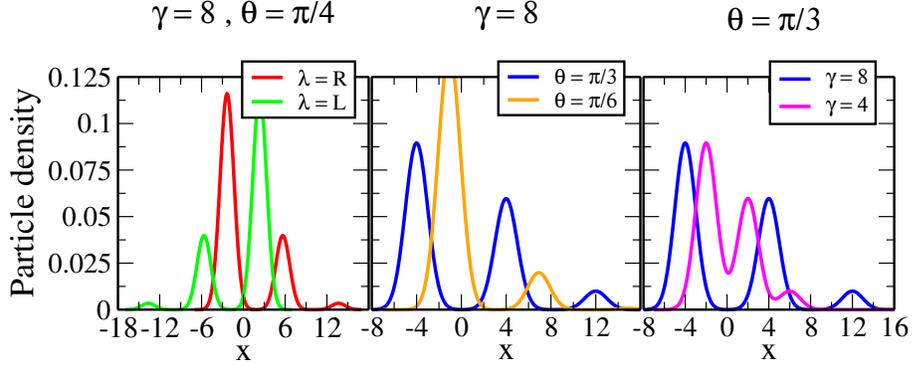
Figure 6.4 – Density profiles $\rho(\mathbf{r}, t)/N$ for $\mathbf{r} = (x, 0, 0)$ and $t = \omega^{-1}$. The position x is measured in units of Γ^{-1}. Left panel: "right moving" versus "left moving" distributions. Notice that the "center of mass" of the distributions is always at $x = 0$. Middle panel: Dependence on the angle θ. At small angles all the weight concentrates in the large peak which is centered near $x = 0$. In the limit $\theta \to \pi/2$ the strength of the SO interaction vanishes $v \to 0$ and the present analysis is not valid. Left panel: Dependence on the relative strength of the spin-orbit coupling, $\gamma = v_a/\sqrt{\omega/m}$. To resolve the peak structure, the spin-orbit coupling energy scale should be larger than the trap level spacing. In the opposite limit interference effects become important (see main text).

Chapter 7

Semi-classical Dynamics and Generalized Spin-Orbit Coupling

7.1   Introduction

This chapter consists of two recent results on spin-orbit coupling. The first part considers the dynamics of the ground state of a trapped spin-orbit coupled system where the trap minimum is instantaneously displaced. The system is considered semi-classically, and depending on the values of the initial conditions and the anisotropy of the spin-orbit coupling, several dynamical regimes are found. Finally an experiment is proposed to use the Berry's phase induced in the pseudo-spin as a signature of spin-orbit coupling.

The second section consists of a proposal for a $3D$ spin-orbit coupling with a vector potential $\mathbf{A} \sim \mathbf{J}$, where $\mathbf{J}$ is the angular momentum operator in pseudo-spin space. This generalized coupling is implemented by including a next-nearest-neighbor coupling to the 4-level ring scheme. The next-nearest coupling scheme produces a tetrahedral coupling topology, and forces the effective momentum transfer of the two-photon transitions to have a tetrahedral geometry. Two limits are considered, and it is found that a $SU(3)$ coupling and a generalized $3D$-$SU(2)$ coupling, with all three spin matrices, is possible.

This work is unpublished and was performed independently by the author. The author would like to thank G. Juzeliunas, I. Spielman, G. Boyd, J. Bagaipo,

and V. Galitski for useful contributions leading to the work in this section.

7.2   Heisenberg Equations of Motion

We consider now an atom with a synthetic spin-orbit coupling in the presence of a harmonic trap of frequency ω. We now express time in units of $1/\omega$, length in units of $\hbar/mv$, and momentum in units of mv, for which the quantum Hamiltonian has the form

$$H/mv^2 = \frac{\mathbf{p}^2}{2} + \frac{1}{2\alpha^2}\mathbf{r}^2 + \Omega(\mathbf{p})\cdot\boldsymbol{\sigma}, \tag{7.1}$$

where $\alpha = mv^2/\hbar\omega = 2E_r/\hbar\omega$ is the ratio of the recoil energy to the trapping energy, $\Delta = v'/v < 1$ is the measurement of the anisotropy of the spin-orbit coupling and $\Omega(\mathbf{p}) = p_x\hat{e}_x + \Delta p_y\hat{e}_y + \delta\hat{e}_z$ is the spin-orbit coupling field with a detuning δ. The Heisenberg equations of the system are found in the usual way [5] to give

$$\dot{\hat{\mathbf{r}}} = \alpha(\hat{\mathbf{p}} + \hat{\sigma}_x\hat{e}_x + \Delta\hat{\sigma}_y\hat{e}_y), \tag{7.2}$$

$$\dot{\hat{\mathbf{p}}} = -\hat{\mathbf{r}}/\alpha, \tag{7.3}$$

$$\dot{\hat{\boldsymbol{\sigma}}} = 2\alpha\tilde{\Omega}(\hat{\mathbf{p}})\times\hat{\boldsymbol{\sigma}}. \tag{7.4}$$

For many experiments, it is reasonable to take $\omega \sim 2\pi * 10\text{Hz}$, and $E_r = \frac{1}{2}mv^2 = \frac{(\hbar k_r)^2}{2m} \sim 2\pi\hbar * 1\text{kHz}$. [27] Thus, an experimentally relevant parameter regime might be $\alpha \sim 100 \gg 1$.

We now propose an experiment where a synthetic spin-orbit coupled system is prepared in one of the ground state,

$$\psi(\mathbf{r}) = \phi_0(\mathbf{r})e^{-ix}\chi(-\hat{e}_x), \tag{7.5}$$

and then the minimum of the harmonic trap is instantaneously displaced. Note that

for $\phi_0(\mathbf{r}) = \left(\frac{1}{\pi \alpha^2}\right)^{1/4} e^{-x^2/2\alpha}$, Eq. 7.5 is the approximate ground state of the system,

neglecting corrections of $\mathcal{O}(1/\alpha)$. Assuming this approximate ground state is value

when the spin-orbit coupling is the largest energy scale in the problem, and that the

trapping potential is a small perturbation. This is precisely the condition given by

$\alpha \gg 1$, and corrections of $1/\alpha$ will be induced by the harmonic trap.

Since the approximate ground state is the product of an orbital coherent state

and a spin coherent state, we expect the system to evolve semi-classically. In what

follows we will consider only the single particle evolution. The treatment will be ap-

proximately valid for a condensate initially prepared with every particle in the state

given by Eq. 7.5. The effect of interactions will not significantly modify the treat-

ment, and the condensate will evolve analogously to the single particle wavepacket.

The approximate ground state has the average momentum, average position,

and a pseduo-spin polarization of

$$\langle \hat{\mathbf{p}} \rangle = -\hat{e}_x, \tag{7.6}$$

$$\langle \hat{\mathbf{r}} \rangle = 0, \tag{7.7}$$

$$\langle \hat{\boldsymbol{\sigma}} \rangle = \hat{e}_x, \tag{7.8}$$

respectively. Since Eq. 7.5 can be expressed as the direct product of a position state

wavefunction and a spin wavefunction, taking the expectation value of Eqns.7.2 -

7.4 in the state 7.5 will be equivalent to replacing $\mathbf{p}$, $\mathbf{r}$ and $\boldsymbol{\sigma}$ with the expectation

values $\langle \mathbf{p} \rangle$, $\langle \mathbf{r} \rangle$ and $\langle \boldsymbol{\sigma} \rangle$. The approximate ground state wavefunction will then act

to set the initial conditions

$$\mathbf{p}(t=0) \quad = \langle \mathbf{p} \rangle \quad = -\hat{e}_x, \tag{7.9}$$

$$\mathbf{r}(t=0) \quad = \langle \mathbf{r} \rangle \quad = 0, \tag{7.10}$$

$$\boldsymbol{\sigma}(t=0) \quad = \langle \boldsymbol{\sigma} \rangle \quad = -\hat{e}_x. \tag{7.11}$$

Note that this replacement cannot be performed for a state where spin and position are entangled, as the expectation value $\langle \mathbf{p} \cdot \boldsymbol{\sigma} \rangle \neq \langle \mathbf{p} \rangle \cdot \langle \boldsymbol{\sigma} \rangle$ in general.

We now treat the Heisenberg equations of motion as semiclassical Hamiltonian equations of motion

$$\dot{\mathbf{r}} \quad = \quad \alpha(\mathbf{p} + \sigma_x \hat{e}_x + \Delta \sigma_y \hat{e}_y), \tag{7.12}$$

$$\dot{\mathbf{p}} \quad = \quad -\mathbf{r}/\alpha, \tag{7.13}$$

$$\dot{\boldsymbol{\sigma}} \quad = \quad 2\alpha \tilde{\Omega}(\mathbf{p}) \times \boldsymbol{\sigma}. \tag{7.14}$$

If at time $t = 0$ we instantaneously shift the minimum of the trap to $\mathbf{r}(0) = \mathbf{r}_0$, the system is defined by the initial conditions $\mathbf{p}(0) = -\hat{e}_x$, $\mathbf{r}(0) = \mathbf{r}_0$, and $\boldsymbol{\sigma} = \hat{e}_x$.

7.3 Adiabatic Dynamics

We can now consider the evolution of the semi-classical equations of motion in the $\alpha \gg 1$ limit. The position and momentum equations immediately decouple to give

$$\ddot{\mathbf{p}} + \mathbf{p} = \sigma_x \hat{e}_x + \Delta \sigma_y \hat{e}_y, \tag{7.15}$$

so the evolution of the position operator can be found by $\mathbf{r}(t) = -\alpha \dot{\mathbf{p}}(t)$. The equation for the spin sector, Eq. 7.14 is driven by a spin-orbit term $\mathcal{O}(\alpha)$. Thus, we

expect that if spin and momentum are aligned or anti-aligned, the spin sector will adiabatically follow the momentum of the particle. This can be solved perturbatively in $1/\alpha$ to give

$$0 = 2\Omega(\mathbf{p}) \times \boldsymbol{\sigma} \tag{7.16}$$

to $\mathcal{O}(1/\alpha)$. This is an effective constraint on $\boldsymbol{\sigma}$ to force $\boldsymbol{\sigma}$ to be aligned or anti-aligned with the effective magnetic field Ω. Considering the initial conditions and normalization, the spin polarization vector is given by

$$\boldsymbol{\sigma}(t) = \frac{(p_x(t), \Delta p_y(t), \delta)^T}{\sqrt{p_x^2(t) + \Delta^2 p_y^2(t) + \delta^2}}. \tag{7.17}$$

Using the adiabatic evolution of the spin polarization, we can derive a set of adiabatic equations for the momentum $\mathbf{p}(t)$:

$$\ddot{\mathbf{p}}_x(t) + \mathbf{p}_x(t) = \frac{p_x(t)}{\sqrt{p_x^2(t) + \Delta^2 p_y^2(t) + \delta^2}}, \tag{7.18}$$

$$\ddot{\mathbf{p}}_y(t) + \mathbf{p}_y(t) = \frac{\Delta^2 p_y(t)}{\sqrt{p_x^2(t) + \Delta^2 p_y^2(t) + \delta^2}}, \tag{7.19}$$

which are correct to $\mathcal{O}(1/\alpha)$.

The adiabatic alignment of the spin polarization and momentum arises naturally from the separation of the time scales of spin evolution and trapping frequency. The spin polarization will undergo Larmor precession on the fast timescale α around the effective magnetic field $\Omega(\mathbf{p})$. However, if the spin and magnetic field are aligned, the spin polarization is constant. The momentum of the system will then evolve on the slow timescale, which will slowly reorient the effective magnetic field $\Omega(\mathbf{p})$. Since the evolution of the spin is much faster than the time dependence of Ω, the spin will adiabatically follow the magnetic field so the spin is always anti-parallel to $\Omega(\mathbf{p})$. If

the initial spin polarization is not anti-parallel to the effective magnetic field, the spin will rapidly Larmor precess around the effective magnetic field. This can be seen in 7.1(b), where we calculate the spin evolution for the non-adiabatic conditions of an initial spin polarization that is offset slightly from the effective magnetic field. The spin precesses on the fast timescale α around the adiabatic trajectory where the initial spin and $\Omega(\mathbf{p})$ are anti-parallel.

7.4 Dynamics and Initial Conditions

The equations of motion are non-linear, and the motion is highly sensitive to initial conditions. We now use Eq 7.18 and Eq. 7.19 to characterize the regimes of motion of the system for various initial conditions and values of Δ and δ. To ensure adiabatic motion, we will continue to assume $\mathbf{p}(0) = -\hat{e}_x$ and $\boldsymbol{\sigma}(0) = \hat{e}_x$. Thus, the one initial condition we consider is is the initial axis of displacement, which gives $\dot{\mathbf{p}}(0) = -\mathbf{r}_0/\alpha$. An initial displacement along $\hat{e}_x$ will not result in interesting dynamics; thus, we consider only initial displacements of the form $\mathbf{r}_0 = y_0\hat{e}_y$. Restoring units we see $y_0 = \tilde{y}_0 mv/\hbar = \tilde{y}_0 * k_L$, where $\tilde{y}_0$ is the dimensionful initial displacement, and k_L is the characteristic wavelength of the optical fields used to induce the spin-orbit coupling. Taking $k_L \sim 2\pi(800nm)^{-1}$, and assuming a trap displacement of $y_0 \sim .1 - 10\mu m$ we see that $\dot{\mathbf{p}}(0) \sim .5 - 50$. This value will be relevant for later calculations.

(a)   (b)
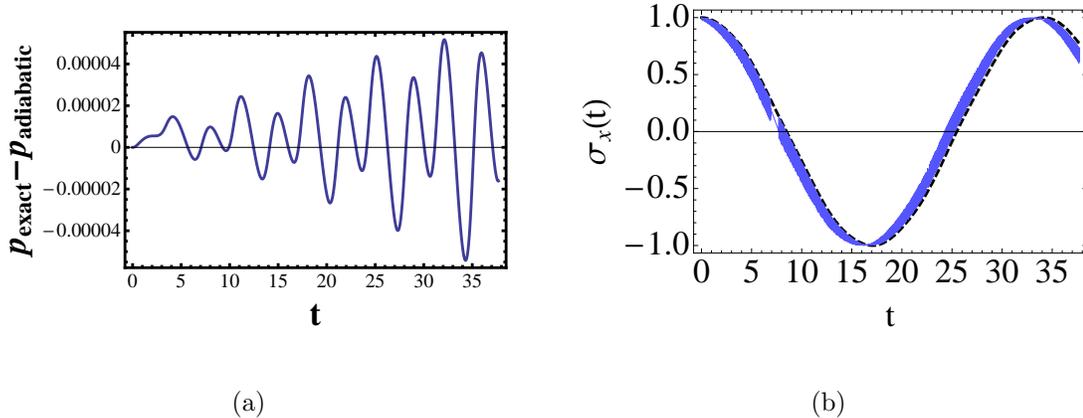
Figure 7.1 – A numerical check of the adiabatic approximation used to derive Eq. 7.18. (a) The time dependence of difference the momentum $p(t) = \sqrt{p_x^2 + p_y^2}$ for the exact solution p_{exact} and the adiabatic solution $p_{adiabatic}$. This difference is $\sim 10^{-3}$, compared to $p(t) \sim 1$, so the approximation is very good. (b) A comparison of the spin component $\sigma_x(t)$ of "adiabatic" initial conditions and non-adiabatic initial conditions. The adiabatic initial conditions (dashed black line) are such that the initial spin and momentum vectors are aligned. $(\mathbf{p}(0) = -\hat{e}_x, \boldsymbol{\sigma}(0) = \hat{e}_x)$ The spin slowly oscillates on a timescale $\mathcal{O}(1)$. The evolution of the spin vector for the non-adiabatic initial conditions (blue) see fast time oscillations $\mathcal{O}(\alpha)$ superposed over the slow time oscillation in the adiabatic setup. These initial conditions are given by $(\mathbf{p}(0) = -\hat{e}_x - .1\hat{e}_y, \boldsymbol{\sigma}(t) = \hat{e}_x)$. In the limit that the initial spin and momentum vectors are perpendicular, the spin and momentum will evolve on timescales much slower than α.

104

7.4.1 Conservation Law

We can derive an approximate conservation law from the adiabatic equations of motion by taking the dot product of $\ddot{\mathbf{p}} + \mathbf{p} = \frac{p_x \hat{e}_x + \Delta^2 p_y \hat{e}_y}{\sqrt{p_x^2(t) + \Delta^2 p_y^2(t) + \delta^2}}$ with $\dot{\mathbf{p}}$:

$$\ddot{\mathbf{p}} \cdot \dot{\mathbf{p}} + \mathbf{p} \cdot \dot{\mathbf{p}} = \frac{p_x \dot{p}_x + \Delta^2 p_y \dot{p}_y}{\sqrt{p_x^2(t) + \Delta^2 p_y^2(t) + \delta^2}}, \tag{7.20}$$

$$\frac{d}{dt}\left(\frac{\dot{p}^2}{2m} + \frac{\mathbf{p}^2}{2m}\right) = \frac{d}{dt}\sqrt{p_x^2(t) + \Delta^2 p_y^2(t) + \delta^2}, \tag{7.21}$$

which gives

$$\frac{\dot{\mathbf{p}}^2}{2} + \frac{\mathbf{p}^2}{2} - \sqrt{p_x^2(t) + \Delta^2 p_y^2(t) + \delta^2} = E, \tag{7.22}$$

where E is a constant of integration. Eq. 7.22 has the form of an energy conservation equation for a momentum-space harmonic oscillator, with an additional potential due to the spin-orbit coupling.

We can now use the order of magnitude of the initial condition to classify the motion into two regimes. The initial conditions give $E = (y_0/\alpha)^2/2 + 1/2 - \sqrt{1 + \delta^2}$. Consider the limit $\Delta \to 1$ and $\delta \to 0$. The conservation equation becomes

$$\frac{\dot{\mathbf{p}}^2}{2} + \frac{(p-1)^2}{2} = \frac{y_0^2}{2\alpha^2}. \tag{7.23}$$

This limit shows that the harmonic trap is displaced around $p = 1$, so the state with lowest potential energy is that with $p = 1$. Thus, for small $\frac{y_0^2}{2\alpha^2} \lesssim 1$, the system will not have enough kinetic energy to undergo large oscillations, and the momentum will oscillate as $p = |\mathbf{p}| = 1 + \delta p$, where $\delta p \ll 1$. However, if $\frac{y_0^2}{2\alpha^2} \gg 1$, the system will have enough energy to overcome the trap, and dynamics with large momenta are possible. This divides the the dynamics of the system into two regimes, that of small initial displacement and that of large initial displacement.

7.4.2 Polar Coordinates

The conservation law above suggests that polar coordinates might be a useful parameterization for finding perturbative solutions to the equations of motion. We will transform the coordinates to

$$p_x = p\cos\theta, \tag{7.24}$$

$$p_y = p\sin\theta, \tag{7.25}$$

where $p = \sqrt{p_x^2 + p_y^2}$ and $\theta = \arctan(p_x/p_y)$. The time derivative becomes [69]

$$\ddot{\mathbf{p}} = (\ddot{p} - p\dot{\theta}^2)\hat{e}_p + (2\dot{p}\dot{\theta} + p\ddot{\theta})\hat{e}_\theta, \tag{7.26}$$

and the term

$$\frac{p_x\hat{e}_x + \Delta^2 p_y\hat{e}_y}{\sqrt{p_x^2(t) + \Delta^2 p_y^2(t) + \delta^2}} = \frac{p\cos\theta(\cos\theta\hat{e}_p - \sin\theta\hat{e}_\theta)}{\sqrt{p_x^2(t) + \Delta^2 p_y^2(t) + \delta^2}}$$

$$+ \frac{\Delta^2 p\sin\theta(\sin\theta\hat{e}_p + \cos\theta\hat{e}_\theta)}{\sqrt{p_x^2(t) + \Delta^2 p_y^2(t) + \delta^2}} \tag{7.27}$$

$$= \frac{p(\cos^2\theta + \Delta^2\sin^2\theta)}{\sqrt{p^2(\cos^2\theta + \Delta^2\sin^2\theta) + \delta^2}}\hat{e}_p$$

$$- \frac{p(1 - \Delta^2)\sin\theta\cos\theta}{\sqrt{p^2(\cos^2\theta + \Delta^2\sin^2\theta) + \delta^2}}\hat{e}_\theta. \tag{7.28}$$

Matching the components of $\hat{e}_p$ and $\hat{e}_\theta$ we get the equations of motion in polar coordinates

$$\ddot{p} + p - p\dot{\theta}^2 = \frac{p(1 - \epsilon\sin^2\theta)}{\sqrt{p^2(1 - \epsilon\sin^2\theta) + \delta^2}}, \tag{7.29}$$

$$2\dot{p}\dot{\theta} + p\ddot{\theta} = -\frac{\epsilon p\sin\theta\cos\theta}{\sqrt{p^2(1 - \epsilon\sin^2\theta) + \delta^2}}, \tag{7.30}$$

where we have used $\cos^2\theta = 1 - \sin^2\theta$ and defined $\epsilon = 1 - \Delta^2$. We see that in the isotropic limit, $\epsilon = 0$, Eq. 7.30 gives a conservation of "angular momentum",

106

$$p^2\dot{\theta} = l.$$

We are now in a place to characterize the regions of dynamics of the system. As discussed earlier, we expect two regimes depending on the magnitude of initial displacement y_0. The initial conditions for $\mathbf{p}$ and $\mathbf{r}$ transform to

$$p(0) = 1, \tag{7.31}$$

$$\dot{p}(0) = 0, \tag{7.32}$$

$$\theta(0) = \arctan(1/0) = 0, \tag{7.33}$$

$$\dot{\theta}(0) = \frac{d}{dt}\arctan\left(\frac{p_x}{p_y}\right)\Big|_{t=0}$$

$$= \left(\frac{\dot{p}_x p_y - \dot{p}_y p_x}{p_x^2 + p_y^2}\right)\Big|_{t=0}$$

$$= -y_0/\alpha \equiv \omega_0. \tag{7.34}$$

We see that the $\epsilon = 0$ angular momentum conservation becomes $p^2\dot{\theta} = \omega_0$. Thus the regime of large or small initial displacement become the regimes of large or small initial angular velocity respectively. In the following sections we characterize the types of motion of the system based upon ω_0.

7.5 Small Initial Displacement

We now consider the limit of small initial displacement. As discussed earlier, in this limit the energy conservation equation forces small radial oscillations around $p = 1 + \delta p$. We can therefore linearize the equations of motion around small momentum oscillations. The dynamics then depends on the value of the anisotropy parameter ϵ. We find there are three regimes. The first is for highly anisotropic systems, where

$\epsilon \simeq 1$. The nearly isotropic limit, $\epsilon \ll 1$, then divides into two sub regimes of small initial displacement, $\omega^2 \ll 3\epsilon > 0$, and $\omega^2 \gtrsim 3\epsilon$. We will demonstrate this behavior in the following sections both analytically and numerically.

7.5.1 Anisotropic Limit, $\epsilon \sim 1$

We now consider the anisotropic limit, and linearize the system around $p = 1 + \delta p$ and $\theta = \delta\theta$. We will neglect all corrections $\mathcal{O}(\delta p^2, \delta p \delta\theta, \delta\theta^2)$. In the end we will justify the linearlization and find the regime of validity for it to remain true.

This linearization gives

$$\delta\ddot{p} + \left(1 - \frac{\delta^2}{(1+\delta^2)^{3/2}}\right)\delta p = \frac{1 - \sqrt{1+\delta^2}}{\sqrt{1+\delta^2}}, \tag{7.35}$$

and

$$\delta\ddot{\theta} + \frac{1 - \Delta^2}{\sqrt{1+\delta^2}}\delta\theta = 0. \tag{7.36}$$

Using the initial conditions in Eq. 7.31 to Eq. 7.34, these equations have the solutions

$$\delta p(t) = \frac{1 - \sqrt{1+\delta^2}}{\sqrt{1+\delta^2}}(1 - \cos(\omega_p t)), \tag{7.37}$$

$$\delta\theta(t) = \frac{\omega_0}{\omega_\theta}\sin(\omega_\theta t), \tag{7.38}$$

where $\omega_p^2 = 1 - \delta^2/(1+\delta^2)^{3/2}$ and $\omega_\theta^2 = \epsilon/\sqrt{1+\delta^2}$. We can now find the regime of validity of this approximation. We require, $\delta^2 \ll 3$ and $\omega_0/\omega_\theta \ll 1$ which gives the constraint $\epsilon \ll \sqrt{1+\delta^2}\omega_0^2$, or $\Delta \ll \sqrt{1 - \omega_0^2\sqrt{1+\delta^2}}$.

Fig. 7.2 shows a numerical calculation of the full equations of motion Eq. 7.12 to Eq. 7.14 for the initial conditions above. We see that the dynamics of the system qualitatively follow the motion described above, i.e., the momentum undergoes small

oscillations around $p = 1$, and the azimuthal angle oscillates around $\theta = 0$. We can explain this behavior by thinking of the system in cartesian coordinates in momentum space. In the strongly anisotropic limit, the system is effectively trapped in momentum space in a harmonic trap centred at $(p_x, p_y) = (1, 0)$. A small coupling between p_x and p_y induce asymmetric and non-closed motion on the oscillations around the center of the trap.

We conclude this analysis by looking at the dynamics of the spin-polarization vector. Since the spin vector does not precess, but merely under goes small oscillations around $\mathbf{p}(0) = -\hat{e}_x$, the effective magnetic field will also not precess. This implies that the spin polarization vector will remain in plane on the Bloch sphere, and will not precess. Therefore, as will be discussed below, in this limit the system will not acquire a Berry's phase. However, as can be seen in Fig. 7.2(d), a detuning will shift the spin polarization off axis, and a small solid angle will be swept out by the spin. This makes a small Berry's phase possible for such a system.

7.5.2   Nearly Isotropic Limit, Intermediate Displacement

In the nearly isotropic limit, $\epsilon \ll 1$ can be used as an expansion parameter. We solve the equations of motion in a perturbation series in ϵ

$$p(t) \;=\; p_0(t) + \epsilon p_1(t) + \epsilon^2 p_2(t) \dots \tag{7.39}$$

$$\theta(t) \;=\; \theta_0(t) + \epsilon \theta_1(t) + \epsilon^2 \theta_2(t) \dots . \tag{7.40}$$

To lowest order, the angular equation of motion is

$$\ddot{p}_0 + p_0 - p_0 \dot{\theta}_0^2 = \frac{p_0}{\sqrt{p_0^2 + \delta^2}}, \tag{7.41}$$
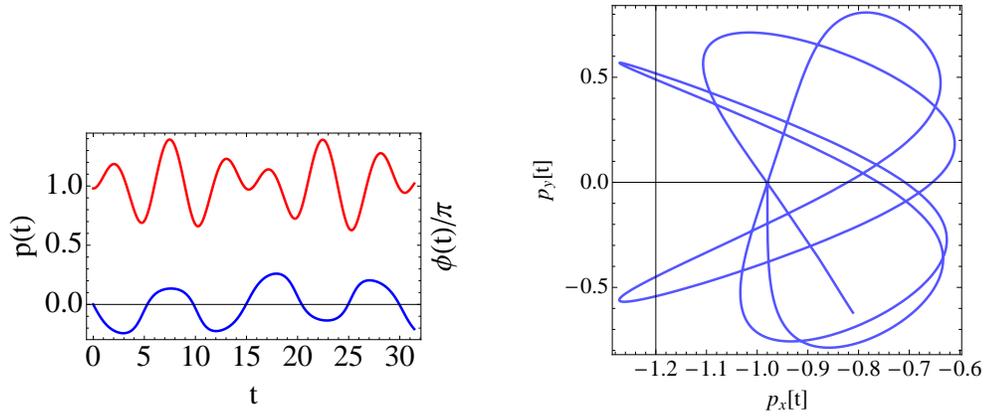
(a) Magnitude and phase of **p** in polar
coordinates.
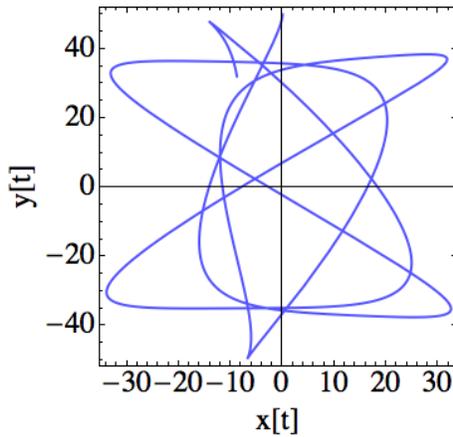
(b) Trajectory of **p**(t).
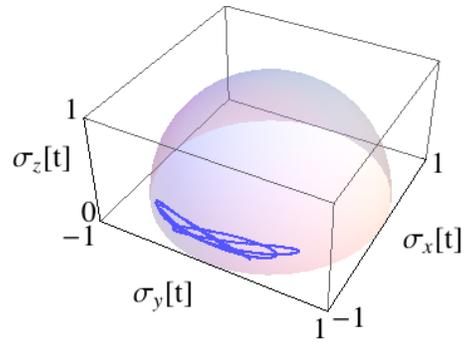
(c) Trajectory of **r**(t).

(d) Precession of the spin vector **σ**

Figure 7.2 – The trajectory of the particle for a small initial displacement with a large anisotropy. ($\epsilon = .31, y_0 = 50/k_R$) (a) Time dependence of the magnitude of momentum, $p(t)$, and the phase $\theta(t)$. (b) A parametric plot of p_x, p_y. (c) A parametric plot of the path the particle orbits in the trap, $(x(t), y(t))$. (d) The spin vector expressed on the Bloch sphere.

and the conservation of angular momentum equation gives

$$p_0^2 \dot{\theta}_0 = \omega_0. \tag{7.42}$$

Recall that the energy conservation term was valid to all orders, so we should still be able to linearize these equations around $p_0 = 1 + \delta p_0$ and $\theta_0 = \omega_0 t + \delta \theta_0$. We will assume δp_0 and $\delta \theta_0$ to be $\mathcal{O}(\omega)$ and $\mathcal{O}(\omega^2)$ respectively, and solve for p_0 and θ_0 to first order in ω. This gives $p_0 = 1$ and $\theta_0 = \omega_0 t$.

The equations of motion to $\mathcal{O}(\epsilon^1, \omega_0^1)$ are

$$\ddot{p}_1 + p_1 - 2\omega_0 \dot{\theta}_1 = -\frac{1}{2}\sin^2(\omega_0 t), \tag{7.43}$$

$$\ddot{\theta}_1 + 2\omega_0 \dot{p}_1 = \sin(\omega_0 t)\cos(\omega_0 t). \tag{7.44}$$

We keep the driving terms on the right hand side to all orders in $\omega_0 t$ to look for the solution at long times. We do not present a full solution, but note that solution to θ_1 is

$$\theta_1 = \frac{t}{4\omega_0} - \frac{\sin(2\omega_0 t)}{8\omega_0^2} + \mathcal{O}(\omega_0^2). \tag{7.45}$$

Consider the behavior of $\theta(t) = \theta_0 + \epsilon \theta_1$ at times $t \sim \pi/4\omega_0$, so that the argument of $\sin(2\omega_0 t) \sim 1$. We now check the validity of the linearization,

$$\theta_0 + \epsilon \theta_1 = \omega_0 t + \epsilon \left(\frac{t}{4\omega_0} - \frac{\sin(2\omega_0 t)}{8\omega_0^2} \right), \tag{7.46}$$

$$\sim \frac{\pi}{4} + \epsilon \left(\frac{\pi}{16\omega_0^2} - \frac{1}{8\omega_0^2} \right) \tag{7.47}$$

$$= \frac{\pi}{4} + \frac{\epsilon}{\omega_0^2} \frac{\pi - 2}{16} \tag{7.48}$$

We see that the linear approximation breaks down if

$$\epsilon/(11\omega_0^2) \gg 1. \tag{7.49}$$

We can subdivide the behavior in the nearly isotropic limit and small initial displacement into two regimes that can be visualized as follows. The momentum

111

space trapping potential has an approximate ring of minima around $p = 1$. However, the small anisotropy will give two local maxima at the bottom of the ring at $\theta = \pi/2, 3\pi/2$. If the initial displacement is sufficiently strong, the particle has enough energy to overcome the local minima and traverse the minima in momentum space. On the other hand, if the initial displacement is sufficiently weak, the particle will not be able to overcome the bumps in the ring minima, and the particle will continue to oscillate around $p_x = -1$.

7.5.3 Small Displacement, Weak Anisotropy

We now consider the dynamics of a weakly anisotropic spin-orbit term $\epsilon \ll \sqrt{1 + \delta^2}\omega_0^2$, but an initial displacement sufficiently strong to produce orbits in momentum space, $\omega_0^2 \gtrsim \epsilon/11$. These initial conditions allows for a linearized solution with $\theta = \omega_0 t$ to lowest order in ϵ, ω_0. Fig. 7.3(a)-(c) gives a numerical solution to the equations of motion in this regime. We see that the linear approximation is justified, with the phase evolving linearly, and the magnitude of momentum oscillation around $p = 1$. Since the dynamics undergo full orbits in momentum space, the spin vector will also undergo orbits. For $\delta = 0$, the orbits will be in the σ_x-σ_y plane of the Bloch sphere, and no Berry's phase will be accumulated. However, adding a $\delta \neq 0$ Zeeman field will shift the precession of the spin off the $\sigma_z = 0$ plane, and allow for a Berry's phase, as is seen in Fig. 7.3(d).
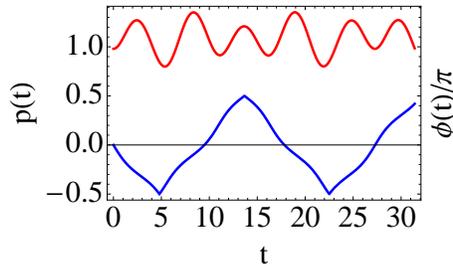
(a) Magnitude and phase of **p** in polar coordinates.
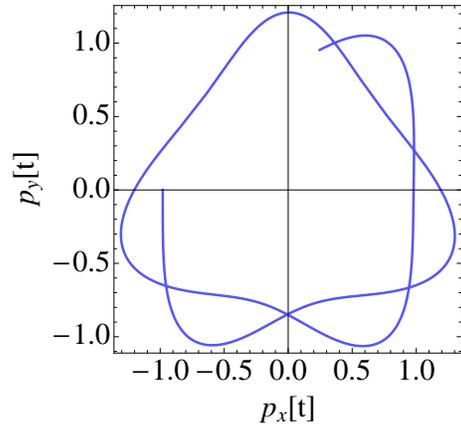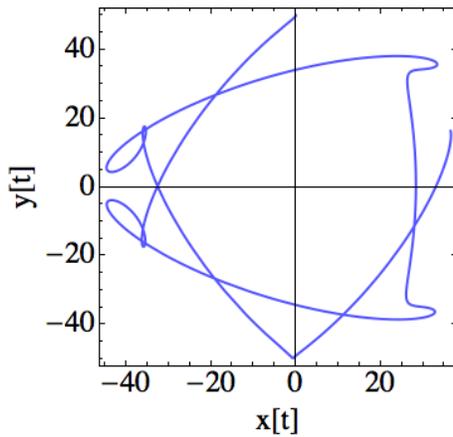
(b) Trajectory of **p**(t).
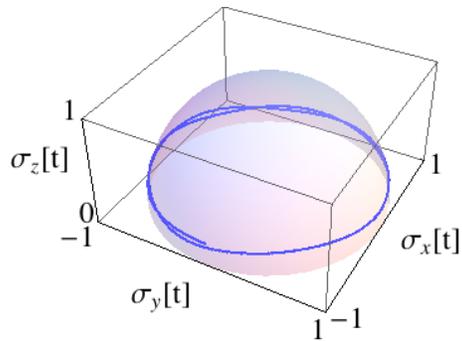
(c) Trajectory of **r**(t).

(d) Precession of the spin vector $\boldsymbol{\sigma}$

Figure 7.3 – The trajectory of the particle for a small initial displacement with a small anisotropy. ($\epsilon = .31, y_0 = 50/k_R$) (a) Time dependence of the magnitude of momentum, $p(t)$, and the phase $\theta(t)$. (b) A parametric plot of p_x, p_y. (c) A parametric plot of the path the particle orbits in the trap, $(x(t), y(t))$. (d) The spin vector expressed on the Bloch sphere.

7.5.4 Very Small Displacement, Weak Anisotropy

We now consider the dynamics of the system in the limit of weak anisotropy and a displacement weaker than the potential barriers due to the trap anisotropy, $\omega_0^2 \ll \epsilon/11$. In this limit the particle will oscillate along the minima of the trap as can be seen in Fig 7.4(b). Since the momentum will not undergo full oscillations, the spin will also not sweep out a solid angle on the Bloch sphere, and no Berry's phase is possible. As in the case of strong anisotropy, a Zeeman field, $\delta \neq 0$ can induce small oscillations off axis to induce a Berry's phase.

7.6 Large Displacement

In the limit of large displacement, the equations of motion cannot be solved perturbatively. An exact solution can be given in terms of inverse elliptic functions, but is not useful for intuition or calculation. The behavior is shown in Fig. 7.5. The phase and momentum are approximately periodic, but the momentum oscillates between 1 and $1 + \omega_0 \gg 1$.

This limit can also be divided into regimes of strong and weak anistropy. Fig. 7.5 shows the behavior in the weakly anisotropic regime with a large initial displacement. The orbits are strongly asymmetric in the $p_x - p_y$ plane. As above, the complete orbit of momentum allows the system to acquire a Berry's phase. Note that in Fig. 7.5(d), the small oscillations on the timescale α are visible. These oscillations are visible because $\dot{p}$ can be non-negligible on the adiabatic timescale. Thus, $\Omega(\mathbf{p})$ may change enough on the Larmor precession timescale for the oscillations to be
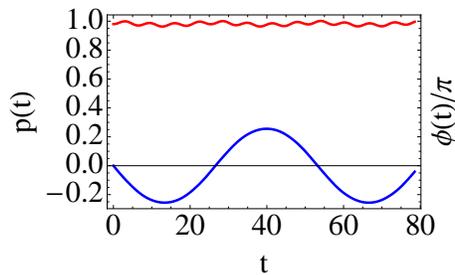
(a) Magnitude and phase of **p** in polar coordinates.
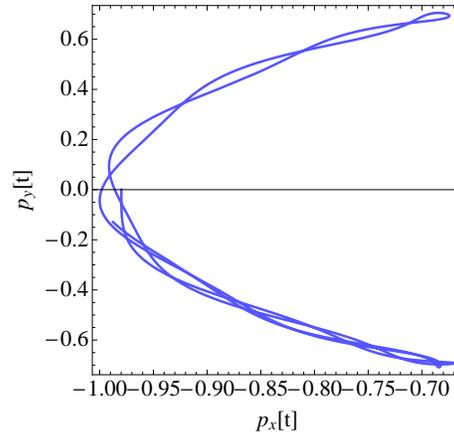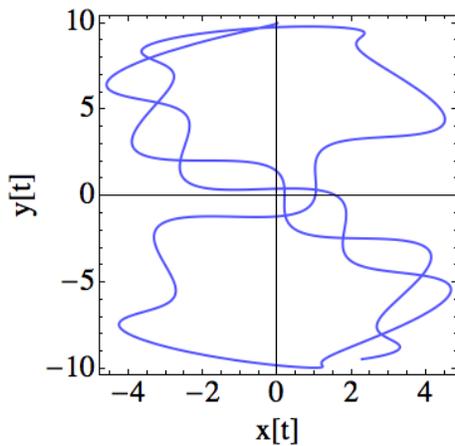
(b) Trajectory of **p**(t).
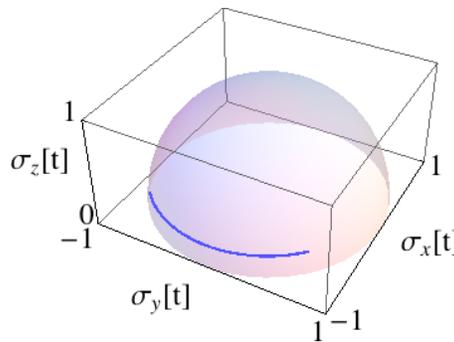
(c) Trajectory of **r**(t).

(d) Precession of the spin vector $\boldsymbol{\sigma}$

Figure 7.4 – The trajectory of the particle for a very small initial displacement with a small anisotropy. ($\epsilon = .14, y_0 = 10/k_R$) (a) Time dependence of the magnitude of momentum, $p(t)$, and the phase $\theta(t)$. (b) A parametric plot of p_x, p_y. (c) A parametric plot of the path the particle orbits in the trap, $(x(t), y(t))$. (d) The spin vector expressed on the Bloch sphere.

detectable.
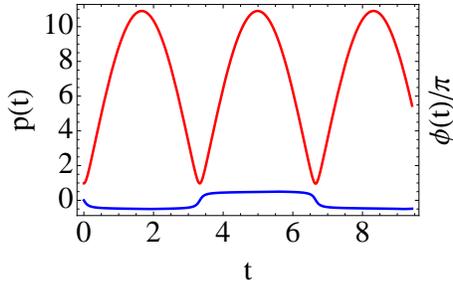
(a) Magnitude and phase of **p** in polar

coordinates.
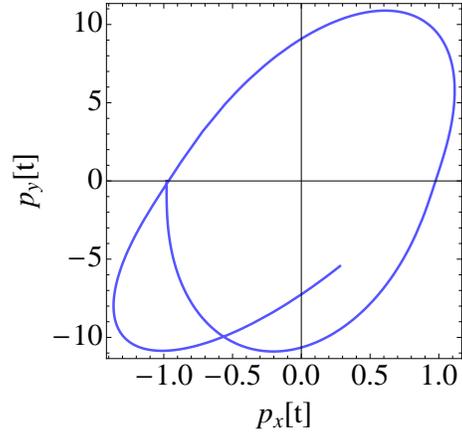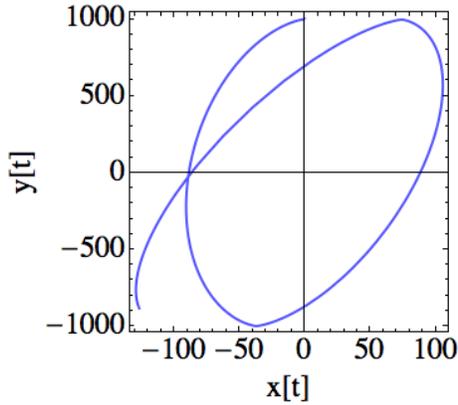
(b) Trajectory of $\mathbf{p}(t)$.
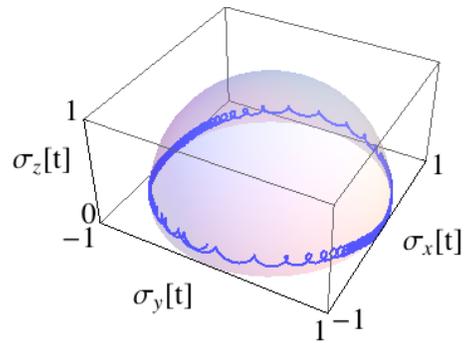
(c) Trajectory of $\mathbf{r}(t)$.

(d) Precession of the spin vector $\boldsymbol{\sigma}$

Figure 7.5 – The trajectory of the particle for a large initial displacement with a small anisotropy. ($\epsilon = .31, y_0 = 1000/k_R$) (a) Time dependence of the magnitude of momentum, $p(t)$, and the phase $\theta(t)$. (b) A parametric plot of p_x, p_y. (c) A parametric plot of the path the particle orbits in the trap, $(x(t), y(t))$. (d) The spin vector expressed on the Bloch sphere.

7.7   Berry's Phase as a Test of non-Abelian Gauge Field.

We now propose an experimental test of the non-Abelian behavior of the spin-orbit coupling. Consider a trapped system of spin-orbit coupled condensates prepared in the approximate ground state given by Eq. 7.5. Turn on a strong optical lattice along the $\hat{e}_z$ direction to produce a system of $2D$ pancakes. If the system is displaced at $t = 0$ by $\mathbf{r}_0 = y_0 \hat{e}_y$, the condensate will begin to oscillate and orbit in one of the regimes given above. As discussed above, the system can acquire a Berry's phase if the momentum undergoes complete orbits, so the spin also undergoes a complete orbit.

Recall that an alternating detuning in the N-level scheme can give rise to a Dresselhaus term, which varies $\Delta < 1$. Thus, by applying a spatial gradient along to the magnetic field along $\hat{e}_z$, we can tune the anisotropy ϵ to be different in each pancake. If the trap minimum is displaced, the condensate in each pancake will orbit according to its own value of the anisotropy. If the orbit is such that the spin precesses, that orbit will acquire a Berry's phase. Note that the single particle energy is degenerate to order $1/\alpha$, so the dynamical phase for each state will be nearly degenerate. The Berry's phase can then be measured by releasing the trap and observing the interference fringes between the pancakes.
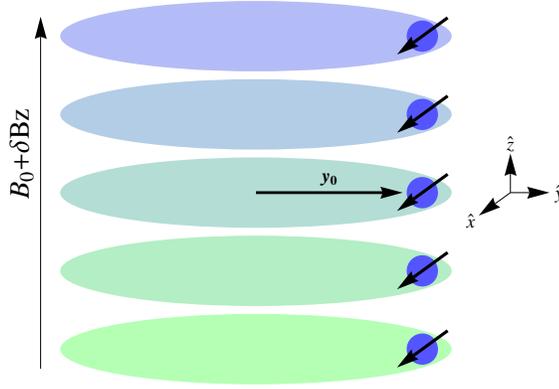
Figure 7.6 – A potential experiment for measuring the Berry's phase due to the spin-orbit coupling. A series of $2D$ pancakes, each with a spin-orbit coupling induced by the N-level scheme. A magnetic field gradient is tuned along the axis perpendicular to plane of confinement. This modifies the two-photon detuning on each level, and in the N-level scheme can vary the magnitude of the anisotropy, ϵ. The experiment is set up so that at $t = 0$, each pancake is prepared in the same ground state with psuedo-spin oriented along $\hat{e}_x$, and then displaced by $y_0\hat{e}_y$. Each system will evolve and accumulate a slightly different Berry's phase that can then be measured in a time-of-flight experiment.

7.7.1 Berry's Phase

We now calculate the Berry's phase of a particle that orbits the trap such that the spin is adiabatically locked to momentum. The adiabatic requirement forces

$$\langle \boldsymbol{\sigma} \rangle = \frac{(p_x, \Delta p_y, \delta)^T}{\sqrt{p_x^2 + \Delta^2 p_y^2 + \delta^2}}, \tag{7.50}$$

which corresponds to a spinor

$$\chi = \begin{pmatrix} \sin\gamma \\ \cos\gamma e^{i\phi} \end{pmatrix}, \tag{7.51}$$

where

$$\arctan \gamma \;=\; \frac{\delta}{\sqrt{p_x^2 + \Delta^2 p_y^2}}, \tag{7.52}$$

$$e^{i\phi} \;=\; \frac{p_x + i\Delta p_y}{\sqrt{p_x^2 + \Delta^2 p_y^2}}. \tag{7.53}$$

The Berry's connection is

$$\mathbf{A}_B \;=\; i\hbar \chi^\dagger \frac{d}{dt}\chi dt \tag{7.54}$$

$$=\; i\hbar \left(\sin\gamma, \cos\gamma e^{-i\phi}\right) \frac{d}{dt} dt \begin{pmatrix} \sin\gamma \\ \cos\gamma e^{i\phi} \end{pmatrix} dt \tag{7.55}$$

$$=\; i\hbar \cos^2 \gamma \, i\dot\phi dt, \tag{7.56}$$

but

$$i\dot\phi \;=\; \frac{d}{dt} \log\left(\frac{p_x + i\Delta p_y}{\sqrt{p_x^2 + \Delta^2 p_y^2}} \right) \tag{7.57}$$

$$=\; -i\Delta \frac{\dot p_x p_y - \dot p_y p_x}{p_x^2 + \Delta^2 p_y^2} \tag{7.58}$$

$$=\; i\Delta \frac{1}{(1 - \epsilon \sin^2 \theta)} \dot\theta, \tag{7.59}$$

which gives the Berry's connection for the ground state as it orbits around the trap center

$$\mathbf{A}_B = -\frac{\Delta p^2}{p^2(1 - \epsilon \sin^2 \theta) + \delta^2} d\theta. \tag{7.60}$$

The Berry's phase is thus

$$\gamma_B = -i \int dt \left(\frac{\Delta p^2}{p^2(1 - \epsilon \sin^2 \theta) + \delta^2} \right) \dot\theta. \tag{7.61}$$

This can be calculated either numerically, or by using the perturbative solutions given above.

Recall that the Berry's phase is only well defined if the system precesses a closed loop in parameter space. It is therefore important to check that this condition is satisfied. Due to the chaotic dynamics of the equations of motion, this condition may not be satisfied. However, if the particle's momentum undergoes a complete orbit around $\mathbf{p} = 0$ in momentum space, it will be guaranteed to undergo a closed loop if it is confined to a $2D$ plane. This then guarantees that the spin will sweep out a closed loop on the Bloch sphere, and Berry's phase will be well defined.

In order for the Berry's phase to be observable it must take a value different from 2π. Examining Eq. 7.60, it is clear that a finite Zeeman field δ is necessary for an observable Berry's phase. At $\delta = 0$, the Berry connection will be $\mathbf{A}_b = \Delta\dot{\theta}/(1 - \epsilon\sin^2\theta)$, which will only deviate slightly from 1 in the nearly isotropic limit, where closed orbits exist for small initial displacements. Thus, a finite detuning is necessary for a significant Berry's phase. Note also that for a detuning $\delta > 1$, the double well structure of the single particle energy spectrum disappears.

7.8   3-D Spin-Orbit Coupling

In this section we propose a modification of the 4-level scheme to allow for a generalized spin-orbit coupling scheme that has all three Pauli matricies, and a vector potential in three dimensions. This coupling arises by adding additional couplings that connect the four states in a tetrahedral topology, as opposed to the ring topology discussed above.

7.8.1 Initial Hamiltonian

Consider now the N-level scheme discussed in Sec. 3.1, with $N = 4$. To generate a $3D$ coupling, consider adding two couplings

$$H'_{al} = \Omega_{13} \left|1\right\rangle \left\langle 3\right| e^{i\mathbf{k}_{13}\cdot\mathbf{r}} + \Omega_{24} \left|2\right\rangle \left\langle 4\right| e^{i\mathbf{k}_{24}\cdot\mathbf{r}} \tag{7.62}$$

that connect the states $\left|1\right\rangle$ to $\left|3\right\rangle$, and $\left|2\right\rangle$ to $\left|4\right\rangle$, as seen in Fig. 7.7. These additional couplings generate a tetrahedral topology to the atom-laser coupling, as opposed to the ring like geometry discussed above.
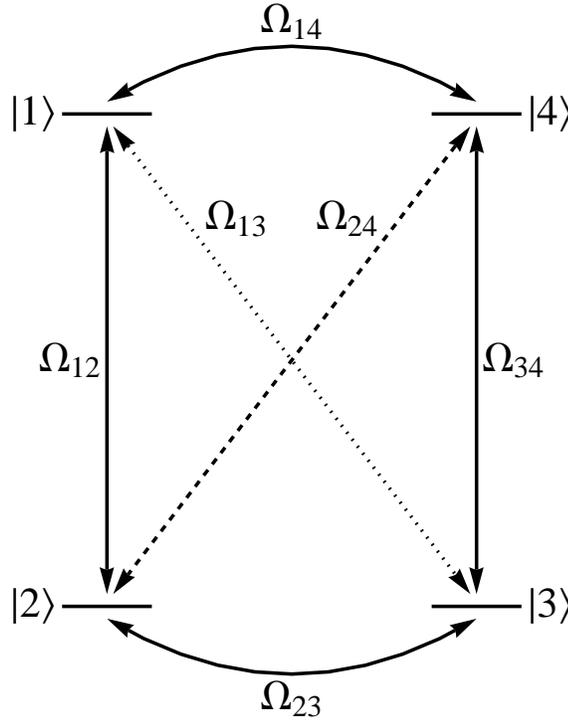
Figure 7.7 – The 4-level coupling scheme needed for a $3D$ spin-orbit interaction. The additional of next-nearest-neighbor couplings Ω_{13} and Ω_{24} form a tetrahedral coupling topology. The momentum transfer of the optical couplings Ω_{ij} forms a tetrahedral geometry.

The tetrahedral topology now modifies the restriction of the effective wavevectors of the two photon transitions required for the net momentum transfer of the optical coupling to vanish. Consider the coupling between the state $|j\rangle$ and $|j+1\rangle$ to be $\Omega_{j,j+1} = \Omega e^{i\phi_{j,j+1} - i\mathbf{k}_{j,j+1}\cdot\mathbf{r}}$, and assume the new couplings to have the form

$$\Omega_{13} = \Omega e^{i\phi_{13} - i\mathbf{k}_{13}\cdot\mathbf{r}}, \tag{7.63}$$

$$\Omega_{24} = \Omega e^{i\phi_{24} - i\mathbf{k}_{24}\cdot\mathbf{r}}. \tag{7.64}$$

The conditions of no net momentum transfer around any closed coupling loop therefore takes the form

$$\mathbf{k}_{12} + \mathbf{k}_{23} - \mathbf{k}_{13} = 0, \tag{7.65}$$

$$\mathbf{k}_{13} + \mathbf{k}_{34} - \mathbf{k}_{14} = 0, \tag{7.66}$$

$$\mathbf{k}_{23} + \mathbf{k}_{34} - \mathbf{k}_{24} = 0. \tag{7.67}$$

This can be immediately satisfied by assuming the wavevectors $\mathbf{k}_{ij}$ to have the form

$$\mathbf{k}_{ij} = \mathbf{K}_i - \mathbf{K}_j, \tag{7.68}$$

where $\mathbf{K}_i$ are vectors from the center to the vertex of a tetrahedron. This can be implemented naturally using two photon transitions where the momentum of the absorbed and emitted beam are $\mathbf{K}_i$ and $\mathbf{K}_j$ respectively.

We can now diagonalize the atom-laser Hamiltonian in a manner analogous to above. We first boost the state $|j\rangle \to e^{-i\mathbf{K}_j\cdot\mathbf{r}}|\tilde{j}\rangle$. This transforms the second

quantized Hamiltonian to the form

$$
\begin{aligned}
\hat{H} &= \sum_{j=1}^{N} \int d^2\mathbf{q} \left(\frac{\hbar^2 |\mathbf{q} - \mathbf{K}_j|^2}{2m} + \delta(-1)^j \right) \tilde{\psi}_j^\dagger(\mathbf{q})\tilde{\psi}_j(\mathbf{q}) \\
&\quad - \sum_{j=1}^{N} \int d^2\mathbf{q} \left(\hbar\Omega e^{i\phi_{ij}} \tilde{\psi}_i^\dagger(\mathbf{q})\tilde{\psi}_j(\mathbf{q}) + H.c. \right).
\end{aligned}
\tag{7.69}
$$

The boosted atom-laser coupling then can be expressed in matrix representation as

$$
H_{al} = \Omega \begin{pmatrix}
0 & e^{i\phi_{12}} & e^{i\phi_{13}} & e^{i\phi_{14}} \\
e^{-i\phi_{12}} & 0 & e^{i\phi_{23}} & e^{i\phi_{24}} \\
e^{-i\phi_{13}} & e^{-i\phi_{23}} & 0 & e^{i\phi_{34}} \\
e^{-i\phi_{14}} & e^{-i\phi_{24}} & e^{-i\phi_{34}} & 0
\end{pmatrix}.
\tag{7.70}
$$

Due to the tetrahedral topology of the optical coupling, it is apparent that only three of the six phases are relevant. This can be seen by considering loops around states, e.g. $1 \to 2 \to 3$, $2 \to 3 \to 4$, etc. There are four loops in a tetrahedron, but only three of them are independent. They can be parametrized in multiple ways, but a suggestive way to deal with them can be seen by applying the transformation

$$
|\tilde{j}\rangle \to e^{i \sum_{l=1}^{j-1}(\gamma_l - \bar{\gamma})} |\tilde{j}\rangle
\tag{7.71}
$$

where $\bar{\gamma} = \sum_j \gamma_j$ is the average phase around the closed loop $|1\rangle \to |2\rangle \to |3\rangle \to |4\rangle \to |1\rangle$. The rephased atom-laser interaction then has the form

$$
H_{al} = \Omega \begin{pmatrix}
0 & e^{i\bar{\gamma}} & e^{i\bar{\phi}} & e^{-i\bar{\gamma}} \\
e^{-i\bar{\gamma}} & 0 & e^{i\bar{\gamma}} & e^{i\bar{\alpha}} \\
e^{-i\bar{\phi}} & e^{-i\bar{\gamma}} & 0 & e^{i\bar{\gamma}} \\
e^{i\bar{\gamma}} & e^{-i\bar{\alpha}} & e^{-i\bar{\gamma}} & 0
\end{pmatrix}.
\tag{7.72}
$$

where $\bar{\gamma}$, $\bar{\phi}$, and $\bar{\alpha}$ are the three phases that cannot be transformed away.

123

7.8.2 Diagonalization

We now diagonalize Eq. 7.72 for two specific limits. The first limit is that of $\bar{\gamma} = \bar{\phi} = \bar{\alpha} = 0$. In this limit, the unitary transformation 3.12 will diagonalize Eq. 7.72. The diagonalized atom-laser term has two eigenvalues, $\lambda = -\Omega, 3\Omega$, with a three-fold degeneracy of the $\lambda = -\Omega$ eigenvalue. This gives degeneracy gives rise to a $SU(3)$ spin-orbit coupling. However, this is analogous to the generalized spin-orbit coupling in Ref. [70].

Another limiting case of interest is that of $\bar{\gamma} = \pi/4$, $\bar{\phi} = \pi$, $\bar{\alpha} = 0$. In this case the effect of 3.12 will be to transform 7.72 to

$$
\tilde{H}_{al} = \Omega \begin{pmatrix} -\sqrt{2} & 0 & 1 & 0 \\ 0 & -\sqrt{2} & 0 & -1 \\ 1 & 0 & \sqrt{2} & 0 \\ 0 & -1 & 0 & \sqrt{2} \end{pmatrix}.
\tag{7.73}
$$

This can be expressed as $H_{al} = \Omega(-\sqrt{2}\hat{I} \otimes \tau_z + \sigma_z \otimes \tau_x)$, where τ_i is the i-th Pauli matrix in the supermatrix space. This suggests H_{al} can be diagonalized with the matrix $U' = \left(\begin{smallmatrix} \cos\theta & -\sigma_z \sin\theta \\ \sigma_z \sin\theta & \cos\theta \end{smallmatrix} \right)$, where $\cos\theta = \sqrt{1/2 - 1/\sqrt{6}}$. The spectrum for this matrix is $\lambda = \pm\sqrt{3}\Omega$, with both eigenvalues doubly degenerate. This gives a two-dimensional degenerate subspace for which a $3D$ spin-orbit coupling can be induced. As before, the action of the unitary matrix U' on the kinetic term will give a vector potential

$$
\mathbf{A} = \frac{1}{2\sqrt{3}}(\mathbf{K}_3 + \mathbf{K}_1 - (\mathbf{K}_4 + \mathbf{K}_2))\sigma_z + \frac{1}{2\sqrt{6}}(\mathbf{K}_3 - \mathbf{K}_1)\sigma_y + \frac{1}{2\sqrt{6}}(\mathbf{K}_4 - \mathbf{K}_2)\sigma_x. \tag{7.74}
$$

This vector potential can be made proportional to $3D$ angular momentum operator,

$\mathbf{A} \sim \mathbf{J}$, by tuning the momenta

$$\mathbf{K}_4 - \mathbf{K}_2 = 2k\hat{e}_x, \tag{7.75}$$

$$\mathbf{K}_3 - \mathbf{K}_1 = 2k\hat{e}_y, \tag{7.76}$$

$$\mathbf{K}_3 + \mathbf{K}_1 = \frac{k}{\sqrt{2}}\hat{e}_z, \tag{7.77}$$

$$\mathbf{K}_4 + \mathbf{K}_2 = -\frac{k}{\sqrt{2}}\hat{e}_z, \tag{7.78}$$

or, equivalently,

$$\mathbf{K}_1 = k\left(-\hat{e}_y + \frac{\hat{e}_z}{\sqrt{2}}\right), \tag{7.79}$$

$$\mathbf{K}_2 = k\left(-\hat{e}_x - \frac{\hat{e}_z}{\sqrt{2}}\right), \tag{7.80}$$

$$\mathbf{K}_3 = k\left(\hat{e}_y + \frac{\hat{e}_z}{\sqrt{2}}\right), \tag{7.81}$$

$$\mathbf{K}_4 = k\left(\hat{e}_x - \frac{\hat{e}_z}{\sqrt{2}}\right). \tag{7.82}$$

This simplifies to give a vector potential of

$$\mathbf{A} = \frac{\hbar k}{\sqrt{6}}(\sigma_x, \sigma_y, \sigma_z). \tag{7.83}$$

The four vectors $\mathbf{K}_1 \ldots \mathbf{K}_4$ can be seen to be the four vectors from the center to the vertices of a tetrahedron. Thus, we constructed a generalized $3D$ spin-orbit coupling for which the vector potential is proportional to the angular momentum operator in psuedo-spin space. This is in contrast to the proof in Sec. III.b of Ref. [70] that claims no $3D$ spin-orbit coupling is possible for which $\mathbf{A} \sim \mathbf{J}$. Notice there is no contradiction with this proof. In the limit of large detuning, the 4-pod scheme of Ref. [70] reduces to the 4-level scheme with the additional couplings added. However, the 4-pod scheme explicitly assumed all single photon phases were

equal. This implies that the phases of the effective two-photon couplings vanish, which reduces to the above $SU(3)$ spin orbit scheme discussed above. Further, the additional phase degrees of freedom allowed with the additional couplings explicitly breaks the symmetry properties of the vector potential required in the proof, and the proof does not apply to our set up.

7.9   Conclusion

In this chapter we propose an experimental consequence of the spin-orbit coupling in a synthetic non-Abelian field. Such a system is found to undergo chaotic dynamics that can be separated into several regimes, each defined by various values of the anisotropy of the spin-orbit coupling and the magnitude of the initial displacement of the trap. For certain regimes, such as that of large initial displacement, or small initial displacement with a nearly isotropic trap, the spin will accumulate a Berry's phase. Finally, we propose an experiment on such a system to measure this Berry's phase that involves a series of $2D$ pancakes, each with their own independent isotropy value. We then consider the effect of next-nearest-neighbor couplings on the 4-level scheme, and find that a $3D$ spin-orbit coupling is possible, in contradiction to the proof in [70].

Chapter 8

Time-dependent accelerometery with Synthetic Gauge Fields

8.1   Introduction

In this chapter we propose a new type of interferometer that uses the optically

induced spin-momentum coupling to measure ac signals. The work in this section

was done in collabortion with Jacob Taylor and Victor Galitski, and was published

in [71].

The optical coupling of the synthetic field provides a continuous coupling of

momentum and spin. This is in contrast to standard interferometry schemes where

spin and momentum coupling is generated only through a set of discrete Raman $\pi/2$

and π pulses. We use the continuous spin-momentum coupling of the gauge field to

produce an interferometer sensitive to high frequency time dependent (or ac) fields.

This is in contrast to current systems whose sensitivity to signals drops above a soft

cutoff frequency of ≤ 10Hz [72, 73]. We specifically propose using a trapped system

of cold bosons under the influence of an optically induced gauge field to measure

weak high-frequency (~ 1kHz) ac gravity signals.

Using time-reversal-like pulses, it is shown that noise can be reduced with a

Carr-Purcell-like pulse sequence. The response function of the system is calculated

for this pulse sequence. We discuss some potential implementations and we estimate

that such a system will have a sensitivity of $S \sim 10^{-7} \frac{\text{m/s}^2}{\sqrt{\text{Hz}}}$. We note that since our
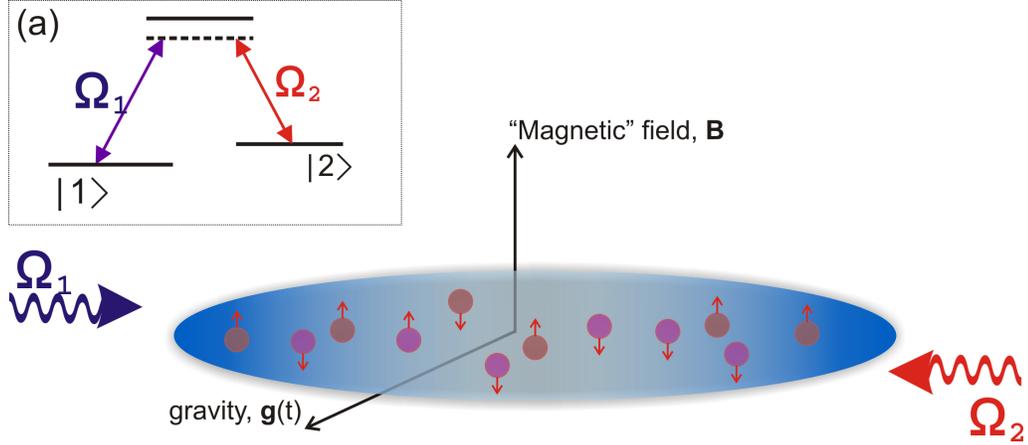
Figure 8.1 – A potential implementation of our interferometer based upon Ref. [4]. The Raman beams $\Omega_{1,2}$ couple a three level atom by two parallel Gaussian profiles with peaks that are spatially offset. The spatial offset of the beams provides a torque on the atoms that looks like a magnetic field. Two of the dressed states couple to a "synthetic gauge field" with opposite charges and become degenerate in the large detuning limit, $\Delta \to \infty$.

system is trapped it can be implemented on an atom chip [74, 75, 76].

8.2   Toy Model

To demonstrate how a synthetic gauge field could be used to make measurements of gravity or acceleration we will begin with a toy model. We note that this model is an idealization of the scheme reviewed Sec. 3.3. As our toy model, we will consider a single particle with a pseudo-spin-1/2 degree of freedom. The pseudo-spins, denoted $|\uparrow\rangle$ and $|\downarrow\rangle$, will be coupled to a synthetic magnetic field proportional to the σ_3 matrix. If there are no other pseudo-spin coupling terms the two uncoupled pseudo-spins will behave as if they are coupled to a magnetic field with charges

of opposite signs. If such a system is placed in a harmonic trap and subject to an external potential $\mathbf{g}(t)$, it's Hamiltonian will be described by

$$H = \frac{[\hat{\mathbf{p}} - \sigma_3 \mathbf{A}(\hat{\mathbf{r}})]^2}{2m} + \frac{1}{2}m\omega_0^2\hat{\mathbf{r}}^2 - m\mathbf{g}(t) \cdot \hat{\mathbf{r}} \qquad (8.1)$$

where $\hat{\mathbf{p}}$ and $\hat{\mathbf{r}}$ are the position and momentum operators respectively, ω_0 is the trapping frequency, m is the mass of the particle, $\mathbf{g}(t)$ is the time dependent external force and $\mathbf{A}(\hat{\mathbf{r}})$ is the spin-orbit coupling field, or vector potential. We confine the particle to a two dimensional plane and chose vector potential to have the form of a magnetic field $\mathbf{A}(\hat{\mathbf{r}}) = m\omega_c x\hat{e}_y$, where ω_c is the characteristic frequency scale of the spin-orbit coupling and $\hat{e}_z$ is the unit vector perpendicular to the plane of confinement.

The system described by Eq. 8.1 only has psuedo-spin dependence in the form of σ_3. This means the dynamics of the two pseudo-spins can be considered independently with σ_3 replaced by a classical parameter $\sigma = \pm 1$. Additionally, the Hamiltonian is quadratic in $\hat{x}$ and $\hat{p}$, so the Heisenberg equations of motion correspond exactly to the Hamiltonian equations of motion. We can thus solve for the dynamics of the system classically, and apply the intuition to the quantum problem. The dynamics given in what follows were found exactly in the quantum regime using both the path integral formalism and by using creation and annihilation operators. The results are given in Appendix A. In what follows we will give a derivation using semi-classical arguments, and supplement with the exact quantum solution where relevant.

As discussed in Chapter 4, gravitational information can be extracted by cre-

ating a superposition of two quantum states (e.g. spin) that follow distinct paths through a gravitational potential. The difference in the potential experienced by the two paths will imprint distinct phases upon the two spin states. Upon overlap of the two states at a future time, a rotation and measurement in the pseudo-spin basis will give the phase information, from which the gravitational potential can be induced. The following discussion will show how the toy model produces two pseudo-spin states that travel along different paths which are sensitive to gravitationally dependent phase information.

The classical paths can be found by solving the Heisenberg equations of motion, and is done in Appendix A. The initial conditions considered are those where a particle starts at rest in the center of the trap, after which the trap minimum is suddenly displaced by a vector $\mathbf{r}_0$. For such an initial condition the paths of the $\sigma = \pm 1$ trajectories are mirrored along the axis of the initial trap displacement, as can be seen in Fig. 8.2(a) and Fig. 8.2(b). These paths are characterized by the two classical frequencies $\omega_{\pm} = \tilde{\omega} \pm \omega_c/2$, with $\tilde{\omega}^2 = \omega_0^2 + (\omega_c/2)^2$. Furthermore, switching the sign of the psuedo-spin, i.e. taking $\sigma \to -\sigma$, will time-reverse the paths in the sense that they will retrace the trajectory they just followed.

8.3 Interferometry in the Toy Model

We can now see how such a toy model can be used to perform time-dependent, or time-independent measurements of acceleration. The mirror symmetry of the two pseudo-spin trajectories can act as the two arms of a Mach-Zehnder interferometer.

The effect of an external force will be to perturb the paths differently. In the case of a constant and uniform gravitational field, the physics is analogous to a normal atom interferometer. The upper arm will be at a higher potential, and therefore will accumulate phase faster than the lower arm. However, if the paths are allowed to perform a full orbit around the trap center, they will interchange the role of the upper and lower arm, and the net phase accumulated will be the same. This implies a time-independent gravitational measurement can only be made at half-orbits.

The situation is more subtle in the presence of a time-dependent external force. In this case, the direction of acceleration can change mid-way through an orbit, and the pseudo-spin with the highest potential will also change. In this case the response of the two arms will not be equal over one orbit, and the system can have a non-zero response even after completing a full orbit. We see this response is maximum for a periodic signal with a frequency near one of the classical frequency ω_-. In this case, one arm will stay at a higher potential for the full orbit since the sign of the driving force will change at half-obits where the response of the two classical paths would switch in the presence of a time-independent potential.

The relation of this behavior to phase information is detailed in the appendix. It is shown that a Gaussian wavepacket will evolve as a coherent state around the classical orbits, accumulating a $\mathbf{g}(t)$ dependent phase with time. Explicitly, such a state evolves as $\psi_\sigma(\mathbf{r}, t) = \phi_0(\mathbf{r} - \mathbf{r}_\sigma(t))e^{iS_\sigma}$, where $\phi_0(\mathbf{r})$ is the harmonic oscillator wavefunction, and $\mathbf{r}_\sigma(t)$, S_σ are the respective classical path and action corresponding to a particle with charge σ.

We become sensitive to this phase in a manner similar to the traditional in-

terferometry schemes discussed in Chapter 4. Begin with a particle in the initial state $|\Psi\rangle = \psi_\uparrow(0)\,|\uparrow\rangle$, where $|\uparrow\rangle$ is the $\sigma = +1$ pseudo-spin state and $\psi_\uparrow(0)$ is the orbital ground state for both $|\uparrow\rangle$ and $|\downarrow\rangle$. Through the application of a $\pi/2$ pulse in pseudo-spin space, the pseudo-spin polarized system is placed in the superopsition $|\Psi\rangle = \frac{|\uparrow\rangle + |\downarrow\rangle}{\sqrt{2}} \psi_\uparrow(0)$. We then displace the trap center which will cause the orbital wavefunctions to orbit around the trap center in the manner described above. The wavefunction evolves to

$$|\Psi\rangle = \frac{1}{\sqrt{2}}\left(e^{iS_\uparrow}\psi_\uparrow(\mathbf{r},t)\,|\uparrow\rangle + e^{iS_\downarrow}\psi_\downarrow(\mathbf{r},t)\,|\downarrow\rangle\right). \tag{8.2}$$

In general the spin states $|\uparrow\rangle$, $|\downarrow\rangle$ are entangled to the orbital states $\psi_\uparrow(\mathbf{r},t)$, $\psi_\downarrow(\mathbf{r},t)$ respectively. However, a pure spin measurement is required for extracting the phase information. This can be performed by waiting for the classical trajectory of the orbital wavefunctions to overlap, i.e. $\psi_\uparrow(\mathbf{r},t_f) = \psi_\downarrow(\mathbf{r},t_f)$. At this point the spin and orbital wavefunctions factor as

$$|\Psi\rangle = \frac{1}{\sqrt{2}}\left(e^{iS_\uparrow}\,|\uparrow\rangle + e^{iS_\downarrow}\,|\downarrow\rangle\right)\psi_\uparrow(\mathbf{r},t_f) \tag{8.3}$$

This places the system in the pseudo-spin state $\frac{1}{\sqrt{2}}(|\uparrow\rangle + e^{i\Delta S}\,|\downarrow\rangle)$ which allows us to measure $\Delta S = S_\uparrow - S_\downarrow$ though a single operator measurement such as $\hat{S}_y$.

As shown in the appendix, the first order phase due to the presence of an external force $\mathbf{g}(t)$ is $\exp(iS_\sigma) = \exp\left[i\frac{m}{\hbar}\int_{t_i}^{t_f}dt\,\mathbf{r}_\sigma(t)\cdot\mathbf{g}(t)\right]$, which is effectively the convolution of the particle's path and the external force $\mathbf{g}(t)$. In an interferometric measurement the phase difference between the two pseudo-spins is what is relevant.

This takes the form

$$\exp(iS_{\mathbf{g}}) = \exp\left[i\frac{m}{\hbar}\int_{t_i}^{t_f}\mathrm{d}t\left(\mathbf{r}_\uparrow(t) - \mathbf{r}_\downarrow(t)\right)\cdot\mathbf{g}(t)\right] \tag{8.4}$$

Which clearly depends only on the difference in the paths $\mathbf{r}_\uparrow$ and $\mathbf{r}_\downarrow$. There is also a higher order term in $g/l_o\omega^2$, where the harmonic oscillator length $l_o = \sqrt{\hbar/m\tilde{\omega}}$.

The mirror symmetry of the two trajectories will be broken if the $\pi/2$-pulse imparts a large momentum to the pseudo-spin $|\uparrow\rangle$. The effect of this symmetry breaking can be solved by either considering a radio frequency Rabi pulse, or two co-propagaing laser pulses. Radio frequency pulses are long wavelength, and therefore will transfer negligible momentum to the atom. A co-propagating two-photon transition will have $k_{eff} = k_1 - k_2$, which can be made small if the energy splitting of the ground states is sufficiently small.

It is of note that for $\mathbf{g}(t) = \text{const}$, this phase correction is independent of σ and the phase response is $\exp(iS_{\mathbf{g}}) = \exp\left[i\frac{m}{\hbar}\mathbf{g}\cdot\int_{t_i}^{t_f}(\mathbf{r}_\uparrow(t) - \mathbf{r}_\downarrow(t))\right]$, which is just the projection of the force $\mathbf{g}$ onto the average of the difference of the two classical paths. A spin polarization measurement can be used to extract this phase information in Eq. 8.3.

If the system is set up to measure weak, time-dependent, gravitational signals, the spin matrix that is used to make the measurement is relevant. For a small phase, a $\hat{S}_y$ spin measurement will be first order in the phase, whereas the phase will enter a $\hat{S}_x$ measurement at second order. It is thus necessary to chose the spin polarization measurement carefully.

To conclude this section, we can express the above set of operations, such as

(a)   (b)
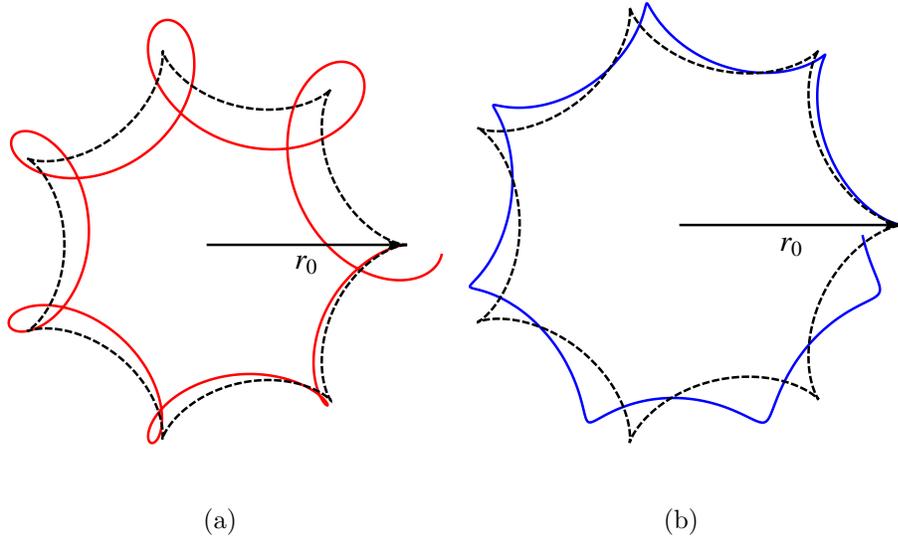
Figure 8.2 – The classical trajectories of a particle initially displace by $\mathbf{r}_0$ and the corresponding perturbed paths for a state with positive (Fig. 8.2(a)) or negative (Fig. 8.2(b)) effective charge. In both cases, the dashed black line is the unperturbed classical path, while the blue(red) line is the perturbed response for a particle with positive(negative) charge. For both plots, the ratio of the two classical frequencies is given by $\omega_+/\omega_- = 6$, and the gravitational perturbation is driving at a frequency of $\omega_g = 1.07\omega_+$. Note that the strength of the perturbation is exaggerated for effect, and larger than the upper bound on the measurable signal given by Eq. 8.15.

displacement, spin rotations, free evolution and a spin polarization measurement as the matrix elements of a quantum mechanical operator. Although the above process was straightforward, an operator description of the above process will make the description and calculation of more general pulse sequences straightforward. We can specifically represent the above pulse sequence as the unitary matrix

$$U_p = R_{\hat{y}}(-\pi/2)U(t)D[R\mathbf{r}_0]R_{\hat{x}}(\pi/2), \tag{8.5}$$

where the displacement vector $D[\boldsymbol{\alpha}]$ is defined in the appendix, and encodes the initial conditions $\mathbf{r}(0) = \mathbf{r}_0$ and $\dot{\mathbf{r}} = 0$, and the time evolution operator $U(t)$ can be found exactly. The expectation value in Eq. 8.6 is then given by $\langle S_z \rangle = \langle 0, \uparrow | U_p^\dagger S_z U_p | 0, \uparrow \rangle$ and can be shown to reproduce Eq. 8.6.

8.4 Response

We now find the response of our interferometer to an arbitrary time varying force. As is shown in the appendix, a spin rotation followed by a spin polarization will give

$$\langle S_z \rangle = \sin \left[2 \int_0^{t'} dt \, (\hat{z} \times \mathbf{r}_0) \cdot \mathbf{g}(t') \, h_\perp(t') \right], \tag{8.6}$$

where $h_\perp(t) = \frac{1}{2\bar{\omega}} (\omega_- \sin(\omega_+ t) - \omega_+ \sin(\omega_- t))$ is the component of motion in the direction perpendicular to the initial axis of displacement. For many purposes the response of the system to certain frequencies is the quantity of interest. To find the frequency response function, first consider the Fourier transform of the signal, $\mathbf{g}(t) = \int \frac{d\omega}{2\pi} e^{-i\omega t} \tilde{\mathbf{g}}(\omega)$. We can then switch the order of the ω and t integrals and perform the $\int_0^t dt$ integral. This allows us to express Eq. 8.6 as $\langle S_z \rangle = \sin \left[\int \frac{d\omega}{2\pi} \tilde{g}_\perp(\omega) F_0(\omega) \right]$
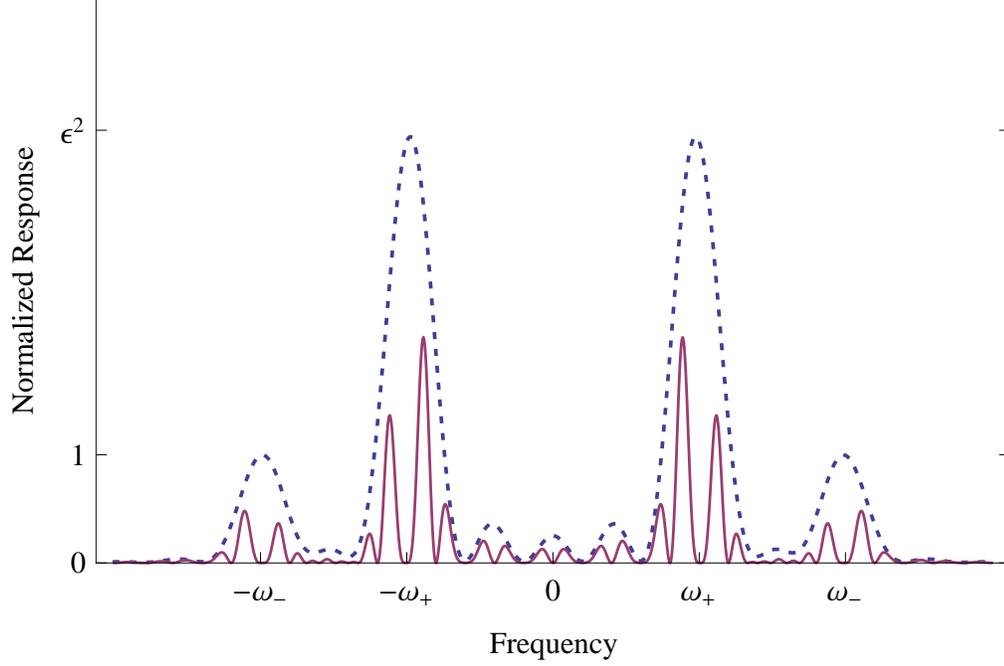
Figure 8.3 – The normalized response function for $\left|\frac{\tilde{\omega}F(\omega)}{r_0 t}\right|^2$ for the pulse sequence U_p, (dashed) or U_{CP}, the Carr-Purcell like pulse sequence (solid). For both sequences we used $t = \frac{10\pi}{\omega_+ + \omega_-} = \frac{5\pi}{\tilde{\omega}}$ and $\epsilon = \omega_+/\omega_-$. Note we have scaled the response for to the CP pulse sequence by a factor of 16 to account for the factor of four increase in interrogation time.

where and

$$F_0(\omega) = \frac{ir_0 t}{\tilde{\omega}} \sum_{\{\sigma, \tau = \pm 1\}} \sigma\tau\, \omega_{-\sigma}\, f(\omega + \tau\omega_\sigma) \tag{8.7}$$

is the full response function of the system. This has the form of a weighted sum of the single frequency response $f(\omega)$, defined by $f(\omega) = \frac{\sin(\omega t/2)}{\omega t/2} e^{-i\omega t/2}$. Note that $f(\omega)$ vanishes at $t = 0$, the lower limit of integration. If we started measurement at $t_i \neq 0$, an additional set of terms would appear in $F_0(\omega)$.

The behavior of the response function can be seen in Fig. 8.3. The peak response of the system is at the frequencies $\omega = \omega_\pm$ with relative peak amplitudes

136

of ω_-/ω_+. The bandwidth of the system varies with the inverse of the interrogation time, $1/t$, giving a large bandwidth for small measurement times. It can also be seen that $F_0(\omega)$ will have non-zero response at $\omega \to 0$, unless the classical frequencies and measurement time satisfy $\omega_+ t = m\pi$ and $\omega_- t = n\pi$, where n and m are integers. This condition can be seen as the constraint that the average time spent off the initial axis of displacement is zero. Intuitively this makes sense, as the average potential seen by either path vanishes, and therefore so does the phase. For some purposes this dc sensitivity is unwanted, however, chosing the classical frequencies so that the sensitivity can vanish may be difficult. Methods for eliminating this response will be discussed below.

8.5   Carr-Purcell and Time Reversal pulses

In order to make a measurement, it is necessary to wait until the orbital wavefunctions overlap as completely as possible. The coherent state waveufunction has a Gaussian profile so a measurement that occurs away from a point of classical overlap will yield $\langle S_z \rangle = e^{-\left(2\frac{r_0}{l_o}h_\perp(\Delta t)\right)^2} \sin\left[2\int_0^{\Delta t} dt\,(\hat{z} \times \mathbf{r}_0) \cdot \delta\mathbf{g}(t)\,h(t)\right]$, which is suppressed by a factor of $A = e^{-\left(2\frac{r_0}{l_o}h_\perp(t)\right)^2}$. This suppression factor will be significant if the system is measured at a time when the classical paths do not overlap. As discussed above, the only measurement points exist on the axis of displacement, but unless the classical frequencies are commensurate, the system will have non-zero dc sensitivity.

This dc sensitivity can be eliminated by using a "time-reversal" pulse. As

discussed in the appendix, a π-pulse, e.g. $R_{\hat{y}}(\pi)$, will act to interchange the two pseudo-spin states. The exchange of $\sigma \to -\sigma$ applied at special points on the classical trajectory will cause the spins to retrace their path, effectively as if the flow of time has been reversed. For the initial conditions given by the trap displacement, these points occur at times

$$t = \frac{2\pi n}{\omega_+ + \omega_-} = \frac{\pi n}{\tilde{\omega}}, \tag{8.8}$$

which can be seen as the cusps in the dotted lines of Figure 8.2. We see that if a time reversal pulse is applied at a time given by Eq. 8.8, then the particle will return to its starting position at a time $2t$. Since a π pulse will interchange both pseudo-spins, both paths will retrace their trajectory and then overlap at the origin.

It is obvious that a single π pulse applied at an arbitrary time given by Eq. 8.8 will have an average non-zero time above the origin, and therefore will have non-zero dc sensitivity. Thus, while a single π pulse can be used to guarantee overlap of the classical trajectories it cannot be used to cancel dc sensitivity. If dc sensitivity is not desired, a second π pulse can be applied at a time $3t$, and then a measurement can be made at a time $4t$. This pulse sequence is analogous to the Carr-Purcell sequence commonly used in NMR [77]. A sample classical trajectory of such a pulse can be seen in Fig. 8.4(a). It can be seen that dc signals will vanish, as the average time spent off of the initial axis is zero.

This pulse sequence has the additional benefit of acting to cancel noise, analogous to the cancellation of inhomogenous dephasing in spin-echo. Such a pulse sequence will act to reduce the effect of random noise, such as $1/f$ electronic noise.

The pulse will cancel the strong effective Zeeman field due to the energy splitting between the dark state and the low energy bright state used as pseudo spins. It will also cancel the weak (compared to the Zeeman splitting), off-diagonal scalar potential that arose in the synthetic magnetic field described in Sec. 3.3.

The operator formalism for calculating the path and classical trajectory now has a clear advantage over the path integral approach. The time evolution operator for a harmonic oscillator in the presence of a time-dependent force takes the form of a time-dependent displacement operator. Thus, the application of multiple time evolution operators sandwiched between time reversal pulses will take the form of a single displacement operator. This is in contrast to the path integral approach, where the propagator between time reversal pulses must be calculated and then an integration must be performed at each step. In what follows the operator formalism will be adopted exclusively.

In the operator language, the Carr-Purcell like pulse sequence can be expressed as

$$U_{CP} = R_{\hat{y}}(-\pi/2)U(4t, 3t)R_{\hat{y}}(\pi)U(3t, t)R_{\hat{y}}(\pi)U(t, 0)D[R\mathbf{r}_0]R_{\hat{y}}(\pi/2). \qquad (8.9)$$

where t is taken to be a special point where time where $R_{\hat{y}}(\pi)$ will time reverse the classical path, and $U(t_f, t_i)$ is the time evolution operator that advances the time from a time t_i to a time t_f, and satisfies the standard properties of the time evolution operator [5]. In the appendix it is shown that the time evolution operator in the presence of a driving term $\mathbf{g}(t)$ takes the form:

$$U(t, 0) = e^{-i\left(\omega_+ a_+^\dagger a_+ + \omega_- a_-^\dagger a_-\right)t} D[\boldsymbol{\gamma}(t)]e^{-i\phi_\gamma(t)}, \qquad (8.10)$$

where $D[\boldsymbol{\gamma}(t)]$ is a displacement operator to account for the driving of the gravitational field, and $e^{-u\phi_\gamma(t)}$ is a phase term that is second order in $\mathbf{g}(t)$, and is path independent. The time evolution between a time t_i and t_f can be found by using the identity $U(t_f, t_i) = U(t_f, 0)U^\dagger(t_i, 0)$.

The full evolution operator U_{CP} can now be calculated. It is found that the modified frequency response function is

$$F(\omega) = 2i\sin(\omega t)\left[F_0(\omega)e^{i\omega t} + F_0^*(\omega)e^{-i\omega t}\right]e^{i2\omega t} \tag{8.11}$$

where $F_0(\omega)$ is the response function given in Eq. 8.7. The complex conjugate term $F_0^*(\omega)$ arises due to the time reversal of the paths. This response function is plotted in Fig. 8.3. The new response function now vanishes at $\omega = 0$ and $\omega = \omega_\pm$, however we still have large sensitivity in the frequency range $\omega = \frac{1}{8}\frac{2\pi}{t}$ around $\omega_\pm$.

8.6 Experimental Setup

We now discuss the experimental details relevant to implement such a measurement device experimentally. The physics described in the toy model can be experimentally realized, at least approximately, in cold atom systems. As discussed in the introduction, there are several possible implementations of synthetic magnetic fields in cold atomic systems. Unfortunately, the only scheme to be experimentally realized to date [23] will not be sufficient, as the effective charges of the two pseudo-spin states do not have opposite signs. However, the scheme given in Ref. [4] does give a set of pseudo-spin states that couple to a synthetic field with equal and opposite charges in the large detuning limit. The two states do have a small energy

(a)   (b)
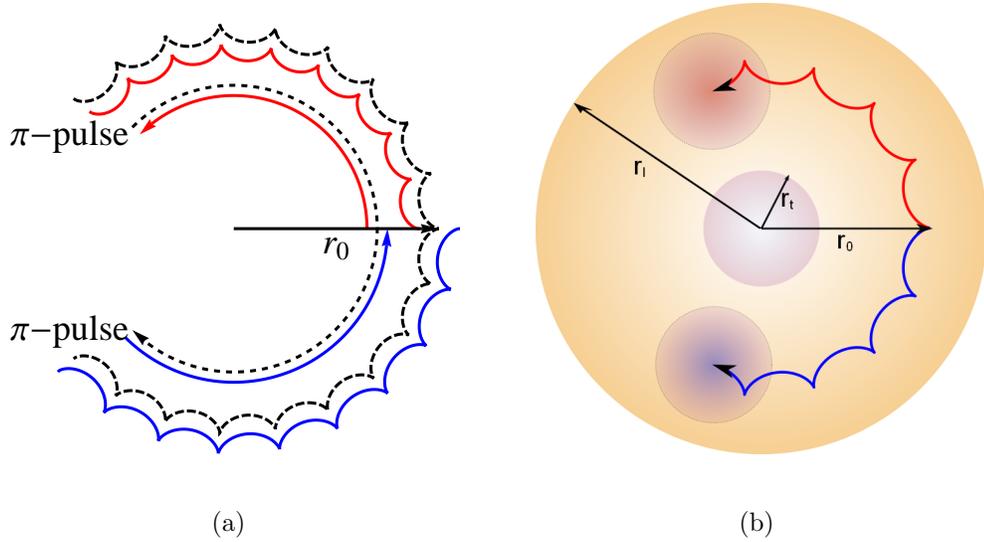
Figure 8.4 – 8.4(a) The classical path a particle will follow with the CP pulse sequence

given by Eq. 8.9. The red path corresponds to the initial free evolution for a time t.

The dashed path is the time reversed path allowed to evolve for a time $2t$. Finally, the

solid blue path is the return trajectory for another t. Note that the three trajectories

will overlap in practice, and have been offset just for a visual aid. The three arcs

correspond to the direction of motion of the classical trajectory. We have chosen

$\epsilon = \omega_+/\omega_- = 22$.

splitting that vanishes in the infinite detuning limit, $\Delta \to \infty$, but through the use

of a Carr-Purcell pulse sequence this energy splitting and phase will average to zero.

We note that the synthetic field in this scheme is not spatially uniform, but this

only adds technical complications and does not fundamentally change the ability for

such a system to make acceleration measurements.

We now must generalize our scheme to a many-atom scheme that is found

in an atom interferometer. The many-particle system of interest is a dilute cold

atoms, as opposed to a BEC. Using such a system allows atom-atom interactions

to be neglected, which could considerably alter the physics in a BEC. A thermal ensemble of cold atoms can be represented using the Glauber P representation [11], where the density matrix

$$\rho = \int \mathrm{d}\alpha \, e^{-|\alpha_+|^2/\langle n_+\rangle - |\alpha_-|^2/\langle n_-\rangle} \, |\alpha\rangle \, \langle\alpha| \tag{8.12}$$

is treated as a sum over coherent states, and $\langle n_i \rangle = [\exp[\hbar\omega_i/kT] - 1]^{-1}$ is the average occupation for the classical mode of frequency ω_i. The use of such a thermal ensemble will suppress the expectation value of the S_z operator by a factor $e^{-\langle n_+\rangle|\gamma_+|^2 - \langle n_-\rangle|\gamma_-|^2}$ relative to the single particle/zero temperature expectation value. The suppression factor $\gamma_\pm$ depends on the pulse sequence used. For example, using the pulse sequence U_p given above we get

$$
\begin{aligned}
\gamma_+ &= \frac{l_o}{2} \int_0^t \mathrm{d}t' \, (g_x + ig_y)e^{i\omega_+ t'}, &(8.13)\\
\gamma_- &= \frac{l_o}{2} \int_0^t \mathrm{d}t' \, (g_y + ig_x)e^{i\omega_- t'}. &(8.14)
\end{aligned}
$$

The frequency response of these suppression factors can most easily be understood by noting the fact that they form a basis for expression the phase response. In other words, the phase term $S_\mathbf{g} \sim \int \mathrm{d}t \, \mathbf{r} \cdot \mathbf{g}$ can be expressed as a superposition of γ_+ and γ_-. For the Carr-Purcell like pulse sequence the form of the suppression factor $\gamma_\pm$ is more complicated, but can it still forms a basis for which we can express the phase. This implies that $\gamma_\pm$ has a similar frequency dependence to $F(\omega)$. This also shows that a pulse sequence designed to eliminate this suppression will also result in a suppression of the signal. Fortunately, this suppression enters quadratically in the external field $\mathbf{g}$, whereas the phase response is first order in $\mathbf{g}$.

We are now in a position to discuss the measurement capabilities of such a system. We first estimate the maximum ac signal such a system can measure. As discussed before, weak ac signals will perturb the classical trajectories so they do not completely overlap. The response of the interferometer is therefore suppressed if the signal is too strong, which fortunately is an effect second order in the external field. It is shown in the appendix that the upper bound for the strength of an ac signal to avoid signal suppression due to the finite temperature is given by

$$g_{max} \leq \frac{1}{\sqrt{\langle n \rangle}} \frac{4\pi\hbar}{mr_0\tau}. \tag{8.15}$$

Assuming this is the maximum signal strength, it is then further shown in the appendix that the sensitivity for such a system is given by

$$S \sim \sqrt{\frac{1}{N\tau}} \frac{2\pi\hbar}{mr_0}, \tag{8.16}$$

where the lifetime of one measurement, $1/\tau = \gamma_{se} + \gamma_{coll}$ is limited by spontaneous emission, γ_{se} and collisions, γ_{coll}.

We see now that the sensitivity of the system depends on the geometry, the hold time, and number of repeated measurements, i.e. atoms. We desire to maximize the system's sensitivity to accelerations (or minimize S). The system has two competing time scales that limit the interrogation time of the atoms, the spontaneous emission rate, γ_{se}, and the collision rate, γ_{coll}. The spontaneous emission rate is independent of the number of atoms, but the collision rate depends on the temperature and number of atoms. Our system is further constrained by the "laser homogeneity" radius, r_l, for which non-linear variations in the laser fields are suppressed.

Taking these considerations into account we can now optimize the sensitivity of the detector. The following analysis is done for a $2D$ system. The effective $2D$ system will use an axial trapping potential of $\omega_\parallel \geq \ln(2)kT/\hbar$ to freeze all motion into a single transverse mode. Thus our system will have $N_l = r_l/d$ layers, where $d = \sqrt{\hbar/m\omega_\parallel}$, providing for an increase in sensitivity of $1/\sqrt{N_l}$. The radius r_l further constrains our sensitivity by bounding the maximum trap displacement by $r_0 = r_l - r_t$, where $r_t = \sqrt{\langle n \rangle}l_o \sim \langle v \rangle/\tilde{\omega}$ is the thermal radius of a thermal ensemble and $\langle n \rangle = kT/\hbar\omega$ and $\langle v \rangle = \sqrt{3kT/m}$ are the respective high temperature thermal occupation number and velocity. (Fig. 8.4(b))

The lifetime of the system will be dominated by spontaneous emission at low densities and collisions at high densities. To optimize the sensitivity we desire to place as many atoms per layer as possible. For a 2D system, the collisional scattering rate is given by $\gamma_{coll} = \frac{N_a \langle v \rangle a^2}{dr_t^2}$, where a is the interparticle scattering length. As the number of atoms increases, the collisional lifetime will decrease until it is equal to the spontaneous emission lifetime, with the crossover happening at $N_c = \frac{\langle v \rangle a^2}{\gamma_{se} dr_t^2}$. At low atom number the sensitivity of the system will decrease with $1/\sqrt{N_a}$ due to the statistical enhancement of the signal to noise ratio. However, above N_c, the $1/\sqrt{N_a}$ gain in sensitivity will begin to counteracted by by a $\sqrt{\tau}$ loss in sensitivity due to the shortened lifetime of the system. In this limit the sensitivity becomes independent of the number of atoms and the sensitivity can be maximized by tuning the trapping frequency to $\omega_{min} = 2\langle v \rangle/r_l$. Note that while the sensitivity of the detector will not be affected by adding more atoms in the large atom limit, the decrease in interrogation time will increase the bandwidth. (See Fig. 8.5(b).) Thus,

the bandwidth can be tuned without a loss in sensitivity in the large atom number limit.

We now estimate the sensitivity of a potential experiment. We will consider a cold gas of ^{87}Rb cooled to $T = 1\mu$K with a frequency scale $\tilde{\omega} = 2\pi$kHz and an axial confinement distance of $d = 1\mu$m. At these temperatures the gas is non-degenerate and is described well by a classical gas. For this temperature we estimate an upper bound of $g \sim 10^{-2}$m/s^2 before exponential suppression of the signal above becomes relevant. We take the spontaneous emission rate to be $\Gamma_{se} = 1/70$ms [26] and laser inhomogeneity radius to be $r_l = 10 - 25\mu$m. In the $N_a \gg N_c$ limit we estimate the sensitivity to be

$$S \sim 10^{-7} \frac{\text{m/s}^2}{\sqrt{\text{Hz}}}.$$ (8.17)

A similar analysis for a $3D$ system gives a sensitivity drop of approximately an order of magnitude. We note that had we instead used a fermionic species we would obtain a similar result since we have two spin species.

8.7 Conclusion and Discussion

In conclusion, we proposed a new method of atom gravimetry that uses the pseudo-spin states of a synthetic magnetic field to continuously couple spin and position. The continuous coupling generates a sensitivity to time-dependent signals on frequency scales that are much shorter than the long time scales a traditional atom interferometer can measure. We then show that noise can be reduced by using time-reversal-like pulses. Finally, the experimental feasibility of such a system is
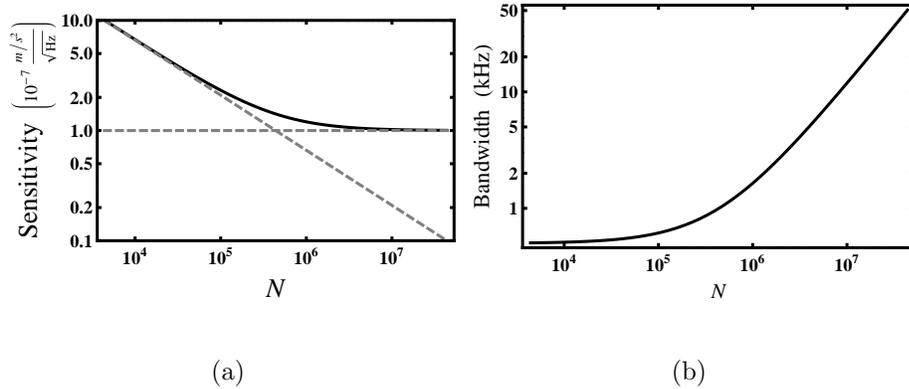
Figure 8.5 – 8.5(a) The dependence of the sensitivity of the system based upon atom number. Below $N_c \sim 10^6$ the sensitivity grows as $\frac{1}{\sqrt{N/N_c}}$. Above N_c the sensitivity $S \sim 10^{-7} \mathrm{m/s^2}/\sqrt{\mathrm{Hz}}$ is independent of the number of particles. 8.5(b) The bandwidth of the system with optimal sensitivity as a function of the number of particles.

considered and the sensitivity is estimated as $S \sim 10^{-7} \mathrm{m/s^2}/\sqrt{\mathrm{Hz}}$. This scheme uses trapped atoms, so it can be naturally implemented on an atom chip.

The concept of a continuous coupling of spin to momentum can also be extended to a continuous coupling of spin and position. We note that in a harmonic trap position and momentum are dual variables, and thus a spin-dependent term in the Hamiltonian that has spatial variation will experience a similar phase accumulation to the system described above. An example would be trapped spin-1 system in the presence of a Zeeman field with a strong spatial variation. In such a system the Zeeman field will act to trap (anti-trap) the $S_z = +1$ and $S_z = -1$ spin states with different trapping potentials. This will play a similar role to the opposite charge couplings to gauge fields given above. However, such a system requires strong magnetic field gradients so it may be impractical. An even simpler generalization of the

ac interferometry scheme could involve two spin states given initial opposite angular momentum around the trap center.

Finally, we note that this system is not limited to measurements of ac signals. Through appropriate modifications of pulse sequences, such a scheme is capable of measurements of dc gravity, gravitational gradients and rotations. Due to electronics noise, the sensitivity of these systems will be significantly lower than existing atom interferometers. However, for some applications they may still be useful due to the ability to place the system on a chip.

Chapter 9

Bulk Spin-Hall Effect

9.1 Introduction

One of the goals of spintronics [42, 43] is to generate spin polarization and transport in semiconducting systems using electric fields. As discussed in Chapter 5, the existence of spin-orbit coupling has allowed for a class of anomalous spin transport mechanisms such as the spin-Hall effect [45, 46, 47, 78, 79], the manifestation of which is spin accumulation on the boundaries of the system. Thus, from an experimental perspective, the spin-Hall effect is a edge phenomena whose manifestation is strongly dependent on boundary conditions. The role of the edge is to create a strong inhomogeneity where a spin density can accumulate. However, if a long length scale inhomogeneity was created in the bulk, by analogy with the edge spin-Hall effect, a spin accumulation would appear. For example, a sinusoidal charge/spin density wave would effectively create multiple boundaries in the bulk to induce a manifestation of the bulk direct/inverse spin-Hall effect.

In this chapter we predict a new manifestation of the inverse spin-Hall effect based upon the work of Koralek et. al. This work was done in collaboration with Tudor Stanescu and Victor Galitski, and was motivated by discussions with Joe Orenstein [57]. This work is similar to the previous sections in that it is driven by spin-orbit coupling. However, the spin-orbit coupling arises as a relativistic

correction that is a result of inversion asymmetry in the crystal structure of the semiconductor. This is in contrast to the previous sections where the effective spin-orbit coupling of atoms arose from an optically induced synthetic field.

The transient spin grating (TSG) technique [80, 81, 82] can be used to induce a sinusoidal spin polarization wave in the bulk, as well as monitor time dependent spin and charge profiles. Within the TSG method, a sinusoidal spin-polarization wave is generated by two interfering non-collinear laser beams with orthogonal linear polarization. This induces a modulation in the index of refraction, which can be measured at subsequent times by the diffraction of a probe pulse. The spin grating acts as a periodic boundary in the bulk of the system; it is expected that a spin-orbit coupled system in the presence of an external electric field oriented perpendicular to the spin polarization-wave-vector will develop a charge density wave with the same wave vector (see Fig. 9.1). Alternatively, if a charge density wave were induced, a corresponding spin modulation would develop.

We develop the theory of the bulk spin-Hall effect in the diffusion limit, in the presence of Rashba [29] and (linear and cubic) Dresselhaus [44] spin-orbit interactions. We focus on the time evolution of a charge density profile induced by an optically generated spin-polarization wave and its dependence on the spin-orbit couplings and on the spin-grating wave-vector. In particular, we determine the optimal parameters for observing the spin-Hall effect with spin gratings. These optimal parameters result from a balance between two competing requirements: 1) to create slowly decaying spin-polarization waves, and 2) to have a strong spin-charge coupling. The first requirement is related to the more general challenge in the field

of spintronics of identifying mechanisms allowing for long spin relaxation times. In the presence of disorder, spin-orbit interactions lead to spin relaxation through the Dyakonov-Perel mechanism [49]. Recently, it was shown that an enhanced spin life time can be realized by tuning the spin-orbit coupling so that the Rashba and the linear Dresselhaus couplings become equal [83, 56, 57, 53, 84]. In this regime, SU(2) spin symmetry is restored, allowing for a long lifetime helical spin density mode [83] termed the "persistent spin helix"[56], provided that the cubic Dresselhaus contribution can be minimized [85]. However, in the persistent spin helix regime the coupling between the spin and the charge channels vanishes and the spin Hall effect cannot be observed. Hence, the second requirement, a strong spin-charge coupling is needed.

9.2   Spin-Charge Diffusion Equations

We consider a two-dimensional electron gas in a III-V type semiconductor quantum well grown along the [001] axis (set as the $\hat{z}$-axis). The spin-orbit coupling Hamiltonian describing the conduction band electrons is $\mathcal{H}_{so} = \mathbf{h}(\mathbf{p}) \cdot \hat{\boldsymbol{\sigma}}$, where $\mathbf{h}(\mathbf{p}) = (h_x, h_y)$ is the momentum-dependent effective "magnetic" field which has contributions due to the Rashba [29], linear and cubic Dresselhaus [44] spin-orbit interaction of the form $\mathbf{h}^R(\mathbf{p}) = \alpha v_F(-p_y, p_x)$, $\mathbf{h}^{D_1}(\mathbf{p}) = \beta_1 v_F(p_x, -p_y)$ and $\mathbf{h}^{D_3}(\mathbf{p}) = -4\beta_3 \frac{v_F}{p_F^2}(p_x p_y^2, -p_y p_x^2)$, respectively. Here v_F and p_F are the Fermi velocity and momentum, respectively, and the coupling constants α, β_1 and β_3 measure the strength of the spin-orbit interaction relative to the Fermi energy.
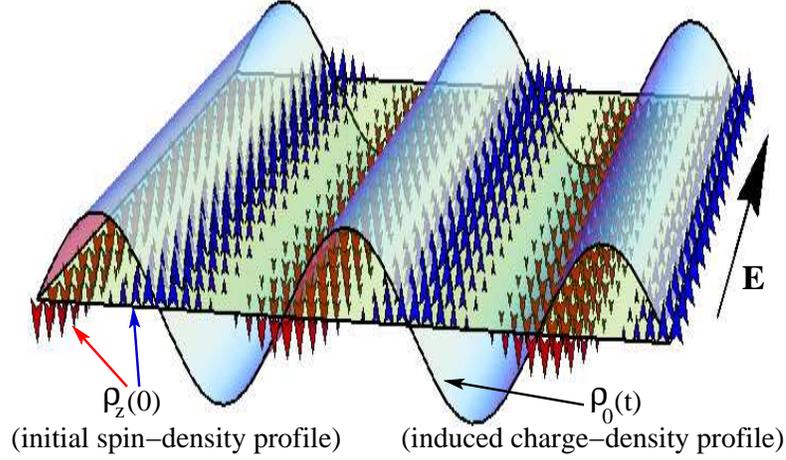
Figure 9.1 – Charge-density profile induced by the relaxation of a spin-density wave in the presence of a uniform electric field. The initial spin density corresponds to a sinusoidal wave with wave-vector $\mathbf{q}$ of the out-of-plane S_z component, as symbolized by the blue (spin up) and red (spin-down) arrows. The in-plane electric field is oriented perpendicular to $\mathbf{q}$. Notice the $\frac{\pi}{2}$ shift of the induced charge-density profile relative to the spin-density wave.

In the presence of disorder, the coupled spin and charge dynamics can be described by a generalized diffusion equation, which in the absence of an external electric field has the form [86, 85]

$$(\partial_t - \mathcal{D}\nabla^2)\rho_i = (\Gamma^{ij} - P^{ijk}\partial_k + \mathbf{C}^{ij} \cdot \nabla)\rho_j, \tag{9.1}$$

where ρ_0 is the charge density and $\rho_{1,2,3} \equiv \rho_{x,y,z}$ are spin densities. The parameters Γ^{ij} describe the Dyakanov-Perel spin relaxation [49], $\mathcal{D} = \tau v_F^2/2$ is the diffusion constant, with τ the mean scattering time, $P^{ijk} = -P^{jik}$ characterize the precession of the spin polarization and $\mathbf{C}^{ij}$ describe the coupling between the spin and charge degrees of freedom. In momentum space, the diffusion equation becomes

$\left[\delta_{ij} - \hat{\Pi}_{ij}(\omega, \mathbf{k})\right] \rho_j = 0$, where $\hat{\Pi}_{ij}$ have coefficients given by Γ^{ij}, P^{ijk} and $\mathbf{C}^{ij}$ [85]. The formal solution of the diffusion equation is $\rho_i(\mathbf{r}, t) = \int d\mathbf{r}' D_{ij}(\mathbf{r}, \mathbf{r}', t)\rho_j(\mathbf{r}', 0)$, where $\rho_i(\mathbf{r}, 0)$ is the initial spin-charge distribution and $\hat{D} = [\hat{1} - \hat{\Pi}]^{-1}$ is the Green's function of the diffusion equation.

The generalization of the spin-charge diffusion formalism developed in Ref. [85] for the case of a uniform electric field amounts to the formal substitution

$$\nabla \rightarrow \nabla + \mu \boldsymbol{E}/2\mathcal{D}, \tag{9.2}$$

where E is a uniform electric field and μ is the mobility of the two-dimensional electron gas. Note that, neglecting the spin-charge coupling, this substitution generates the standard drift-diffusion equation for the charge channel, while the description of the spin sector is in agreement with a semi-classical kinetic theory of electron spin transport derived using the Keldysh Green's function formalism [87, 88]. The substitution (9.2) is valid as long as non-linear contributions of order $\mathcal{O}(E^2)$ are small and assuming that the effects of the electron-electron Coulomb interaction can be neglected. Without loss of generality, we focus on the geometry corresponding to Fig. 9.1 and consider a system with an initial out of plane spin-density wave (SDW), $\rho_z(r, 0) = n_0\cos(qr_+)$, oriented along the [110] direction ($\mathbf{e}_+$) and a weak constant electric field, $\mathbf{E} = E_0\mathbf{e}_-$, oriented along $[1\bar{1}0]$ ($\mathbf{e}_-$). In momentum space, the substitution (9.2) becomes $\mathbf{k} \rightarrow \mathbf{k} - i\mu\mathbf{E}/\mathcal{D}$ and the inverse of the Green's function

is

$$
\hat{1} - \hat{\Pi}(\omega, q) =
\begin{pmatrix}
s - 1 & i\lambda_- \tilde{E} & \lambda_+ q & 0 \\
i\lambda_- \tilde{E} & s - \frac{\gamma_R \gamma_D}{2} & 0 & -i\gamma_+ q \\
\lambda_+ q & 0 & s + \frac{\gamma_R \gamma_D}{2} & -\gamma_- \tilde{E} \\
0 & i\gamma_+ q & \gamma_- \tilde{E} & s + 1
\end{pmatrix},
\tag{9.3}
$$

where $\tilde{E} = \mu E L_s / 2\mathcal{D}$ is a dimensionless measure of the electric field strength and

$s = -i\omega(q) + q^2 + 1$. All lengths are measured in units of spin relaxation length,

$L_s = 1/2 p_F \Delta$ and times in units of spin relaxation time, $\tau_s = 2\tau/g^2\Delta$, where

$\Delta = (\alpha^2 + (\beta_1 - \beta_3)^2 + \beta_3^2)^{1/2}$ and $g = 2 v_F p_F \tau$ is a dimensionless conductance. The

spin-spin coupling parameters [85], $\gamma_\pm = \gamma_R \pm \gamma_D$, with $\gamma_R = 2\alpha/\Delta$ and $\gamma_D =$

$2(\beta_1 - \beta_3)/\Delta$, are independent of the overall strength of the spin-orbit interaction

$\Gamma = (\alpha^2 + \beta_1^2 + \beta_3^2)^{1/2}$ and lie within a disc of radius 2. The spin-charge coupling

parameters [85], $\lambda_\pm = \lambda_1 \pm \lambda_2$, with $\lambda_1 = [(3\beta_3 - \beta_1)(\alpha^2 - \beta_1^2 + \beta_3^2) - \beta_1\beta_3^2]/\Delta$ and

$\lambda_2 = \alpha(\alpha^2 - \beta_1^2 + 6\beta_3^2)/\Delta$, are quadratic in the spin-orbit interaction strength.

9.3   Charge Density Wave

The induced charge density $\rho_0(\mathbf{r}, t)$ is determined by the matrix element $D_{03} = $

$\sum_{l=0}^{3} A_l(\mathbf{q}) e^{-i\omega_l(\mathbf{q})t}$ of the inverse Green's function. Here $i\omega_l(\mathbf{q})$ are the relaxation

modes obtained from the equation $\det\left[\hat{1} - \hat{\Pi}(\omega, \mathbf{q})\right] = 0$ and $A_l(\mathbf{q})$ are momentum-

dependent amplitudes. To order $\mathcal{O}(\tilde{E}^2)$ the relaxation times are independent of the

electric field, while the amplitudes have a linear dependence, $A_l(\mathbf{q}) = i(\mu E/v_F) q \tilde{A}_l(q)$,

with $\tilde{A}_l(q)$ being an even function of momentum and $q = \mathbf{q} \cdot \mathbf{e}_+$. Note that, if one

initially generates a charge density profile, the external electric field induces a spin
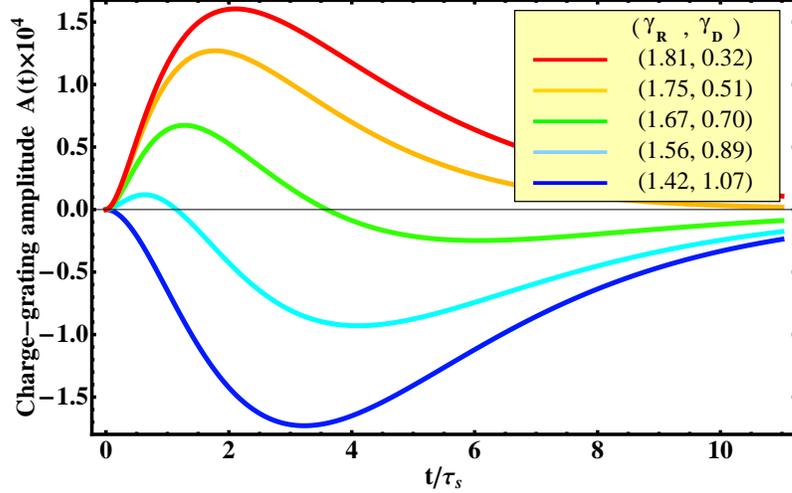
Figure 9.2 – Time dependence of the induced charge-density waveamplitude A(t) for various values of the dimensionless spin orbit coupling parameters (γ_R, γ_D), for an spin-orbit coupling strength $\Gamma = .001$. The wave-vector $\mathbf{q} \parallel \mathbf{e}_+$ has a fixed value, $q = 0.6/L_s$. The amplitude of the induced wave varies non-monotonically and is characterized by a peak value A_{max} and an exponential decay at large times.

wave with a spatial and time dependence determined by $\hat{D}_{30} = -\hat{D}_{03}$. Hence the present analysis applies to both the direct and the inverse spin Hall effect. Explicitly, an initial out-of-plane spin density wave $\rho_z(r, 0) = n_0 \cos(qr_+)$ induces a time-dependent charge density wave

$$\rho(\mathbf{r}, t) = n_0 \sin(qr_+)\frac{\mu E}{v_f} \sum_{l=0}^{3} q\tilde{A}_l(q)e^{-i\omega_l(q^2)t} \tag{9.4}$$

Note that the induced charge density wave (CDW) is phase shifted by $\pi/2$ relative to the initial SDW (see Fig. 9.1) and has a time dependent amplitude $n_0(\mu E/v_F)A(t)$ where $A(t) = \sum_{l=0}^{3} q\tilde{A}_l(q)e^{-i\omega_l(q^2)t}$. The general behavior of the induced CDW amplitude $A(t)$ is shown in Fig. 9.2. At $t = 0$ the amplitude of the CDW vanishes, as the system is initially uniform, while at long times $A(t)$ decays exponentially with

a characteristic lifetime $1/(i\omega_l(q))$ given by the lowest frequency relaxation mode. At intermediate times of order τ_s the CDW amplitude has one maximum and/or one minimum. The largest absolute value defines the peak amplitude A_{max}.

The strength of the Rashba and Dresselhaus spin-orbit interaction in GaAs quantum wells can be adjusted by varying the doping asymmetry or the width of the quantum wells. Values in the range of $\alpha = 0.5 \times 10^{-3}$ to $\alpha = 1.5 \times 10^{-3}$ and $\beta_1 = 1 \times 10^{-3}$ to $\beta = 3 \times 10^{-3}$ with $\beta_3 = 0.3 \times 10^{-3}$ [57] can be experimentally achieved, thus most of region in the vicinity of the boundary of the radius 2 disc in the (γ_R, γ_D) parameter space can be probed. Scaling α, β_1 and β_3 equally will not change the spin-spin couplings γ_R or γ_D, but it will change the spin-charge couplings λ_+ and λ_- which are quadratic in the overall spin-orbit coupling strength Γ. The amplitudes $\tilde{A}_l(q)$ depend linearly on λ_+ and λ_- with higher order corrections of order $\lambda_{\pm}^3$. Thus for experimentally realizable two-dimensional spin-orbit interacting electron systems characterized by $\Gamma \ll 1$, the higher order corrections due to the spin-charge couplings are negligible and the amplitude $A(t)$ is approximately linear in the spin-charge couplings. Since the factor of q in $A(t)$ gives a contribution of $1/\Gamma$, as the wave-vector is measured in units of $1/L_s$, we conclude that the amplitude $A(t)$ of the induced CDW depends linearly on the overall spin-orbit interaction strength Γ. This proportionality relation holds as long as we express the wave-vector in units of $1/L_s$. Furthermore, we find that the induced CDW amplitude $A(t)$ is independent of the dimensionless conductance g, provided time is measured in units of $1/\tau_s$. Consequently, the bulk manifestation of the spin-Hall effect proposed here, can be enhanced by reducing the carrier density of system, which will increase the
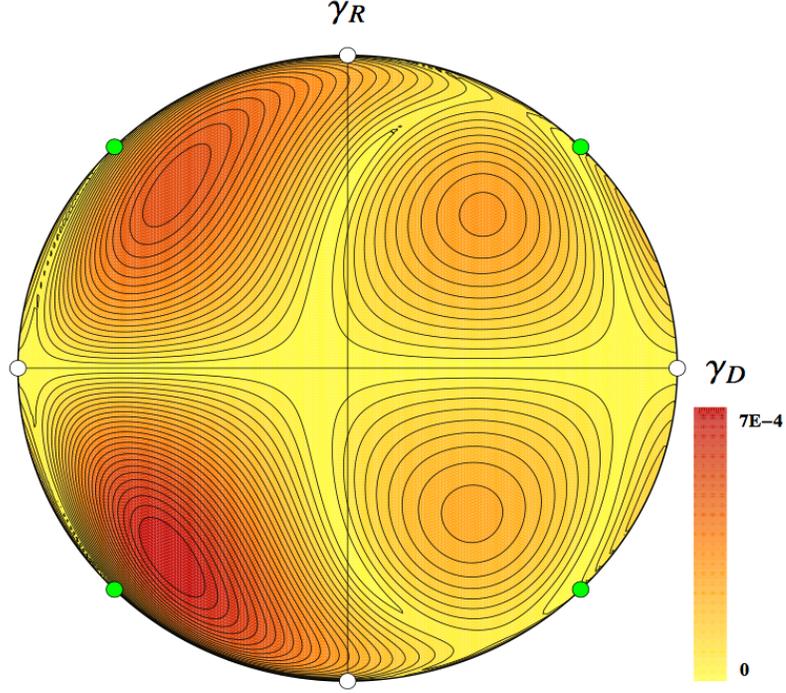
Figure 9.3 – Dependence of the absolute value of the peak amplitude A_{max} on the spin-orbit parameters (γ_D, γ_R) for a fixed value of the overall spin-orbit interaction strength, $\Gamma = .001$, and $q = 0.7/L_s$. A_{max} vanishes for pure Dresselhaus spin-orbit coupling, $\gamma_R = 0$ (horizontal axis and horizontal pair of white dots), pure Rashba coupling, $(\gamma_D = 0, \gamma_R = \pm 2)$ (vertical pair of white dots), and at the symmetry points $(\gamma_D = \pm\sqrt{2}, \gamma_R = \pm\sqrt{2})$ (green dots). The maximum of the peak amplitude corresponds to $(\gamma_D, \gamma_R) = (-1.08, -1.25)$ (inside the lower left quarter of the parameter space, $A_{max} = 7.8 \times 10^{-4}$), while three other local maxima are located at $(\gamma_D, \gamma_R) = (-1, 1.24)$ (upper left quarter, $A_{max} = -5.5 \times 10^{-4}$), $(0.80, 1.06)$ (upper right, $A_{max} = 3.2 \times 10^{-4}$), and $(0.76, -0.98)$ (lower right, $A_{max} = -2.8 \times 10^{-4}$). All these maxima involve large relative contributions of the cubic Dresselhaus coupling, $\beta_3/\Gamma = 0.5 \div 0.68$.

ratio between the strength of the spin-orbit interaction and the Fermi energy.

Next, we study the dependence of the induced charge density wave amplitude on the ratio between various components of the spin-orbit interaction for a fixed value of the overall spin-orbit coupling strength Γ. Fig. 9.3 shows the maximum amplitude of the CDW, A_{max}, for the experimentally relevant spin-orbit coupling strength $\Gamma = 0.001$ and wave-vector $q = 0.7/L_s$. The peak amplitude vanishes for pure Dresselhaus spin-orbit coupling, $\gamma_R = 0$, pure Rashba coupling, $(\gamma_D = 0, \gamma_R = \pm 2)$, and at the symmetry points $(\gamma_D = \pm\sqrt{2}, \gamma_R = \pm\sqrt{2})$ which support the persistent spin helix modes (see Fig. 9.3). This is consistent with previous results showing that, at least in uniform and stationary conditions, the spin Hall conductivity in systems with pure Rashba or pure linear Dresselhaus spin-orbit interaction vanishes [89, 90, 91, 92]. Our analysis reveals the absence of any manifestation of the spin-Hall effect for these types of spin-orbit interactions in non-uniform systems and under time-dependent conditions. The absolute maximum of the peak amplitude, $A_{max} = 7.8 \times 10^{-4}$, is realized for $(\gamma_D, \gamma_R) = (-1.08, -1.25)$. The corresponding original spin-orbit couplings are $(\alpha, \beta_1, \beta_3) = (-7.4, 0.3, 6.7) \times 10^{-4}$. Several other local maxima (minima) can be identified throughout the parameter space (see Fig. 9.3). To enhance the peak amplitude of the induced charge profile, one has to consider systems with strong cubic Dresselhaus spin-orbit coupling. This condition is opposite to that required for the realization of the persistent spin helix mode [85, 57]. Note that the diagram in Fig. 9.3 has no particular symmetry, as a result of the nontrivial dependence of the spin-charge coupling parameters $\lambda_\pm$ on the spin-orbit couplings.
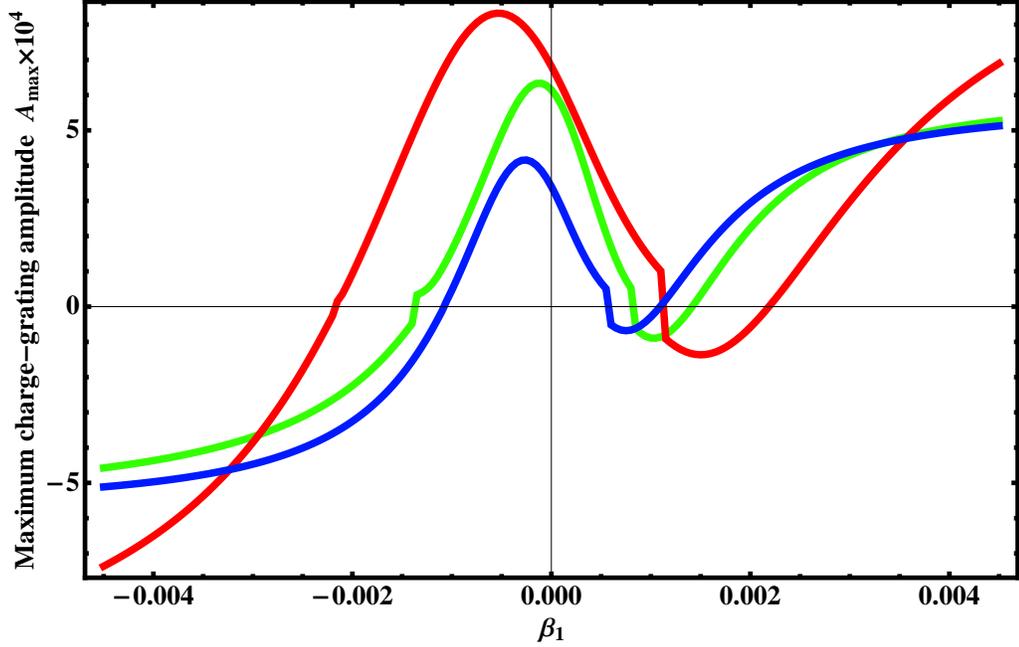
Figure 9.4 – Dependence of the peak amplitude on the linear Dresselhaus coupling for various values of the cubic Dresselhaus and Rashba couplings. The arrows mark the values of β_1 where the A_{max} changes from an absolute minimum of $A(t)$ to an absolute maximum (cf. Fig. 9.2).

We consider now the case of a fixed cubic Dresselhaus coupling in the range $\beta_3 = 2 \times 10^{-4} \div 4 \times 10^{-4}$, which is experimentally relevant for GaAs quantum wells. The dependence of the peak amplitude on the tunable parameters α and β_1 is shown in Fig. 9.4. We stress that both the absolute value and the sign of the spin-orbit coupling constants are important in determining the strength of the spin-Hall effect. Finally, we note that the peak amplitude also depends on the wave-vector q. A_{max} vanishes in the limits $q \to 0$ and $q \to \infty$ and is maximized in the range $0.5 \leq qL_s \leq 0.7$. Increasing the spin-orbit interaction strength enhances the bulk spin-Hall effect, provided it is observed at larger wave-vector values.

For completeness we note that, if the initial spin-density waves have an arbitrary orientation of the q-vector, a CDW is induced even in the absence of an external electric field. However, this wave is in-phase with the initial spin wave. Adding an external electric field perpendicular to the wave-vector induces an additional charge density component characterized by a $\pi/2$ phase shift, as described above, and causes the spin and charge profiles to drift along a direction parallel to the q-vector, i.e., perpendicular to the electric field. The induced CDW has the form

$$
\begin{aligned}
\rho(\mathbf{r}, t) &= n_0 \sum_{l=0}^{3} e^{-i\omega_l(\mathbf{q})t} \left\{ a_l(\mathbf{q}) \cos\left[\mathbf{q}\cdot\mathbf{r} + \left(\mathbf{q}\times\tilde{\mathbf{E}}\right)_z \tilde{\Omega}_l(\mathbf{q})t \right] \right. \\
&\quad + \left. \left(\mathbf{q}\times\tilde{\mathbf{E}}\right)_z \tilde{A}_l(\mathbf{q}) \sin\left[\mathbf{q}\cdot\mathbf{r} + \left(\mathbf{q}\times\tilde{\mathbf{E}}\right)_z \tilde{\Omega}_l(\mathbf{q})t \right] \right\},
\end{aligned}
\tag{9.5}
$$

where $a_l(\mathbf{q})$ are the amplitudes of the in-phase charge component and $\omega_l(\mathbf{q})$ are the corresponding frequencies. The electric field induces out-of-phase waves with amplitudes $\tilde{A}_l(\mathbf{q})$ and generates oscillatory components of the relaxation modes proportional to $\tilde{\Omega}_l(\mathbf{q})$.

9.4 Conclusion

In summary, we show that a non-homogeneous spin-orbit interacting system supports bulk manifestations of the spin-Hall effect. By extending the spin-charge diffusion equations to the case of a constant electric field we find that a spin-density wave allowed to relax in the presence of an external electric field induces a charge density wave that is characterized by the same wave-vector as the spin-density wave but has a phase shift of $\pm\pi/2$. The amplitude of the induced charge-density wave

varies non-monotonically in time and is characterized by a peak value and an exponential decay at large times. We show how to maximize the effect by tuning the relative strengths of the spin-orbit interactions. Finally, we mention that similar non-homogeneous perturbations may lead to bulk manifestations of the topological quantum spin-Hall effect [93, 94] in spin-orbit interacting insulators [95].

Chapter 10

Conclusion

In this dissertation we have presented a series of experimental proposals related to the field of spintronics and spin-orbit coupling. In the first proposal we considered the effects of a synthetic spin-orbit coupled pseudo-spin-1/2 degree of freedom induced by an optically induced non-Abelian gauge field. The spin-orbit interaction couples spin and momentum to generate a momentum space double well structure in the single particle energy spectrum. The minima of the double wells is degenerate due to a time-reversal-like symmetry. If the many-body Hamiltonian preserves this symmetry the many-body ground state must also be degenerate, as is the case for density-density interactions. We then consider the low temperature ground state for a many-body system of Bosons, where condensation is expected to take place. In the limit of vanishing interactions, the many body ground state wavefunction is found to be a superposition of all particles in the left well, and all particles in the right well. Such a state is known as a $N00N$ state, and has potential applications for interferometry and metrology. Finally, we give an experimental signature of a double well condensate that can be observed using time-of-flight imaging. It is found that the different momentum components will result in different peaks in a time-of-flight image.

We then discuss the semiclassical dynamics of a trapped spin-orbit coupled

system. Non-linear dynamics are found for a system that is initially trapped and displaced. We classify the dynamics of the system based on the anisotropy of the spin-orbit dispersion, and the magnitude of the initial displacement. In the presence of a pseudo-spin Zeeman field the system can acquire a Berry's phase. We propose an experiment to measure this phase using a system of pancakes formed from a strong axial trapping lattice.

We propose a generalized spin-orbit coupling based upon the 4-level scheme. It is found that by adding next-nearest-neighbor couplings, a $3D$ spin-orbit coupling can be generated. For certain configurations of the optical fields it is found that a full $3D$ spin-orbit coupling can be induced. This spin-orbit coupling can be shown to be described by a vector potential that is proportional to the angular momentum operator in pseudo-spin space.

In the third proposal, we use an optically induced synthetic magnetic field to generate two pseudo-spin states, each of which is coupled to an effective magnetic field, but with opposite charges. We consider a toy model for this Hamiltonian, and demonstrate the ability of such a setup as an atom interferometer capable of measuring time-dependent accelerations. The synthetic gauge field can be thought of as continuously imparting an acceleration dependent phase on each of the spins. Time reversal like pulses are used to reduce noise. The response function for the system with and without time reversal pulses is calculated. The sensitivity of such a system is estimated to be $S \sim 10^{-7} \frac{\mathrm{m/s^2}}{\sqrt{\mathrm{Hz}}}$.

Finally we propose a bulk manifestation of the spin-Hall effect. We first extend the spin-charge diffusion equations to the case of arbitrary Rashba and linear and

cubic Dresselhaus spin orbit couplings. Using the spin-charge diffusion equations it is found that if the wavevector of the spin-density wave is oriented perpendicular to an applied electric field, then a charge-density wave will be induced. The charge-density wave is phase shifted by $\pi/2$ relative to the charge-density wave, and has a time-dependent amplitude that decays at long times. The values of the spin-orbit coupling parameters are found for which the effect will be maximized. The ability to create bulk spin or charge densities will open the door for new spintronic devices.

Appendix A

Exact solutions to the Toy Model Hamiltonian from Ch. 8

A.1 Path Integral Approach

In this section we use the path integral approach [5] to derive the exact quantum wave function and phase evolution in the toy model given by Eq. 8.1. Using this formalism we will show that the wavefunction evolves as $\psi(\mathbf{r}, t = 0) = \psi(\mathbf{r} - \mathbf{r}_{cl}(t), t)e^{i\phi_g(t)}$, where $\mathbf{r}_{cl}(t)$ is the classical trajectory of the quantum particle, and $\phi_g(t)$ is the first order phase acquired due to the gravitational force the particle experiences.

To begin, take the expression for the propagator written using the configuration space path integral:

$$\langle \mathbf{r}_f, t_f | \mathbf{r}_i, t_i \rangle = \int_{\mathbf{r}[t_i]}^{\mathbf{r}[t_f]} \mathcal{D}[\mathbf{r}[t]] e^{\frac{i}{\hbar} S[\mathbf{r}(t), \dot{\mathbf{r}}(t)]}, \tag{A.1}$$

where

$$S[\mathbf{r}(t), \dot{\mathbf{r}}(t)] = \int_0^t dt \left(\frac{1}{2} m \dot{\mathbf{r}}^2(t) - \frac{1}{2} m \omega_0^2 \mathbf{r}^2(t) + m \omega_c x \dot{y} + m \mathbf{g}(t) \cdot \mathbf{r} \right) \tag{A.2}$$

is the classical action for the path $\mathbf{r}(t)$ corresponding to the Hamiltonian in Eq. 8.1. We can solve the path integral exactly by using the method of steepest descent [69, 96] and expand the action as

$$S = S_0 + \frac{\delta S}{\delta \mathbf{r}} \cdot \delta \mathbf{r} + \frac{\delta^2 S}{\delta \mathbf{r}_i \delta \mathbf{r}_j} \delta \mathbf{r}_i \delta \mathbf{r}_j \tag{A.3}$$

where the series exactly terminates after the second order term because the action is at most quadratic in $\mathbf{r}(t)$. The method of steepest descent involves setting $\frac{\delta S}{\delta \mathbf{r}} = 0$ which gives the classical equations of motion $\frac{d}{dt}\left(\frac{\delta L}{\delta \mathbf{r}}\right) - \frac{\delta L}{\delta \mathbf{r}} = 0$ where $L[\mathbf{r}(t), \dot{\mathbf{r}}(t)] = \frac{1}{2}m\dot{\mathbf{r}}^2(t) - \frac{1}{2}m\omega^2\mathbf{r}^2(t) + m\omega_c x\dot{y} + m\mathbf{g}(t)\cdot\mathbf{r}$ is the classical Lagrangian. Explicitly, these equations of motion take the form:

$$\ddot{\mathbf{r}} + \omega_0^2\mathbf{r} + \omega_c\hat{z}\times\dot{\mathbf{r}} = \mathbf{g}(t). \tag{A.4}$$

The propagator then becomes

$$\langle \mathbf{r}_f, t_f | \mathbf{r}_i, t_i\rangle = F_0(t_f, t_i)e^{iS_0}, \tag{A.5}$$

where

$$F_0(t_f, t_i) = \int_{\delta\mathbf{r}(t_i)=0}^{\delta\mathbf{r}(t_f)=0} \mathcal{D}[\mathbf{r}[t]]e^{\frac{i}{\hbar}S[\delta\mathbf{r}(t),\delta\dot{\mathbf{r}}(t)]} \tag{A.6}$$

is the fluctuation determinant [96]. The fluctuation determinant is independent of the boundary conditions, and thus takes the form of a time-dependent normalization coefficient. We will ignore this term and concentrate on the physics contained in the e^{iS_0} term. We will see later that the same physics can be found by using the operator formalism.

The effects of the gravitation field can be treated by separating the solution to the equations of motion into the homogeneous and particular solutions, $\mathbf{r}(t) = \mathbf{r}_h(t) + \mathbf{r}_p(t)$, where $\mathbf{r}_h(t)$ satisfies the equation of motion with $\mathbf{g} = 0$, and $\mathbf{r}_p(t)$ satisfies the equation of motion with $\mathbf{g} \neq 0$. The boundary conditions for $\mathbf{r}(t)$ can be satisfied by setting $\mathbf{r}_p(t_i) = \mathbf{r}_p(t_f) = 0$ and allowing $\mathbf{r}_h(t)$ to satisfy the boundary conditions $\mathbf{r}_h(t_i) = \mathbf{r}_i$ and $\mathbf{r}(t_f) = \mathbf{r}_f$. Performing this separation, and applying the

165

equation of motion transforms the action to the form

$$S_0 = S_h + S_p + S_g, \tag{A.7}$$

where

$$
\begin{aligned}
S_h &= \int_{t_i}^{t_f} dt \left(\frac{1}{2} m \dot{\mathbf{r}}_h^2(t) - \frac{1}{2} m \omega_0^2 \mathbf{r}_h^2(t) + m \omega_c x_h \dot{y}_h \right), \tag{A.8} \\
S_p &= \int_{t_i}^{t_f} dt \left(\frac{1}{2} m \dot{\mathbf{r}}_p^2(t) - \frac{1}{2} m \omega_0^2 \mathbf{r}_p^2(t) + m \omega_c x_p \dot{y}_p + m \mathbf{g} \cdot \mathbf{r}_p \right), \tag{A.9} \\
S_g &= \int_{t_i}^{t_f} dt \, m \mathbf{g} \cdot \mathbf{r}_h. \tag{A.10}
\end{aligned}
$$

Note that while the actions S_h and S_p have the same form, this substitution has allowed us to separate the effect of the driving field into a path independent term, S_p, a term independent of gravity S_h, and coupling term S_g.

A.1.1 Evolution of a Wavepacket

We now consider the effect of the propagator on the initial state

$$\phi(\mathbf{r}) = N \exp \left[-\frac{(\mathbf{r} - \mathbf{r}_0)^2}{2\sigma^2} \right] = \phi_0(\mathbf{r} - \mathbf{r}_0) \tag{A.11}$$

where $\sigma^2 = \frac{m\tilde{\omega}}{\hbar}$ and $\phi_0(\mathbf{r})$ is the quantum harmonic oscillator ground state. This state corresponds to taking the quantum ground state of a harmonic oscillator with frequency $\tilde{\omega}$, and displacing it in position space by a vector $\mathbf{r}_0$. We expect the system will evolve as a quantum wavepacket where the expectation value of position and momentum corresponds to the evolution of the classical system with the same initial conditions.

To demonstrate this behavior, evolve the state in Eq. A.11 using the propagator in the path integral formulation:

$$\psi(\mathbf{r}_f, t_f) = \int d\mathbf{r}_i \, \langle \mathbf{r}_f, t_f | \mathbf{r}_i, t_i \rangle \phi(\mathbf{r}_i, t_i). \tag{A.12}$$

A change of variables substitution in the integral will move the initial displacement of the ground state wavefunction to the evolution of the propagator

$$\psi(\mathbf{r}_f, t_f) = \int d\mathbf{r}_i \, \langle \mathbf{r}_f, t_f | \mathbf{r}_i + \mathbf{r}_0, t_i \rangle \phi_0(\mathbf{r}_i, t_i). \tag{A.13}$$

It is now desirable to express the propagator $\langle \mathbf{r}_f, t_f | \mathbf{r}_i + \mathbf{r}_0, t_i \rangle$ in terms of the propagator calculated in the previous section, $\langle \mathbf{r}_f, t_f | \mathbf{r}_i, t_i \rangle$. To do this, take the expression for the propagator in the path integral formalism:

$$\langle \mathbf{r}_f, t_f | \mathbf{r}_i + \mathbf{r}_0, t_i \rangle = \int_{\mathbf{r}(t_i)=\mathbf{r}_i-\mathbf{r}_0}^{\mathbf{r}(t_f)=\mathbf{r}_f} \mathcal{D}[\mathbf{r}(t)] \exp\left[i \int dt \, L[\mathbf{r}(r), \dot{\mathbf{r}}(t)]\right]. \tag{A.14}$$

A change of variables of $\mathbf{r}(t) \to \mathbf{r}(t) - \mathbf{r}_c(t)$ will leave the measure of the path integral unchanged. We will chose $\mathbf{r}_c(t)$ to be a solution to the $\mathbf{g} = 0$ equation of motion with the intial conditions $\mathbf{r}_c(t_i) = \mathbf{r}_0$ and $\dot{\mathbf{r}}_c(t_i) = 0$. Thus, $\mathbf{r}_c(t)$ is the classical trajectory that a particle will follow if it is initially at the origin at rest, and then instantaneously displaced to a position $\mathbf{r}_c(t_i) = \mathbf{r}_0$ at a time t_i.

It is important to make a distinction between two "classical" paths. The path $\mathbf{r}(t) = \mathbf{r}_h(t) + \mathbf{r}_p(t)$ of the previous section is the path that minimizes the action of the path integral. It satisfies the classical equation of motion, but is defined by the boundary conditions of the propagator. The path $\mathbf{r}_c(t)$ is the classical path a particle will travel if it is initially held at $\mathbf{r}_c(0) = \mathbf{r}_0$ and $\dot{\mathbf{r}}_c(0) = 0$, and then allowed to freely evolve along the classical equations of motion.

The action can then be separated into different contributions corresponding to the paths $\mathbf{r}(t)$ and $\mathbf{r}_c(t)$. The net result of the change of variables will be to modify the homogeneous and gravitational actions S_h and S_g. The gravitational coupling action becomes

$$S_g[\mathbf{r}_h(t) - \mathbf{r}_c(t)] = \int_{t_i}^{t_f} dt\, m\mathbf{g} \cdot (\mathbf{r}_g - \mathbf{r}_c) = S_g + S_{gc} \qquad (A.15)$$

where the $\mathbf{r}_c(t)$ term is just a new phase factor. The homogenous action can be separated in a similar way (dropping the h subscript on $\mathbf{r}_h(t)$)

$$
\begin{aligned}
S_h\left[\mathbf{r}(t) - \mathbf{r}_c(t), \dot{\mathbf{r}}(t) - \dot{\mathbf{r}}_c(t)\right] &= \int dt\, L\left[\mathbf{r}(t) - \mathbf{r}_c(t), \dot{\mathbf{r}}(t) - \dot{\mathbf{r}}_c(t)\right] \qquad (A.16)\\
&= \int dt\, \left[\frac{1}{2}m(\dot{\mathbf{r}} - \dot{\mathbf{r}}_c)^2 - \frac{1}{2}m\omega_0^2(\mathbf{r} - \mathbf{r}_c)^2 + m\omega_c(x - x_c)(\dot{y} - \dot{y}_c)\right]\\
&= \int dt\, \left[\left(\frac{1}{2}m\dot{\mathbf{r}}_c^2 - \frac{1}{2}m\omega_0^2\mathbf{r}_c^2 + m\omega_c x_c\dot{y}_c\right) + \right.\\
&\qquad \left(\frac{1}{2}m\dot{\mathbf{r}}^2 - \frac{1}{2}m\omega_0^2\mathbf{r}^2 + m\omega_c x\dot{y}\right) +\\
&\qquad \left. (-m\dot{\mathbf{r}} \cdot \dot{\mathbf{r}}_c + m\omega_c\mathbf{r} \cdot \mathbf{r}_c - m\omega_c x_c\dot{y} - x\dot{y}_c)\right] \qquad (A.17)
\end{aligned}
$$

The last term can be simplified using integration by parts

$$
\begin{aligned}
\int_{t_i}^{t_f} dt\, \left[-m\dot{\mathbf{r}} \cdot \dot{\mathbf{r}}_c + m\omega_c\mathbf{r} \cdot \mathbf{r}_c - m\omega_c(x_c\dot{y} + x\dot{y}_c)\right] &= m\int_{t_i}^{t_f} dt\, \left[\mathbf{r} \cdot \left(\ddot{\mathbf{r}}_c + \omega_0^2\mathbf{r}_c + \omega_c\hat{z} \times \mathbf{r}_c\right)\right] +\\
&\qquad \left[-m\mathbf{r} \cdot \dot{\mathbf{r}}_c - m\omega_c x_c y\right|_{t_i}^{t_f} \qquad (A.18)\\
&= \left[-m\mathbf{r} \cdot \dot{\mathbf{r}}_c - m\omega_c x_c y\right|_{t_i}^{t_f} \qquad (A.19)\\
&= \mathbf{r}(t_f) \cdot \mathbf{p}_c(t_f) - \mathbf{r}(t_i) \cdot \mathbf{p}_c(t_i) \qquad (A.20)
\end{aligned}
$$

where the term under the integral vanished due to the equations of motion for $\mathbf{r}_c(t)$. The momentum $\mathbf{p}_c(t) = m\dot{\mathbf{r}}_c + m\omega_c x_c\hat{e}_y$ is the classical momentum of the system in the Hamiltonian formalism. Note that $\mathbf{p}_c$ is not a gauge invariant quantity, even

though $\dot{\mathbf{r}}_c$ is. We therefore desire a choice of gauge where $\mathbf{p}_c(t_i) = 0$. Under this gauge transformation, denoted by the function $\Lambda(\mathbf{r}, t)$, the propagator transforms as $\langle \mathbf{r}_f, t_f | \mathbf{r}_i, t_i \rangle \rightarrow e^{i\left(\Lambda(\mathbf{r}_f, t_f) - \Lambda(\mathbf{r}_i, t_i)\right)} \langle \mathbf{r}_f, t_f | \mathbf{r}_i, t_i \rangle$ and the wavefunction transforms as $\psi(\mathbf{r}, t) \rightarrow e^{i\Lambda(\mathbf{r}, t)} \psi(\mathbf{r}, t)$. Thus, a wavefunction propagated forward in time will transform as

$$\psi(\mathbf{r}_f, t_f) = \int d\mathbf{r}_i \langle \mathbf{r}_f, t_f | \mathbf{r}_i, t_i \rangle \psi(\mathbf{r}_i, t_i) \tag{A.21}$$

$$\rightarrow \int d\mathbf{r}_i \, e^{i\left(\Lambda(\mathbf{r}_f, t_f) - \Lambda(\mathbf{r}_i, t_i)\right)} \langle \mathbf{r}_f, t_f | \mathbf{r}_i, t_i \rangle e^{i\Lambda(\mathbf{r}_i, t_i)} \psi(\mathbf{r}_i, t_i) \tag{A.22}$$

$$= e^{i\left(\Lambda(\mathbf{r}_f, t_f)\right)} \int d\mathbf{r}_i \langle \mathbf{r}_f, t_f | \mathbf{r}_i, t_i \rangle \psi(\mathbf{r}_i, t_i) \tag{A.23}$$

$$= e^{i\left(\Lambda(\mathbf{r}_f, t_f)\right)} \psi(\mathbf{r}_f, t_f) \tag{A.24}$$

which is consistent with the transformation of a wavefunction under a change of gauge. Is is therefore possible to calculate the propagator in a gauge for which the canonical momentum $\mathbf{p}_c(t_i) = 0$ vanishes on the lower limit of Eq. A.20. This gauge is always possible for a spatially uniform magnetic field, and would correspond to a gauge with the vector potential $A(\mathbf{r}) \propto \hat{e}_z \times \mathbf{r}_0$ is perpendicular to the axis of initial displacement, $\mathbf{r}_0$.

Using these simplifications, the homogenous part of the action can be expressed as

$$S_0[\mathbf{r} - \mathbf{r}_c, \dot{\mathbf{r}} - \dot{\mathbf{r}}_c] = S_{h0} + S_c + \mathbf{r}(t_f) \cdot \mathbf{p}_c(t_f) + S_{g0} + S_{gc}. \tag{A.25}$$

The term $S_0[\mathbf{r}, \dot{\mathbf{r}}]$ is the action of a path not shifted by $\mathbf{r}_c(t)$. The action $S_c[\mathbf{r}_c, \dot{\mathbf{r}}_c]$ is a phase that arises due to the motion around the classical trajectory $\mathbf{r}_c$. The term $\mathbf{r}(t_f) \cdot \mathbf{p}_c(t_f)$ will be shown to correspond to the classical momentum of the wavepacket. It is key to note that of these contributions to the action, only S_{h0}

169

and S_{g0} depend on the on the path $\mathbf{r}(t)$ at more than the boundary point $\mathbf{r}(t_f)$. Therefore these terms can be factored out of the path integral. This factorization can be used to convert the initial displacement into a final displacement along the classical trajectory

$$
\begin{aligned}
\langle \mathbf{r}_f, t_f | \mathbf{r}_i + \mathbf{r}_0, t_i \rangle &= e^{iS_{gc}} e^{iS_c} e^{i\mathbf{r}_f(t_f)\cdot \mathbf{p}_c(t_f)} \int_{\mathbf{r}(t_i)=\mathbf{r}_i}^{\mathbf{r}(t_f)=\mathbf{r}_f - \mathbf{r}_c(t_f)} \mathcal{D}[\mathbf{r}(t)] \exp\left[i \int dt\, L[\mathbf{r}(r), \dot{\mathbf{r}}(t)] \right] \\
&= e^{iS_{gc}} e^{iS_c} e^{i\mathbf{r}_f(t_f)\cdot \mathbf{p}_c(t_f)} \langle \mathbf{r}_f - \mathbf{r}_c(t_f), t_f | \mathbf{r}_i, t_i \rangle.
\end{aligned}
\tag{A.26}
$$

Where the propagator $\langle \mathbf{r}_f - \mathbf{r}_c(t_f), t_f | \mathbf{r}_i, t_i \rangle$ is expressed as the wavefunction shifted around the classical trajectory $\mathbf{r}_c(t)$. For the purposes of this section, we desire to simply show that the time evolution of the wavepacket $\phi(\mathbf{r})$ has the form

$$
\begin{aligned}
\psi(\mathbf{r}_f, t_f) &= \int d\mathbf{r}_i \, \langle \mathbf{r}_f, t_f | \mathbf{r}_i, t_i \rangle \phi(\mathbf{r}_i) && \text{(A.27)} \\
&= \int d\mathbf{r}_i \, \langle \mathbf{r}_f, t_f | \mathbf{r}_i - \mathbf{r}_0, t_i \rangle \phi_0(\mathbf{r}_i) && \text{(A.28)} \\
&= e^{iS_{gc}} e^{iS_c} e^{i\mathbf{r}_f \cdot \mathbf{p}_c(t_f)} \int d\mathbf{r}_f \, \langle \mathbf{r}_f - \mathbf{r}_c(t_f), t_f | \mathbf{r}_i, t_i \rangle \phi_0(\mathbf{r}_i) && \text{(A.29)} \\
&= e^{iS_{gc}} e^{iS_c} e^{i\mathbf{r}_f \cdot \mathbf{p}_c(t_f)} \phi_0(\mathbf{r}_f - \mathbf{r}_c(t_f), t_f) && \text{(A.30)}
\end{aligned}
$$

where $\phi_0(\mathbf{r}, t)$ is the evolution of the undisplaced harmonic oscillator ground state. Using the properties of the harmonic oscillator ground state, we immediately see that at a time t, this wavepacket has the average value of momentum of $\langle \hat{\mathbf{p}} \rangle = \mathbf{p}_c(t)$, and the average position of $\langle \hat{\mathbf{r}} \rangle = \mathbf{r}_c(t)$. Therefore, the effect of the initial displacement of the harmonic oscillator ground state is to evolve the system as a Gaussian wavepacket around the classical trajectory with the phase factor e^{iS_c}. The first order phase response of the system to a gravitational field around the classical

trajectory is given by

$$e^{iS_{gc}/\hbar} = e^{-i\frac{m}{\hbar}\int dt\, \mathbf{g}\cdot\mathbf{r}_c}. \tag{A.31}$$

This behavior will be derived using coherent states in the following section.

A.2 Operators and Coherent States

The physics in the proceeding section can also be derived using coherent states and quantum mechanical operators. We reiterate that since the Hamiltonian is quadratic in the operators $\hat{\mathbf{r}}$ and $\hat{\mathbf{p}}$, we can explicitly diagonalize the system using creation and annihilation operators. To diagonalize our system, we consider the toy Hamiltonian given by 8.1 in the symmetric gauge:

$$H = \frac{\left(\mathbf{p} - \frac{1}{2}\sigma_3 m\omega_c \hat{e}_z \times \mathbf{r}\right)^2}{2m} + \frac{1}{2}m\omega_0^2 \mathbf{r}^2 \tag{A.32}$$

where we have set $\mathbf{g}(t) = 0$, and will restore it later. The change in gauge will not be relevant for the quantities of interest, and if necessary we can return to the Landau gauge at any time with the gauge transformation defined by $U = \exp[im\omega_c xy/2]$. The advantage of using the symmetric gauge is that the Hamiltonian can be expressed as:

$$H = \frac{1}{2m}\sum_j \left[\mathbf{p}^2 + m^2\left(\omega_0^2 + \left(\frac{\omega_c}{2}\right)^2\right)\mathbf{r}^2 - \sigma_3\omega_c\mathbf{p}\times\mathbf{r}\right]. \tag{A.33}$$

We now define the creation and annihilation operators $\mathbf{c}^\dagger = \frac{1}{\sqrt{2m\tilde{\omega}}}\left(m\tilde{\omega}\mathbf{r} - i\mathbf{p}\right)$ and $\mathbf{c} = \frac{1}{\sqrt{2m\tilde{\omega}}}\left(m\tilde{\omega}\mathbf{r} + i\mathbf{p}\right)$ where $\tilde{\omega}^2 = \omega_0^2 + \left(\frac{\omega_c}{2}\right)^2$. These operators satisfy the standard

commutation relations for creation and annihilation operators [5]

$$[c_i, c_j^\dagger] \ = \ \delta_{ij} \tag{A.34}$$

$$[c_i, c_j] \ = \ 0 \tag{A.35}$$

$$[c_i^\dagger, c_j^\dagger] \ = \ 0. \tag{A.36}$$

Inverting these operators gives $r_i = \sqrt{\frac{\hbar}{2m\tilde{\omega}}}(c_i^\dagger + c_i)$ and $p_i = i\sqrt{\frac{\hbar m\tilde{\omega}}{2}}(c_i^\dagger - c_i)$ which can be used to express Eq. A.33 as

$$H/\hbar \ = \ \tilde{\omega}(\mathbf{c}^\dagger \cdot \mathbf{c} + 1) - i\sigma_3\frac{\omega_c}{2}(\mathbf{c}^\dagger - \mathbf{c}) \times (\mathbf{c}^\dagger + \mathbf{c}) \cdot \hat{e}_z) \tag{A.37}$$

$$= \ \tilde{\omega}(\mathbf{c}^\dagger \cdot \mathbf{c} + 1) - i\sigma_3\omega_c\mathbf{c}^\dagger \times \mathbf{c} \cdot \hat{e}_z. \tag{A.38}$$

We can diagonalize the term last term of Eq. A.38 by noting $\mathbf{c}^\dagger \times \mathbf{c} \cdot \hat{e}_z = i\tau_{ij}^y c_i^\dagger c_j$ where τ^y is the second Pauli matrix in the $\hat{e}_x - \hat{e}_y$ space. We then see that a $\pi/2$-rotation about τ^x will bring Eq. A.38 to a diagonal form. Explicitly, this rotation takes the form $R = e^{-i\frac{\pi}{4}\tau^x} = \frac{1}{\sqrt{2}}(1 - i\tau^x)$, and the diagonal Hamiltonain is

$$H = \omega_+ a_+^\dagger a_+ + \omega_- a_-^\dagger a_- + \tilde{\omega} \tag{A.39}$$

where we have set $\hbar = 1$ and the operators $a_\lambda^\dagger = R_{\lambda,i}^\dagger c_i^\dagger$ and $a_\lambda = R_{\lambda,i} c_i$ are the respective creation and annihilation operators for a for a mode with classical frequency ω_λ. It is clear that this unitary rotation will preserve the canonical commutation relations. Also of note is that the classical frequencies discussed in the previous section arise naturally through diagonalization of the quantum Hamiltonian.

Finally, it is important to note that Eq. A.39 has implicit spin dependence in the frequencies $\omega_\pm$. For example, the frequency ω_+ for the state $|\downarrow\rangle$ is the same

as the frequency ω_- for the state $|\uparrow\rangle$. Note however, the creation and annihilation operators $a_\pm$ have no spin dependence. This indicates that the mode corresponding to $a_\pm$ will rotate with frequency $\omega_\uparrow$, $\omega_\downarrow$ for the respective state $|\uparrow\rangle,|\downarrow\rangle$. Therefore, a π-pulse, which will invert $|\uparrow\rangle \to |\downarrow\rangle$ and $|\downarrow\rangle \to |\uparrow\rangle$, will act to interchange the frequencies at which the classical modes rotate.

A.2.1   Effect of Gravity

We now restore the external force applied in the original Hamiltonian given by Eq. 8.1. In term of the operators c_j, the external force takes the form:

$$
\begin{aligned}
H_g &= m\mathbf{g}(t) \cdot \sqrt{\frac{\hbar}{2m\tilde{\omega}}} (\mathbf{c}^\dagger + \mathbf{c}) & \text{(A.40)} \\
&= \sqrt{\frac{m\hbar}{2\tilde{\omega}}} \mathbf{g}(t) \cdot (\mathbf{a}^\dagger R^\dagger + R\mathbf{a}) & \text{(A.41)} \\
&= (\tilde{\boldsymbol{\eta}}(t) \cdot \mathbf{a}^\dagger + \tilde{\boldsymbol{\eta}}^*(\mathbf{t}) \cdot \mathbf{a}) & \text{(A.42)}
\end{aligned}
$$

where $\tilde{\boldsymbol{\eta}}(t) = \sqrt{\frac{m\hbar}{2\tilde{\omega}}} R\mathbf{g}(t)$. The total Hamiltonian of the system in the presence of gravity is therefore

$$
H = \omega_+ a_+^\dagger a_+ + \omega_- a_-^\dagger a_- + \tilde{\boldsymbol{\eta}}(t) \cdot \mathbf{a}^\dagger + \tilde{\boldsymbol{\eta}}^*(\mathbf{t}) \cdot \mathbf{a}. \tag{A.43}
$$

We would like to find the time evolution operator for this Hamiltonian. This can be done by moving to a frame rotating by $U_\omega(t) = e^{-i(\omega_+ a_+^\dagger a_+ + \omega_- a_-^\dagger a_-)t}$. In the new frame, the Hamiltonian takes the form

$$
H' = \boldsymbol{\eta}(t) \cdot \mathbf{a}^\dagger + \eta^*(\mathbf{t}) \cdot \mathbf{a} \tag{A.44}
$$

where the rotating $\eta(t)$ are given by

$$
\begin{pmatrix} \eta_+ \\ \eta_- \end{pmatrix} = \begin{pmatrix} \tilde{\eta}_+ e^{-i\omega_+ t} \\ \tilde{\eta}_- e^{-i\omega_- t} \end{pmatrix}. \tag{A.45}
$$

The time evolution operator, $U(t) = U_\omega(t)U_d(t)$, can thus be found by solving the equation of motion

$$
i\dot{U}_d(t) = \left(\boldsymbol{\eta}(t) \cdot \mathbf{a}^\dagger + \boldsymbol{\eta}^*(\mathbf{t}) \cdot \mathbf{a} \right) U_d(t). \tag{A.46}
$$

subject to the initial conditions $U_d(0) = \hat{I}$. Since the commutator of the creation operators, $[a_\lambda, a_\mu^\dagger] = \delta_{\lambda,\mu}$, are constants, the commutators will themselves commute with any of the operators $\{a_\lambda, a_\mu^\dagger\}$. Therefore, Eq. A.46 can be integrated exactly to give $U_d(t)$. We claim that

$$
U_d(t) = \exp\left[-i \int \mathrm{d}t \, \left(\boldsymbol{\eta}(t) \cdot \mathbf{a}^\dagger + \boldsymbol{\eta}^*(\mathbf{t}) \cdot \mathbf{a} \right) \right] e^{-i\phi_\eta(t)} \tag{A.47}
$$

satisfies this equation of motion, where $\phi_\eta(t)$ is just an overall phase factor. The phase can be found by substituting this solution into Eq. A.46. Using the identity

$$
\frac{d}{\mathrm{d}t} e^{X(t)} = \int_0^1 e^{sX(t)} \frac{\mathrm{d}X(t)}{\mathrm{d}t} e^{(1-s)X(t)} \mathrm{d}s \tag{A.48}
$$

gives

$$
\begin{aligned}
i\frac{d}{\mathrm{d}t} U_d(t) &= \dot{\phi}_\eta U_d(t) + \left(\boldsymbol{\eta}(t) \cdot \mathbf{a}^\dagger + \boldsymbol{\eta}^*(\mathbf{t}) \cdot \mathbf{a} \right) U_d(t) + \\
&\quad \int_0^t \mathrm{d}t' \, \left(\boldsymbol{\eta}(t) \cdot \boldsymbol{\eta}^*(t') + \boldsymbol{\eta}^*(t) \cdot \boldsymbol{\eta}(t') \right) U_d(t) \tag{A.49}
\end{aligned}
$$

In arriving at the last equation we exploited the fact that $\exp\left[-i \int \mathrm{d}t \, \left(\boldsymbol{\eta}(t) \cdot \mathbf{a}^\dagger + \boldsymbol{\eta}^*(\mathbf{t}) \cdot \mathbf{a} \right) \right]$ is a displacement operator [11]. The action of a displacement operator $D[\alpha] =$

174

$\exp\left(\alpha a^\dagger - \alpha^* a\right)$ is to displace an annihilation operator $D[\alpha] a D[\alpha] = a + \alpha$. We therefore can express the time evolution operator as $U_d(t) = D[\boldsymbol{\gamma}(t)] e^{-i\phi_\gamma(t)}$, where $\boldsymbol{\gamma}(t) = -i \int_0^t dt'\, \boldsymbol{\eta}(t)$. We see by comparing Eq. A.49 and Eq. A.46 that the phase $\phi_\gamma(t)$ is given by

$$\phi_\gamma(t) = \int_0^t d\tau \int_0^\tau d\tau' \left(\boldsymbol{\eta}(\tau) \cdot \boldsymbol{\eta}^*(\tau') + \boldsymbol{\eta}^*(\tau) \cdot \boldsymbol{\eta}(\tau')\right). \tag{A.50}$$

The overall time evolution operator therefore takes the form

$$U(t) = e^{-i\left(\omega_+ a_+^\dagger a_+ + \omega_- a_-^\dagger a_-\right)t} D[\boldsymbol{\gamma}(t)] e^{-i\phi_\gamma(t)}. \tag{A.51}$$

The form of the time evolution can be interpreted as follows. The external force displaces the evolution away from the classical trajectory that is defined by the evolution of the free system. The overall phase has an implicit dependence on the frequencies $\omega_\pm$, and therefore can be relevant for spin-dependent measurements.

A.2.2 Single Pulse and Measurement

We can now replicate the result given in the path integral section. Consider the sequence of operations given to perform an interferometric measurement as discussed in Chapter 8. Such a measurement sequence is schematically given by:

1. Prepare a spin-polarized ground state defined by $|\psi\rangle = |\uparrow\rangle |0\rangle$, where $|0\rangle$ is the orbital ground state.

2. Apply a spin-rotation, $U_{\pi/2}(\hat{y})$.

3. Displace the trap minimum by a vector $\mathbf{r}_0$. This is equivalent to applying the

175

displacement matrix $D[\boldsymbol{\alpha}]$ where

$$\boldsymbol{\alpha} = \sqrt{\frac{m}{4\hbar\tilde{\omega}}} \begin{pmatrix} (\tilde{\omega} - \omega_c/2)x_0 - i(\tilde{\omega} - \omega_c/2)y_0 \\ (\tilde{\omega} + \omega_c/2)y_0 - i(\tilde{\omega} + \omega_c/2)x_0 \end{pmatrix} \tag{A.52}$$

encodes the initial conditions that $\mathbf{r}(0) = \mathbf{r}_0$ and $\dot{\mathbf{r}}(0) = 0$.

4. Allow the system to freely evolve under the evolution of $U(t)$.

5. At a future time, t, when the particles overlap, make a S_z, spin polarization measurement.

The application of steps 1 to 4 act to prepare the time evolved states

$$|\psi_f\rangle = U(t)D[\boldsymbol{\alpha}]U_{\pi/2}(\hat{y})\left|\uparrow\right\rangle|0\rangle. \tag{A.53}$$

The step 5 amounts to taking the expectation value

$$\langle S_x\rangle = \langle\psi_f| S_x |\psi_f\rangle. \tag{A.54}$$

This can also be expressed as the $\left|\uparrow\right\rangle|0\rangle$ matrix element of the operator

$$U = U_{\pi/2}^\dagger(\hat{y})D^\dagger[\boldsymbol{\alpha}]U^\dagger(t)S_x U(t)D[\boldsymbol{\alpha}]U_{\pi/2}(\hat{y}). \tag{A.55}$$

We will now calculate this matrix element. Recall that $U(t)$ has an implicit σ_z dependence in the classical frequencies $\omega_\pm$. This dependence can be rotated by expressing $S_z = U_{\pi/2}(\hat{y})S_x U_{\pi/2}^\dagger(\hat{y})$. The rotation operators can then be used to rotate the implicit σ_z operators in $U(t)$ to $-\sigma_x$ operators. The rotation $\pi/2$ rotation around $\hat{e}_y$ can then be regrouped to rotate $U(t)$. After inserting $\hat{I} = D[\boldsymbol{\alpha}]D^\dagger[\boldsymbol{\alpha}]$ after the S_x operator, and associating the unitary transformations $D[\boldsymbol{\alpha}]$ and $U_{\pi/2}(\hat{y})$ with $U(t)$, we obtain

$$U = U_{\hat{y}}^\dagger(t)S_x U_{\hat{y}}(t) \tag{A.56}$$

176

where

$$U_{\hat{y}}(t) = D^\dagger[\boldsymbol{\alpha}]U_{\pi/2}^\dagger(\hat{y})U(t)U_{\pi/2}^\dagger(\hat{y})D[\boldsymbol{\alpha}] \tag{A.57}$$

is the rotated and displaced time evolution operator. This operator can be explicitly calculated at all times, but a solution is only relevant at times when the two trajectories overlap. Consider the special case where the ratio of the classical frequencies is rational, i.e. $\omega_+ = \frac{p}{q}\omega_-$ with p and q integers. In this case the paths of the two spins will overlap at time intervals of $t = 2\pi\frac{q}{\omega_-}$. Using the operator identity $e^{i2\pi a^\dagger a} = \hat{I}$, the time evolution operator becomes $U(t) = D[\boldsymbol{\gamma}(t)]e^{-i\phi_\gamma(t)}$. The displacement term of the time evolution operator then becomes $D^\dagger[\boldsymbol{\alpha}]D[\boldsymbol{\gamma}(t)]D[\boldsymbol{\alpha}] = e^{\boldsymbol{\alpha}^*\cdot\boldsymbol{\gamma}(t)-\boldsymbol{\alpha}\cdot\boldsymbol{\gamma}^*(t)}D[\boldsymbol{\gamma}(t)]$. Using the original definition of $\boldsymbol{\gamma}(t)$, the phase factor can be expressed as

$$\begin{aligned}
\boldsymbol{\alpha}^* \cdot \boldsymbol{\gamma}(t) - \boldsymbol{\alpha} \cdot \boldsymbol{\gamma}^*(t) &= -i \int_{t_i}^{t_f} dt \, (\boldsymbol{\alpha}^* \cdot \boldsymbol{\eta}(t) + \boldsymbol{\alpha} \cdot \boldsymbol{\eta}^*(t)) \tag{A.58} \\
&= -i \int_{t_i}^{t_f} dt \, (\mathbf{r}(t) \cdot \mathbf{g}(t)) \tag{A.59}
\end{aligned}$$

where the last relation can be seen since $\boldsymbol{\alpha}$ contains the initial conditions of the classical system, and $\boldsymbol{\eta}(t)$ has a factor that corresponds to the time evolution of a coherent state.

These operators reduce $U_{\hat{y}}(t)$ to

$$U_{\hat{y}}(t) = e^{-i\int dt\,(\mathbf{r}'(t)\cdot\mathbf{g}(t))}e^{-i\phi'_\gamma(t)}D[\boldsymbol{\gamma}'] \tag{A.60}$$

where the primes represent an internal rotation of the spin operator from σ_z to σ_x. At this point the only dependence on the orbital degrees of freedom are contained in the operator $D[\boldsymbol{\gamma}']$. This can be treated by commuting the term $D^\dagger[\boldsymbol{\gamma}']$ through

177

the S_z operator at the cost of a negative sign in the coefficients of σ_x. The orbital components can then be calculated by taking the matrix element $\langle 0|\, D[\boldsymbol{\gamma}' - \boldsymbol{\gamma}'']\, |0\rangle = e^{-|\gamma'' - \gamma'|^2}$, which gives an overall a spin-independent suppression factor. This factor is a result of the incomplete overlap of the two spin states that overlap across different spin trajectories.

Finally, the $|\uparrow\rangle$ matrix element can be taken to find the expectation value of a spin measurement. The remaining spin-dependent terms are the phase $e^{-i\frac{m}{\hbar}\int \mathrm{d}t\, \mathbf{g}\cdot\mathbf{r}_c}$ and $e^{-i\phi_\gamma}$. The expectation value to first order in $\mathbf{g}$ then becomes

$$\langle S_z\rangle = \sin\left[2\frac{m}{\hbar}\int \mathrm{d}t\, \mathbf{g}\cdot\mathbf{r}_c\right]. \tag{A.61}$$

Terms second order in $\mathbf{g}$ will result in both a correction to the phase, and an exponential suppression factor $e^{-|\gamma'' - \gamma'|^2}$ due to the driving field.

A.2.3   Carr-Purcell Sequence and Measurement

The methods in the preceding section can be naturally extended to include the effect of time reversal pulses. Consider the Carr-Purcell pulse sequence discussed in Sec. 8.5. The pulse sequence

1. Apply a $U_{\hat{y}}(\pi/2)$ spin rotation;

2. Displace by $D[\boldsymbol{\alpha}]$;

3. Evolve for a time t;

4. Apply a $U_{\hat{y}}(\pi)$ spin rotation;

5. Evolve for a time $2t$;

6. Apply a $U_{\hat{y}}(\pi)$ spin rotation;

7. Evolve for a time t;

can be described by the operator

$$U_{CP} = U_{fk}(t)U_{\hat{y}}(\pi)U_{kj}(t)U_{\hat{y}}(\pi)U_{ji}(t)D[\boldsymbol{\alpha}]U_{\hat{y}}(\pi/2), \qquad (\text{A.62})$$

where $U_{ij} = U(t_j, t_i)$ is the time evolution operator from the time t_i to t_j. This operator can be simplified in a manner similar to the case without time reversal. We express the first and second operator $U_{\hat{y}}(\pi)$ in Eq. A.62 as $U_{\hat{y}}(\pi) = U_{\hat{y}}(\pi/2)U_{\hat{y}}(\pi/2)$ and $U_{\hat{y}}(\pi) = -U_{\hat{y}}(-\pi/2)U_{\hat{y}}(-\pi/2)$. The rotations can then be applied to the time evolution operators to give

$$U_{CP} = U_{\hat{y}}(\pi/2)\tilde{U}_{fk}(t)\tilde{U}'_{kj}(t)\tilde{U}_{ji}(t)D[\boldsymbol{\alpha}] \qquad (\text{A.63})$$

where $\tilde{U},(\tilde{U}')$ represents an evolution operator that was rotated by $-\pi/2$, $(\pi/2)$ around the $\hat{y}$-axis. This can be further simplified if the free evolution parts of the time evolution operator, $\tilde{U}_\omega(t_j, t_i)$, are separated from the displacement operators, $\tilde{D}[\gamma(t_j, t_i)]$. This can be done by commuting the operators $\tilde{U}_\omega$ through the operators $\tilde{D}$. Doing this gives

$$U_{C-P} = -U_{\hat{y}}(-\pi/2)\tilde{U}_\omega(t_f, t_k)\tilde{U}'_\omega(t_k, t_j)\tilde{U}_\omega(t_j, t_i)\tilde{D}[\boldsymbol{\gamma}_{fk}]\tilde{D}[\boldsymbol{\gamma}'_{kj}]\tilde{D}[\boldsymbol{\gamma}_{ji}]D[\boldsymbol{\alpha}]e^{-i\phi}.$$

$$(\text{A.64})$$

The displacement vectors are defined by

$$\boldsymbol{\gamma}_{ji} = -i \int_i^j dt' \begin{pmatrix} \eta_+ e^{-i\omega_+ t'} \\ \eta_- e^{-i\omega_- t'} \end{pmatrix}, \tag{A.65}$$

$$\boldsymbol{\gamma}_{kj} = -i \int_j^k dt' \begin{pmatrix} \eta_+ e^{-i\omega_- t'} e^{i\omega_+ (t_j - t_i)} \\ \eta_- e^{-i\omega_+ t'} e^{i\omega_- (t_j - t_i)} \end{pmatrix}, \tag{A.66}$$

$$\boldsymbol{\gamma}_{fk} = -i \int_j^k dt' \begin{pmatrix} \eta_+ e^{-i\omega_+ t'} e^{i\omega_+ (t_j - t_i) - i\omega_- (t_k - t_j)} \\ \eta_- e^{-i\omega_- t'} e^{i\omega_- (t_j - t_i) - i\omega_+ (t_k - t_j)} \end{pmatrix}, \tag{A.67}$$

and the phase $\phi = \tilde{\phi}_\gamma(t_f, t_k) + \tilde{\phi}'_\gamma(t_k, t_j) + \tilde{\phi}_\gamma(t_j, t_i)$ is the sum of the phases second order in $\mathbf{g}$ for each of the time evolution operators. We will ignore this phase as a second order correction, but note it can be calculated exactly if necessary. Assuming the time intervals take the form $t_j - t_i = t_f - t_k = \Delta t$ and $t_k - t_j = 2\Delta t$, the product of the three free evolution operators gives

$$U_{\omega,\text{total}} = \tilde{U}_\omega(t_f, t_k)\tilde{U}'_\omega(t_k, t_j)\tilde{U}_\omega(t_j, t_i) = \exp\left[2\left(\omega_+ + \omega_-\right)\left(a_+^\dagger a_+ + a_-^\dagger a_-\right)\Delta t\right]. \tag{A.68}$$

Therefore, if the π-pulses are applied at time intervals of $\Delta t = \frac{2\pi}{\omega_+ + \omega_-}$, corresponding to cusps in the cyclotron motion, the factor $U_{\omega,\text{total}} = \hat{I}$.

The phase $e^{-i\frac{m}{\hbar}\int_{t_i}^{t_f} dt\, \mathbf{g}\cdot\mathbf{r}_c}$ then arises in a manner similar to the single pulse case. When the operator $D[\boldsymbol{\alpha}]$ is commuted through the operator $\tilde{D}[\boldsymbol{\gamma}'_{ij}]$, an additional phase of $e^{\boldsymbol{\alpha}\cdot\boldsymbol{\gamma}^*_{ji} - \boldsymbol{\alpha}^*\cdot\boldsymbol{\gamma}_{ji}}$ appears. The three terms defined by Eq. A.65 - Eq. A.67 will combine to give a total phase of

$$e^{-i\frac{m}{\hbar}\int_{t_i}^{t_f} dt\, \mathbf{g}\cdot\mathbf{r}_{CP}}, \tag{A.69}$$

180

where the path $\mathbf{r}_{CP}$ is the classical path a particle would undertake after the Carr-Purcell time reversal sequences are applied. It is defined by

$$
\mathbf{r}_{CP} = \begin{cases} \mathbf{r}_c(t) & 0 \leq t \leq \Delta t \\ \mathbf{r}_c(2\Delta t - t) & \Delta t \leq t \leq 3\Delta t \\ \mathbf{r}_c(t - 4\Delta t) & 3\Delta t \leq t \leq 4\Delta t \end{cases} \tag{A.70}
$$

and is shown in Fig. 8.4(a). The expectation value of S_z can then be found in a manner similar to the above section. The result is analogous

$$
\langle S_z \rangle = \sin\left[2\frac{m}{\hbar}\int dt\, \mathbf{g} \cdot \mathbf{r}_{CP}\right]. \tag{A.71}
$$

As above, there is an additional factor that results in the suppression of the signal, as well as an additional phase. Both of these effects are second order in $\mathbf{g}$, and are therefore ignored. They can be calculated exactly if necessary.

Bibliography

[1] D. L. Campbell, G. Juzeliūnas, and I. B. Spielman, Realistic rashba and dressehaus spin-orbit coupling for neutral atoms.

[2] A. Peters, K. Y. Chung, and S. Chu, Nature **400**, 849 (1999).

[3] T. D. Stanescu, C. Zhang, and V. Galitski, Phys. Rev. Lett. **99**, 110403 (2007).

[4] S.-L. Zhu, H. Fu, C.-J. Wu, S.-C. Zhang, and L.-M. Duan, Phys. Rev. Lett. **97**, 240401 (2006).

[5] J. J. Sakurai, *Modern Quantum Mechanics (Revised Edition)* (Addison Wesley, 1993).

[6] T. D. Stanescu, B. Anderson, and V. Galitski, Phys. Rev. A **78**, 023616 (2008).

[7] B. Anderson, T. D. Stanescu, and V. Galitski, Phys. Rev. B **81**, 121304 (2010).

[8] D. A. Steck, Quantum and atom optics.

[9] M. Lukin, P285b course notes.

[10] C. Cohen-Tannoudji, J. Dupont-Roc, and G. Grynberg, *Atom - Photon Interactions: Basic Process and Appilcations* (Wiley-Interscience, 1992).

[11] R. J. Glauber, Phys. Rev. **131**, 2766 (1963).

[12] E. Jaynes and F. Cummings, Proceedings of the IEEE **51**, 89 (1963).

[13] M. J. Snadden, J. M. McGuirk, P. Bouyer, K. G. Haritos, and M. A. Kasevich, Phys. Rev. Lett. **81**, 971 (1998).

[14] J. M. McGuirk, G. T. Foster, J. B. Fixler, M. J. Snadden, and M. A. Kasevich, Phys. Rev. A **65**, 033608 (2002).

[15] H. Müller, S.-w. Chiow, S. Herrmann, S. Chu, and K.-Y. Chung, Phys. Rev. Lett. **100**, 031101 (2008).

[16] S. Dimopoulos, P. W. Graham, J. M. Hogan, and M. A. Kasevich, Phys. Rev. Lett. **98**, 111102 (2007).

[17] S. Dimopoulos, P. W. Graham, J. M. Hogan, and M. A. Kasevich, Phys. Rev. D **78**, 042003 (2008).

[18] D. Loss and D. P. DiVincenzo, Phys. Rev. A **57**, 120 (1998).

[19] R. Feynman, International Journal of Theoretical Physics **21**, 467 (1982), 10.1007/BF02650179.

[20] M. A. Nielsen and I. L. Chuang, *Quantum Computation and Quantum Information* (Cambridge University Press, 2000).

[21] G. Juzeliūnas, J. Ruseckas, P. Öhberg, and M. Fleischhauer, Phys. Rev. A **73**, 025602 (2006).

[22] I. B. Spielman, Phys. Rev. A **79**, 063613 (2009).

[23] Y. J. Lin, R. L. Compton, K. Jimenez-Garcia, J. V. Porto, and I. B. Spielman, Nature **462**, 628 (2009).

[24] J. Ruseckas, G. Juzeliūnas, P. Öhberg, and M. Fleischhauer, Phys. Rev. Lett. **95**, 010404 (2005).

[25] L.-H. Lu and Y.-Q. Li, Phys. Rev. A **76**, 023410 (2007).

[26] Y.-J. Lin *et al.*, Phys. Rev. Lett. **102**, 130401 (2009).

[27] Y. J. Lin, K. Jimenez-Garcia, and I. B. Spielman, Nature **471**, 83 (2011).

[28] J. R. Kuklinski, U. Gaubatz, F. T. Hioe, and K. Bergmann, Phys. Rev. A **40**, 6741 (1989).

[29] E. I. Rashba, Sov. Phys. Solid State **2**, 1109 (1960); Yu.A. Bychkov and E.I. Rashba, J. Phys. C **17**, 6093 (1984).

[30] D. R. Yennie, Rev. Mod. Phys. **59**, 781 (1987).

[31] R. B. Laughlin, Phys. Rev. B **23**, 5632 (1981).

[32] N. Cooper, Advances in Physics **57**, 539 (2008), http://www.tandfonline.com/doi/pdf/10.1080/00018730802564122.

[33] J. I. Cirac, P. Maraner, and J. K. Pachos, Phys. Rev. Lett. **105**, 190403 (2010).

[34] J. F. Clauser, Physica B+C **151**, 262 (1988).

[35] M. de Angelis *et al.*, Measurement Science and Technology **20**, 022001 (2009).

[36] A. D. Cronin, J. Schmiedmayer, and D. E. Pritchard, Rev. Mod. Phys. **81**, 1051 (2009).

[37] J. B. Fixler, G. T. Foster, J. M. McGuirk, and M. A. Kasevich, Science **315**, 74 (2007), http://www.sciencemag.org/content/315/5808/74.full.pdf.

[38] M. J. Biercuk, H. Uys, J. W. Britton, A. P. VanDevender, and J. J. Bollinger, Nat Nano **5**, 646 (2010).

[39] A. Bertoldi *et al.*, The European Physical Journal D - Atomic, Molecular, Optical and Plasma Physics **40**, 271 (2006), 10.1140/epjd/e2006-00212-2.

[40] A. B. Chatfield, *Fundamentals of High Accuracy Inertial Navigation* (American Institute of Aeronautics and Astronautics, 1997).

[41] T. van Zoest *et al.*, Science **328**, 1540 (2010), http://www.sciencemag.org/content/328/5985/1540.full.pdf.

[42] S. A. Wolf *et al.*, Science **294**, 1488 (2001), http://www.sciencemag.org/content/294/5546/1488.full.pdf.

[43] I. Žutić, J. Fabian, and S. Das Sarma, Rev. Mod. Phys. **76**, 323 (2004).

[44] G. Dresselhaus, Phys. Rev. **100**, 580 (1955).

[45] Y. K. Kato, R. C. Myers, A. C. Gossard, and D. D. Awschalom, Science **306**, 1910 (2004), http://www.sciencemag.org/content/306/5703/1910.full.pdf.

[46] J. Wunderlich, B. Kaestner, J. Sinova, and T. Jungwirth, Phys. Rev. Lett. **94**, 047204 (2005).

[47] V. Sih *et al.*, Phys. Rev. Lett. **97**, 096605 (2006).

[48] M. I. Dyakonov and V. I. Perel, Physics Letters A **35**, 459 (1971).

[49] I. Dyakonov and V. I. Perel, Sov. Phys. JETP **33**, 1053 (1971).

[50] V. M. Galitski, A. A. Burkov, and S. Das Sarma, Phys. Rev. B **74**, 115331 (2006).

[51] V. M. Galitski, A. A. Burkov, and S. Das Sarma, Phys. Rev. B **74**, 115331 (2006).

[52] W.-K. Tse, J. Fabian, I. Žutić, and S. Das Sarma, Phys. Rev. B**72**, 241303 (2005).

[53] P. G. Silvestrov, V. A. Zyuzin, and E. G. Mishchenko, Phys. Rev. Lett.**102**, 196802 (2009).

[54] M. E. Peskin and D. V. Schroeder, *An Introduction To Quantum Field Theory* (Westview Press, 1994).

[55] A. M. Polyakov, Nuclear Physics B **120**, 429 (1977).

[56] B. A. Bernevig, J. Orenstein, and S.-C. Zhang, Phys. Rev. Lett. **97**, 236601 (2006).

[57] J. D. Koralek *et al.*, Nature **458**, 610 (2009).

[58] A. A. Abrikosov, L. P. Gor'kov, and E. Dzyaloshinskii, Methods of quantum field theory in statistical physics, Prentice- Hall, Englewood Cliffs, NJ, 1963.

[59] S. A. Brazovskii, Sov. Phys. JETP **41**, 85 (1975).

[60] B. Binz, A. Vishwanath, and V. Aji, Phys. Rev. Lett. **96**, 207202 (2006).

[61] A. V. Chubukov, V. M. Galitski, and V. M. Yakovenko, Phys. Rev. Lett. **94**, 046404 (2005).

[62] J. Schmalian and M. Turlakov, Phys. Rev. Lett. **93**, 036405 (2004).

[63] A. Posazhennikova, Rev. Mod. Phys. **78**, 1111 (2006).

[64] A. B. Kuklov and B. V. Svistunov, Phys. Rev. Lett. **89**, 170403 (2002).

[65] S. Ashhab and A. J. Leggett, Phys. Rev. A **68**, 063612 (2003).

[66] B. C. Sanders, Phys. Rev. A **40**, 2417 (1989).

[67] P. Kok, H. Lee, and J. P. Dowling, Phys. Rev. A **65**, 052104 (2002).

[68] J. Higbie and D. M. Stamper-Kurn, Phys. Rev. A **69**, 053605 (2004).

[69] G. B. Arfken, H. J. Weber, and F. Harris, *Mathematical Methods for Physicists* (Academic Press, 2000).

[70] G. Juzeliūnas, J. Ruseckas, and J. Dalibard, Phys. Rev. A **81**, 053403 (2010).

[71] B. M. Anderson, J. M. Taylor, and V. M. Galitski, Phys. Rev. A **83**, 031602 (2011).

[72] S. Dimopoulos, P. W. Graham, J. M. Hogan, M. A. Kasevich, and S. Rajendran, Phys. Rev. D **78**, 122002 (2008).

[73] M. Hohensee *et al.*, General Relativity and Gravitation **43**, 1905 (2011), 10.1007/s10714-010-1118-x.

[74] Y. Shin *et al.*, Phys. Rev. Lett. **92**, 050405 (2004).

[75] T. Schumm *et al.*, Nat Phys **1**, 57 (2005).

[76] W. Hänsel, J. Reichel, P. Hommelhoff, and T. W. Hänsch, Phys. Rev. A **64**, 063607 (2001).

[77] H. Y. Carr and E. Purcell, Phys. Rev. **94**, 630 (1954).

[78] J. Sinova *et al.*, Phys. Rev. Lett. **92**, 126603 (2004).

[79] S. Murakami, N. Nagaosa, and S.-C. Zhang, Science **301**, 1348 (2003), http://www.sciencemag.org/content/301/5638/1348.full.pdf.

[80] A. R. Cameron, P. Riblet, and A. Miller, Phys. Rev. Lett. **76**, 4793 (1996).

[81] N. Gedik and J. Orenstein, Opt. Lett. **29**, 2109 (2004).

[82] C. P. Weber *et al.*, Nature **437**, 1330 (2005).

[83] J. Schliemann, J. C. Egues, and D. Loss, Phys. Rev. Lett. **90**, 146801 (2003).

[84] N. S. Averkiev and L. E. Golub, Phys. Rev. B**60**, 15582 (1999).

[85] T. D. Stanescu and V. Galitski, Phys. Rev. B **75**, 125307 (2007).

[86] A. A. Burkov, A. S. Núñez, and A. H. MacDonald, Phys. Rev. B **70**, 155308 (2004).

[87] M. Hruška, i. c. v. Kos, S. A. Crooker, A. Saxena, and D. L. Smith, Phys. Rev. B **73**, 075306 (2006).

[88] V. V. Bryksin and P. Kleinert, Phys. Rev. B**76**, 075340 (2007).

[89] O. V. Dimitrova, Phys. Rev. B **71**, 245327 (2005).

[90] J.-i. Inoue, G. E. W. Bauer, and L. W. Molenkamp, Phys. Rev. B **70**, 041303 (2004).

[91] E. G. Mishchenko, A. V. Shytov, and B. I. Halperin, Phys. Rev. Lett. **93**, 226602 (2004).

[92] O. Chalaev and D. Loss, Phys. Rev. B**71**, 245318 (2005).

[93] C. L. Kane and E. J. Mele, Phys. Rev. Lett. **95**, 226801 (2005).

[94] B. A. Bernevig and S.-C. Zhang, Phys. Rev. Lett. **96**, 106802 (2006).

[95] V. Galitski and T. D. Stanescu, unpublished.

[96] H. Kleinert, *Path Integrals in Quantum Mechanics, Statistics, Polymer Physics, and Financial Markets,* (World Scientific Publishing Co., 2006).